University of South Bohemia

Faculty of Science

mTOR-regulated translation during first the wave of inner cell generation in mouse preimplantation embryos

MASTER´S THESIS

Bc. Pavlína Černá

Supervisor of the master´s thesis: doc. Alexander W. Bruce, Ph.D.

Co-supervisor of the master´s thesis: Lenka Gahurová, Ph.D.

České Budějovice 2022

Černá, P., 2022: **mTOR-regulated translation during the first wave of inner cell generation in mouse preimplantation embryos**, Mgr. Thesis, in English. – 98 p. Faculty of Science, University of South Bohemia, České Budějovice, Czech Republic.

Annotation

The aim of this master thesis was to investigate the role of mTOR and connected pathways in early mouse preimplantation development.

Prohlašuji, že svou diplomovou práci jsem vypracovala samostatně pouze s použitím pramenů a literatury uvedených v seznamu citované literatury.

V Českých Budějovicích 13.4.2022

Acknowledgements

I would like to thank my supervisor Alexander W. Bruce for giving me an opportunity to work in his laboratory and especially for his endless patience with me finishing this thesis simultaneously with my work. My biggest gratitude belongs to Lenka Gahurová who showed me how interesting and exciting work with murine embryos can be. She was always ready to help, advice and encourage, which I deeply appreciate. Also, many thanks to other members of Laboratory of Early Mammalian Developmental Biology especially Pablo Bora for cooperation during microinjection experiments. Last but not the least my deepest gratitude belongs to my supportive family, who have always been by my side.

Abstract

Mouse preimplantation development proceeds over 4.5 days and starts with oocyte fertilization and finishes with uterine implantation of the blastocyst embryo. The embryo undergoes at least seven rounds of mitotic cell division, with the generated blastomeres being assigned specific cell fates by the peri-implantation blastocyst stage; the trophectoderm (TE - a differentiating and extraembryonic progenitor lineage of the placenta), primitive endoderm (PrE - a differentiating extraembryonic lineage that gives rise to the yolk sac) and epiblast (EPI - a progenitor pool for all the cell types of the foetus). Accordingly, the first cell fate decision initiates with spatial segregation of 16-cell stage blastomeres that arise following the division of polarised 8-cell stage blastomeres. Depending on axes of cell division and regulative mechanisms influencing spatial positioning, resulting blastomeres can remain polarised and reside on the outside of the embryo or become internalised as apolar cells (repeated by 16-cell stage outer-blastomeres in the next round of division). Under cellular mechanisms governed by, but not limited to, the influence of intracellular polarity, relative cellular position, differential cell signalling and transcription factor regulated gene expression, outer blastomeres specify as TE and the inner-cell-mass (ICM) remains pluripotent; eventually segregating into EPI and PrE. The mTOR signalling pathway is a central regulator of cell growth and metabolism. Active mTOR signalling promotes mRNA translation, particularly recalcitrant mRNAs containing so called 5'UTR TOP-motifs, and is known to regulate chromosomal segregation, spindle position and polar body extrusion in mouse oocytes. mTOR, acting as part of the mTORC1 complex, regulates translation via direct phosphorylation of substrates; including the translational inhibitor protein 4EBP1, to liberate the translation initiation factor eIF4E (an essential component of the 7-methyl-guanosine-RNA-cap binding complex eIF4F). Herein, it is confirmed *in vitro* culture of mouse embryos in the presence of the mTORC1 inhibitor Rapamycin (during the 8- to 16-cell transition), significantly impairs the generation of inner blastomeres; with similar phenotypes obtainable by targeting other mTOR-related pathways (*i.e.* AMPK, p38-MAPK, AKT, RSK and

MEK1/2). Moreover, clonal overexpression of a recombinant non-phosphorylatable 4EBP1 mutant also impairs 16-cell stage inner blastomere generation; linking mTOR activity, regulation of protein translation and spatial allocation of TE and ICM founder cells (although over-expression of recombinant EIF4E could not rescue the impaired inner cell phenotype mediated by mTOR inhibition). Overall, data in this thesis place mTOR signalling, and that of related signalling pathways, as important components of relative blastomere spatial positioning, contributing to the first cell-fate decision of mouse preimplantation development.

Abbreviations

AJs - adherens junctions

AKT - serine/threonine protein kinase protein

AMOT – Angiomotin protein

AMPK - adenosine monophosphate activated kinase protein

Amp^r - ampicillin resistance

BSA – bovine serum albumin

CDC42 - cell division control protein 42 homolog

CDK1 - cyclin dependent kinase 1 protein

CDX2 - caudal-related homeobox 2 transcription factor protein

eEF-2K - eukaryotic elongation factor 2 kinase protein

EIF4E - eukaryotic initiation factor 4E protein

eIF4G - eukaryotic initiation factor 4G protein

EPI - epiblast

ERK - extracellular signal regulated kinase protein

ESC – embryonic stem cell

FGF4 – fibroblast growth factor 4 protein

FGFR - fibroblast growth factor receptor protein

GATA4/6 – GATA binding protein 4/6 (transcription factor)

HA-tag - Hemagglutinin epitope tag

hCG - human chorionic gonadotrophic hormone

ICM - inner cell mass

IVT - *in vitro* transcription

JNK – jun-amino terminal kinase protein

LARP1 - la-related protein 1

LATS - large tumor suppressor kinase protein

MAPK - mitogen activated kinase protein

MCS - multiple cloning site

mLST8 - mammalian lethal with SEC13 protein 8

mTOR – mammalian target of Rapamycin protein

NANOG – homeobox transcription factor NANOG protein

OCT4 - octamer-binding transcription factor 4 protein

PARD3/6 - Partitioning defective 3/6 protein homolog

PCR - polymerase chain reaction

PDCD4 - programmed cell death 4 protein

PI3K - phosphoinositide 3-kinase protein

PLK1 - polo-like-kinase 1 protein

PMSG - pregnant mare serum gonadotrophin

PP2A - Protein phosphatase 2A proteiun

PrE - primitive endoderm

RAC1 - Rac family small GTPase 1 protein

Raptor - regulatory associated protein of mTOR protein

RDB - for rhodamine-conjugated dextran micro-bead

RHOA – Ras homolog family member A protein

RSK - ribosomal s6 kinase protein

RT – room temperature

SAD - small apical domain

SOX2 - SRY-box transcription factor 2 protein

S6K1 - p70 ribosomal S6 kinase 1 protein

TAZ – transcriptional coactivator with a PDZ binding motif protein

TBE (Tris-Borate-EDTA)

TE – trophectoderm

TEAD4 – transcriptional enhanced associate domain 4 transcription factor protein

TOP - terminal oligopyrimidine

UTR - untranslated region

YAP – Yes associated protein

ZGA – zygotic genome activation

4EBP1 - 4E binding protein

Table of contents.

1. Introduction.

1.1. Mouse preimplantation embryo development.

1.1.1. The preimplantation mouse embryo.

Preimplantation mouse development (Fig. 1) takes 4.5 days. It starts with the fertilization of the oocyte and ends in the implantation of a blastocyst embryo (comprising >128 cells and defined by the presence of fluid filled cavity) into the maternal uterus. During this time the embryo goes through at least seven rounds of mitotic cell division. Such successive rounds of mitosis produce progressively smaller cells, referred to in the preimplantation embryo as blastomeres, and arise from so-called cleavage divisions in which resulting daughter cells do not grow during interphase. Consequently, the combined cytoplasmic volume of all cells of the embryo, up to the peri-implantation blastocyst stage is equivalent to that of the initially fertilised oocyte (Nagy *et al.*, 2003). During preimplantation development the individually generated blastomeres adopt specific fates that enable blastocyst implantation and continued post-implantation stages of development. Such cell fate adoption occurs during two distinct temporal phases. The first cell fate decision occurs between the 8- and 32-cell stages, when blastomeres either contribute to an outer-residing population of differentiating trophectoderm cells (TE – extraembryonic progenitors of the future placenta) or are allocated to the completely surrounded and pluripotent inner cell mass (ICM). Whereas the second cell fate decision involves the subsequent segregation of blastocyst ICM cells between the differentiating primitive endoderm (PrE – another extraembryonic lineage that later gives rise to the yolk sac membranes and resides at the interface of the ICM and blastocyst cavity) and the pluripotent epiblast (EPI – a progenitor pool for all the cells types of the subsequently derived foetus and the post-natal adult, that is found deep within the ICM) (Chazaud and Yamanaka, 2016).

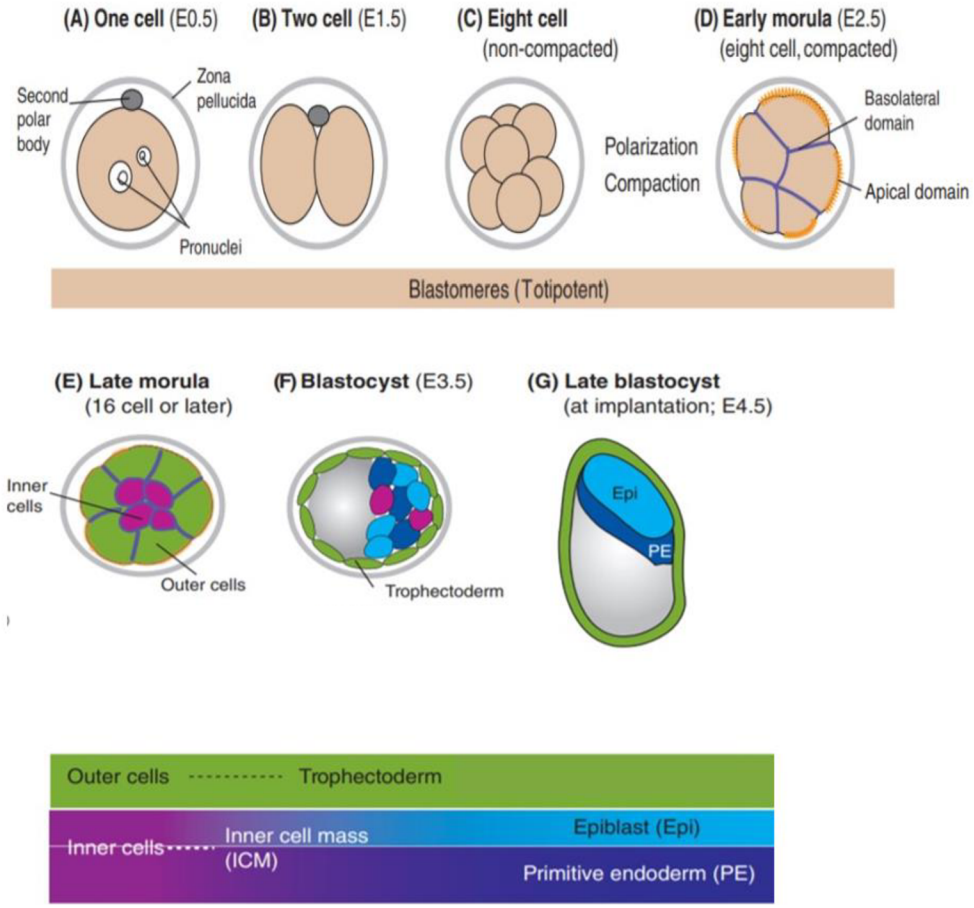

Fig. 1: Preimplantation mouse embryo development: growing number of embryo cells during the individual stages after cleavage cell divisions of the embryo. The first wave of cell internalisation is observable from the 8- to 16-cell stages and results in the appearance of the first inner cell population. The second wave of outer daughter cell internalisation takes place as a result of the 16- to 32-cell transition. Consequently, outer residing TE cell become set apart from ICM in what is termed the first cell fate decision and the PrE and EPI lineages are later segregated within the ICM during the second cell fate decision (Rossant and Tam, 2009).

1.1.2. Preimplantation mouse embryo potency and morphology.

It is documented that the preimplantation stages of mouse embryo development are extremely flexible, robust and plastic. For example, perturbation experiments demonstrate that either the loss of individual blastomeres or the combining of embryonic blastomeres of distinct genetic origin (to form chimaeras) can be fully compensated without significant consequences for the proper development of blastocysts capable of implantation and supporting the birth of viable pups. Indeed, individual/isolated 2-cell stage blastomeres are totipotent; meaning they can give rise to blastocyst embryos and live pups after uterine transfer, as they

are able to ultimately derive both the extraembryonic tissues (arising from TE and PrE) and all embryonic/foetal cell types (resulting from the EPI) (Tarkowski, 1959; Morris, Guo and Zernicka-Goetz, 2012). An application of this strict definition of totipotency shows that isolated blastomeres from 4-8 cell stage embryos are not capable of supporting full development on their own (*i.e.* they have lost totipotent properties), nevertheless they are still considered pluripotent as they are able to contribute to all three blastocyst lineages when combined with other cells as chimeric embryos and form developmentally viable blastocysts (Tarkowski and Wróblewska, 1967; Rossant, 1976). Indeed, research has proven this pluripotent character persists until the early stages of blastocyst formation at the 32-cell stage (the point at which TE cell fate specification is irreversibly committed – (Posfai *et al.*, 2017)), as reformed chimeric aggregates consisting of individually separated 16- and early (uncavitated) 32- cell stage embryo blastomeres, of either exclusively inner or outer cells or a mixture of both, can produce normal peri-implantation stage blastocysts that are developmentally viable to term following uterine transfer (Ziomek and Johnson, 1982; Suwińska *et al.*, 2008). Hence, individual blastomeres of the developing preimplantation mouse embryo retain maximal cell fate plasticity until the initiation of blastocyst formation and furthermore, the embryo as a whole preserves its ability to ultimately self-organise into a late blastocyst appropriately comprised of three distinct cell types/tissue layers.

The first obvious morphological transition observed during preimplantation mouse embryo development occurs during the 8-cell stage; whereby the embryo undergoes a process of compaction (Fig. 1). As the embryo compacts, inter-cellular contacts are maximalised (as mediated by the cell adhesion molecule E-cadherin and the formation of Adherens junctions – AJs) and the boundaries of individual cells become obscured. Concomitantly, individual 8-cell blastomeres undergo a process of apical-basolateral polarisation, typified by the asymmetrical intra-cellular distribution of specific cytoplasmic polarity factors to either the cell contactless apical membranes or cell contacted basolateral membrane domains and the restriction of plasma membrane microvilli to the apical surface. Such factors include Ezrin/EZR (apically localised and plays a role in formation and stabilization of microvilli (Dard *et al.*, 2004)), PARD6 (also apically localised and essential for TE formation (Alarcon, 2010)) and PARD3 (targeted to tight

junctions, at the interface of the apical and lateral domains, to play a role in maturation/maintenance of the TE (Vinot *et al.*, 2005)). As described below the adoption of such apical-basolateral polarity and its subsequent inheritance is central to the first cell fate specification decision (*i.e.* TE versus EPI).

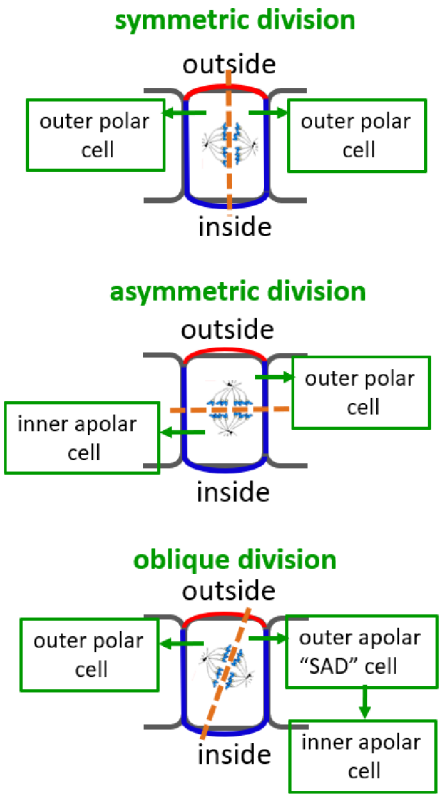

Fig. 2: Types of possible 8-cell stage and outer 16-cell stage blastomere cleavage division with regard to spindle orientation and intra-cellular apical (red) and basolateral (blue) polarity. During symmetric divisions (upper panel) the axis of cell division (as defined by the dashed orange line) along the radial axis of the embryo with the mitotic spindle axis (defined by the two opposing spindle poles) being at a perpendicular angle. Post-cell division this results in two outer-residing daughter cells each exhibiting equal apical-basolateral polarity (green arrows). During asymmetric divisions (central panel) the plane of cell division is perpendicular to the radial axis and results in the generation of an outer and polarised daughter cell and an inner apolar daughter. In reality most divisions represent varying degrees of oblique divisions (lower panel) in which both daughter cells inherit unequal amounts of apical-basolateral polarity, with those inheriting less more prone to eventual internalisation (*as discussed below*) (Author: Lenka Gahurová).

As compacted 8-cell stage embryos enter the 8- to 16-cell transition individually polarised blastomeres can divide in one of three distinct manners (Fig. 2). The first is termed as a conservative/symmetric division and it is typified by the

mitotic spindle axis aligning perpendicular to the radial axis of the embryo (*i.e.* across the intra-cellular apical-basolateral axis of polarity). As a result, both daughter cells inherit approximately equal amounts of apical and basolateral membrane domains and maintain a surface position on the outside of the embryo (and can contribute progeny cells to the future TE). Although it is argued localisation of apical/basolateral polarity factors is temporarily lost during mitosis itself (Johnson, 2009) both the resulting daughter cells of symmetric/conservative divisions re-establish intra-cellular apical-basolateral polarity as they enter inter-phase, and thus retain their polarity (incidentally, the apical plasma membrane surface typified by the presence of microvilli appears not to be affected by entry into mitosis). The second cell division type called differentiative/asymmetric, involves spindle alignment parallel to the radial embryonic axis and results on one daughter cell inheriting the entire apical domain and an outer position, whilst the second daughter comprises only previously basolateral membranes and is completely internalised within the embryonic cell mass. Accordingly, the resulting outer 16-cell stage daughters retain polarity and can contribute future TE cells, whereas their internalised sisters become apolar and populate the nascent ICM. The final type of division, that via live-cell time-lapse microscopy observation appears to be most common (Sutherland, Speed and Calarco, 1990; Morris *et al.*, 2010; Watanabe *et al.*, 2014), is referred to as oblique and is associated with mitotic spindle angles that are slightly off-set from the radial axis of the embryo and result in daughter cell couplets inheriting differing amounts of the apical domain resulting in one polarised blastomere retaining an outer position (and contributing future TE cells – as described above for daughters of symmetric/conservative divisions) and the other retaining a comparatively small apical domain contact with the outer surface of the embryo (that we term 'SAD' – Small Apical Domain), or a cell contactless domain devoid of apical polarity factors, that is most likely to internalise (via an intrinsic mechanism actomyosin contraction – (Samarage *et al.*, 2015)) to the nascent ICM during the ensuing 16-cell stage (Sutherland, Speed and Calarco, 1990; Anani *et al.*, 2014). The differential spatial segregation and inheritance of apical-basolateral polarity of 8-cell daughter blastomeres represents the first wave of potential internalisation of apolar cells to the nascent ICM. However, this process is repeated during the following 16- to 32-cell

transition, whereby polarised outer 16-cell stage blastomeres can contribute an additional population of inner cells in a second wave of cell internalisation (to accompany the already internalised and dividing cells from the first wave). Therefore, it is at this early blastocyst 32-cell stage, that the pluripotent ICM comprises its initial full complement of EPI and PrE progenitors (save for an extremely infrequent and minimal in size third internalisation event (Morris *et al.*, 2010)) and the outer polarised and differentiating TE cells initiate their irreversible cell fate commitment (Posfai *et al.*, 2017). Factors influencing the frequency of the adoption of each of the three described division types, or whether they represent inherent randomness, are not completely understood. However, Ajduk and co-workers report the intra-cellular position of nuclei long the radial axis (*i.e.* the intra-cellular axis of apical-basolateral polarity), as mediated by the action of microtubules and kinesin motor proteins driving nuclei more basally, influences the probability of ensuing symmetric/conservative or asymmetric/differentiative cell divisions; specifically, that apical positioned nuclei strongly correlate with symmetric/conservative divisions and asymmetric/differentiative cell divisions can only occur from nuclei positions more basally (although such positions can also yield the alternative division type - Ajduk et al. 2014). Additionally, the work of Korotkevich *et al*., has also shown an important role of the 8-cell stage apical domain towards orientating ensuring divisions to favour generation of apolar inner cell populations (*i.e.* favouring degrees of division that could be classified as asymmetric/differentiative, or at least oblique - Korotkevich et al. 2017).

1.1.3. Historical models of mouse preimplantation embryo cell fate acquisition.

In relation to the first cell fate decision (the separation of differentiating TE cells from pluripotent ICM cells), two historical models, often portrayed as being conflicting, have gained traction. The first, as proposed by Tarkowski and Wroblewska, is referred to as the *positional/inside-outside model*. The second was defined by Johnson and Ziomek and is known as the *polarity model*. According to the positional model, an individual blastomeres (post-8-cell stage) cell fate depends on its relative spatial position in the embryo. It is argued, spatial positioning information is used by outer cells to specify TE differentiation and

equally for inner cells to maintain ICM pluripotency; as such, if individual cells are experimentally transferred from one spatial position to the opposing one, they are able to change/adapt their fate accordingly (Tarkowski and Wróblewska, 1967). The polarity model states that it is not cell positioning *per se* that dictates appropriate cell fate specification but rather the presence or absence of intra-cellular apical-basolateral polarity that promotes TE differentiation or pluripotency, respectively. Therefore it is the post-cell division inheritance of the apical domain (*i.e. de facto* polarisation) that is the key to unlocking the first cell fate decision (Johnson and Ziomek, 1981). However, in recent years multiple lines of experimental evidence have begun to demonstrate the strong inter-dependency of intra-cellular polarity and the relative spatial positioning of individual blastomeres in the embryo and their ultimate TE versus ICM cell fate (as reviewed – Mihajlovic and Bruce, 2017); this has led to the proposition of a refined hybrid model, termed the *polarity dependent cell positioning model*. This model stipulates the polarity (or the degree of apical polarity) status of a blastomere as being not only important in driving TE differentiation (as will be discussed in the following section relating to molecular mechanisms) but also ensuring an appropriate and continuing residency on the outer surface of the embryo. As such, if polarity is compromised, either experimentally or as a result of an oblique cell division, the apolar cell will internalise into the pluripotent ICM (or in more rare cases initiate re-polarisation (Mihajlovic and Bruce, 2017)).

Regarding the second cell fate decision (the specification and segregation of differentiating PrE from pluripotent EPI within the maturing mouse blastocyst ICM) a number of models also have been provided. The oldest of which suggests surface ICM cells in contact with the expanding fluid filled cavity receive from it an instructive cue to differentiate *in situ* (Enders, Allen, Given, Randall and Schlafke, 1978; Gardner, 1982). Although recent reports have implicated a role for increasing blastocyst cavity volume (as mediated by the osmotic transfer of water across the encapsulating and epithelialized TE monolayer, via the action of Na^+/K^+ ATPases and aquaporins – reviewed in Rossant a Tam 2009)) in facilitating PrE differentiation and its segregation from the EPI (Ryan *et al.*, 2019), the lack of definitive cavity derived signalling molecule detracts from this *induction model*. Moreover, the discovery that specified PrE and EPI progenitors arise only at the mid-blastocyst stage and in an essentially randomised pattern

throughout the ICM, referred to as the *salt and pepper pattern*, that then sorts into the distinct late blastocyst tissue layers (via a combination of active cell movement and apoptosis) further argues again the induction model. There is some discord within the literature as to how the salt and pepper pattern of PrE and EPI progenitors emerge. Some researchers favour a mechanism by which essentially bipotent early blastocyst ICM cells, comprising essentially similar transcriptomic profiles (Ohnishi *et al.*, 2014), nevertheless go on to display *stochastic patterns of gene transcription* that via positive and negative feedback mechanisms initiate and reinforce the necessary gene expression patterns to drive ICM cell fate segregation, through the salt and pepper stage (Yamanaka, Lanner and Rossant, 2010). Whilst appealing, mathematical modelling indicates stochastic processes alone are unlikely to be the driving force establishing the salt and pepper pattern (Bessonnard *et al.*, 2014). An alternative mechanism, termed the *time inside-time outside model*, suggests an individual early blastocyst ICM cell's developmental history influences its ultimate EPI versus PrE fate (Zernicka-Goetz, Morris and Bruce, 2009; Bruce and Zernicka-Goetz, 2010). According to this model, an ICM cell is more likely to contribute EPI progenitors if it were derived from the first wave of cell internalisation (at the 8- to 16-cell transition) and is strongly biased to produce PrE progeny if internalised within the second wave (at the 16- to 32-cell transition). Evidence from recorded cell lineage tracing analysis of time-lapse microscopy mouse embryos support the time inside-time outside model (Morris *et al.*, 2010); although the strength of the relationship is strongly dependent on the number of initially internalised cells in the first wave (Morris *et al.*, 2013). The combined facts that the nascent ICM cells of 16-cell stage mouse embryo upregulate expression of the *Fgf4* (fibroblast-growth factor 4 – encoding FGF4 required to drive PrE differentiation, (Yamanaka, Lanner and Rossant, 2010)) gene (Guo *et al.*, 2010) and second wave ICM cells also express elevated levels of FGFR2 (fibroblast-growth factor receptor 2 (Morris *et al.*, 2013; Krupa *et al.*, 2014)) are supportive of the time inside-time outside model.

1.1.4. Molecular mechanisms of cell fate derivation in mouse preimplantation development.

Before the 2-cell stage, the mouse embryo relies on maternally provided mRNAs and proteins to underpin its necessary functions. During the 2-cell stage, the genome becomes transcriptionally active, with control of development passing from maternal to embryonic control, in a process called zygotic genome activation (ZGA – note, there is a minor and gene specific ZGA that occurs in the zygote but the major burst of generalised ZGA occurs during the 2-cell stage). The onset of ZGA, which is uniquely early in mice compared to other mammals (typically initiating around the 8- or 16-cell stage) is accompanied by the targeted destruction of the maternally provided mRNAs but maternal proteins can persist and be functional until the end of the preimplantation developmental period (Aoki, Worrad and Schultz, 1997; Johnson and McConnell, 2004).

For the purposes of this thesis introduction, it can be considered that no substantial/functionally relevant molecular differences exist between blastomeres of the same mouse embryo up until beyond the 8-cell stage (Anani *et al.*, 2014). However, there are multiple reports that detail inter-blastomere molecular heterogeneities in expressed mRNA transcripts and/or post-translation histone/chromatin modifications at both the 4- and 8-cell stages (Torres-Padilla *et al.*, 2007; Jedrusik *et al.*, 2008; Goolam *et al.*, 2016) and embryological evidence supporting reduced developmental potency of specific blastomeres, emanating from defined cell division orientation patterns, prior to the 8- to 16-cell stage transition (Piotrowska-Nitsche *et al.*, 2005; Bischoff, Parfitt and Zernicka-goetz, 2008; Tabansky *et al.*, 2013).

However, the first cell fate decision (*i.e.* TE versus ICM) can be considered to initiate from the 8-cell stage, during which all blastomeres increase cell contacts during embryo compaction and establish an intra-cellular axis of apical-basolateral polarity (as described above). After the 8- to 16-cell transition, the spatially distinct outer-polarised and apolar inner cells display differentiational activation of the hippo-signalling pathway. This is manifest in the opposing subcellular localisation of the hippo-effector transcriptional co-activator proteins YAP and TAZ (herein collectively referred to as YAP). Specifically, in outer polarised cells YAP is nuclear (indicative of a supressed hippo-signalling pathway) and in apolar inner cells it is sequestered to the cytoplasm (reporting an

active hippo-signalling pathway). The establishment of such spatially distinct differential hippo-signalling is an absolute prerequisite for both outer cell TE differentiation (Nishioka *et al.*, 2009) and specification of ICM pluripotency (Wicklow *et al.*, 2014) and is predicated on the polarisation status of individual blastomeres. This is because from the 8-cell stage, the hippo-signalling pathway activator protein AMOT (Angiomotin) becomes weakly expressed and specifically localises at the apical domain (without activating the hippo-pathway). However, at the 16-cell stage, AMOT localises around the cortical membranes of apolar inner cells (at AJs – centres of intra-cellular hippo-signalling) but is excluded from the similar basolateral membranes of outer cells, remaining sequestered to the apical domain (Figs. 3 & 4). Therefore, it is the apical sequestration of AMOT in polarised outer cells that inhibits outer cell hippo-signalling activation, and it is the lack of a sequestration mechanism in apolar inner cells that promotes activation of the pathway. Indeed, experiments prove that if AMOT is absent in nonpolar cells, they loose their pluripotency and initiate the expression of trophectodermal genes; *e.g.*, the TE required transcription factor *Cdx2* (Hirate, Hirahara, K. I. Inoue, *et al.*, 2013; Leung and Zernicka-Goetz, 2013). Moreover, disruption of outer cell apical polarity causes aberrant activation of the hippo-pathway and adoption of pluripotent gene expression patterns (Hirate, Hirahara, K. I. Inoue, *et al.*, 2013; Anani *et al.*, 2014; Kono, Tamashiro and Alarcon, 2014; Mihajlovic and Bruce, 2016). Mechanistically, it is known that AMOT sequestration to the apical domain, not only relies on apical domain polarity factors but its interaction with cortical F-actin. However in apolar inner cells, AMOT can interact with plasma membrane localised AJ hippo-signalling centres (as facilitated by binding of the NF2/merlin protein (Cockburn *et al.*, 2013)), where it is phosphorylated by the hippo-effector kinases LATS1/2 (on Serine 179/S176). Such, phosphorylation both decreases AMOT's affinity for F-actin and promotes its association with LATS1/2 to facilitate high levels of kinase activity, in a positive feed-forward regulatory loop. Accordingly, LATS1/2 can go on to phosphorylate the YAP co-activator protein (at S112) and prevents its translocation to the nucleus (via promoting an association with cytoplasmic 14-3-3 scaffold proteins) and thus blocks the transcription of TE specific genes by the transcription factor TEAD4 (already recruited to TE gene specific promoters, such as *Cdx2*, but requiring binding of

YAP to activate transcription) and simultaneously permits pluripotent gene expression (*e.g.* SOX2 and NANOG transcription factors - Fig.3). However, as AMOT is sequestered by binding F-actin at the polarised apical domain in outer cells, here LATS1/2 remains inactivated, YAP unphosphorylated and free to enter the nucleus, resulting in TEAD4 dependent expression of TE specific genes (Nishioka *et al.*, 2009; Cockburn *et al.*, 2013; Hirate, Hirahara, K. I. Inoue, *et al.*, 2013; Leung and Zernicka-Goetz, 2013) and the concomitant suppression pluripotency transcription genes, such as *Sox2* and *Nanog*, via an unknown but TEAD4 dependent mechanism (Wicklow *et al.*, 2014)(Fig.4).

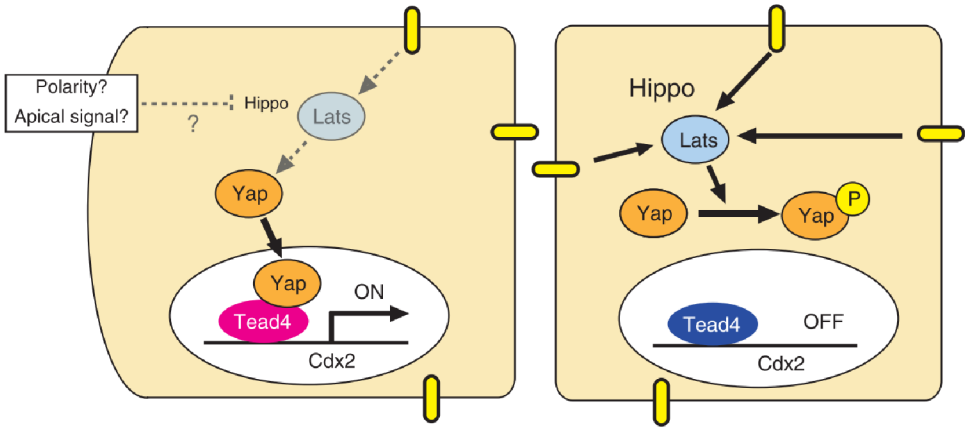

Fig. 3: Mechanism of differential hippo signalling pathway (in)activation in preimplantation stage mouse embryos. In inner cells (right) LATS1/2 phosphorylates the YAP co-activator protein (at adherens junctions/AJs – yellow oblongs) and prevents its translocation to the nucleus and thus blocks the transcription of TE specific genes (*e.g. Cdx2*) by the transcription factor TEAD4 and simultaneously permits pluripotent gene expression (*e.g.* SOX2 and NANOG transcription factors). Whereas in outer cells (left) LATS1/2 activation at AJs is prevented, allowing unphosphorylated YAP to enter the nucleus and together with TEAD4 activate the expression of TE specific genes (*e.g. Cdx2).* (Sasaki, 2010)

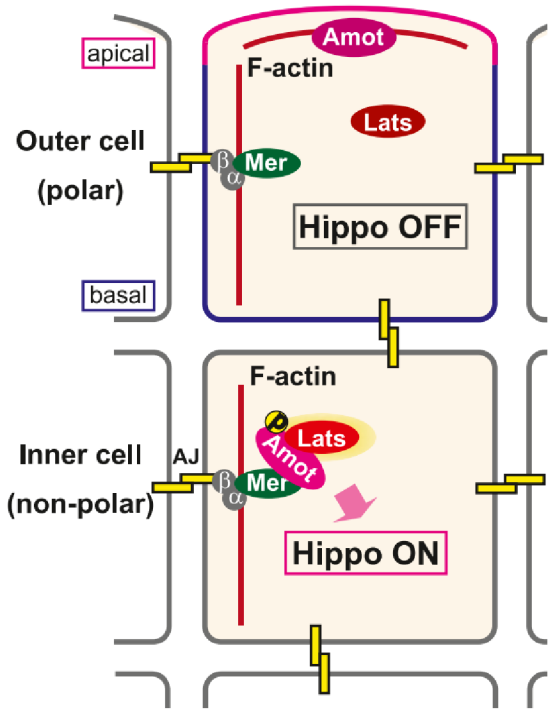

Fig. 4: Mechanism of differential hippo signalling pathway (in)activation in preimplantation stage mouse embryos. In outer cells (upper) the hippo-signalling pathway activator protein AMOT is sequestered by binding F-actin at the polarised apical domain (red), causing adherens junction (AJ) localised LATS1/2 to remain inactivated, YAP unphosphorylated and free to enter the nucleus to result in TEAD4 dependent expression of TE specific genes; plus the concomitant suppression pluripotency transcription genes, such as *Sox2* and *Nanog*, via an unknown but TEAD4 dependent mechanisms; *i.e.* the hippo-signalling pathway is inactive/off. In apolar inner cells (lower) AMOT is not sequestered, interacts with LATS1/2 at AJs and results in LATS1/2 activation and phosphorylation of YAP. Phosphorylated YAP is prevented from entering the nucleus and hence TEAD4 specific activation of TE-related genes is blocked, in favour of the activation of pluripotency related gene expression*; i.e.* the hippo-signalling pathway is active/on (Hirate, Hirahara, K. Inoue, *et al.*, 2013).

In relation to the second cell-fate decision, it is known the specified late peri-implantation mouse blastocyst EPI state is characterised by expression of the pluripotency transcription factors NANOG and SOX2, whereas the PrE is distinguished by exclusive expression of the transcription factors GATA6, SOX17 and GATA4 (Artus, Piliszek and Hadjantonakis, 2011). Interestingly, NANOG/SOX2 and GATA6 expression overlaps in all the ICM cells of the early 32-cell blastocyst (indicative of an uncommitted cell fate) but as blastocyst development matures their expression becomes mutually exclusive and randomly distributed throughout the ICM. This is reflective of the mid-blastocyst stage salt and pepper pattern of PrE (GATA6+) and EPI (NANOG/SOX2+) progenitors referred to the above section (Chazaud *et al.*, 2006). These EPI and PrE progenitors then sort via a mechanism of active movement and apoptosis of

inappropriately positioned PrE or EPI specified cells (Chazaud *et al.*, 2006; Plusa *et al.*, 2008; Meilhac *et al.*, 2009; Morris *et al.*, 2010). In the specified and differentiating PrE lineage there is a subsequent and sequential induction in the expression of the transcription factors SOX17, GATA4 and SOX7 (Morris *et al.*, 2010; Niakan, Kathy *et al.*, 2010; Artus, Piliszek and Hadjantonakis, 2011). Interestingly, the classically recognised (largely from embryonic stem cell/ESC culture studies – cell lines derived from the blastocyst ICM) pluripotency transcription factor OCT4 is expressed in all ICM cells until the peri-implantation stage and is essential for blastocyst survival. It is proposed it is essential for directly promoting gene expression patterns required for EPI pluripotency (via dimerisation with SOX2) and indirectly sustains PrE differentiation by activating expression and secretion of FGF4 ligands (further discussed below). However, it is known OCT4 is also required to cell-autonomously support PrE differentiation directly (Frum *et al.*, 2013) and it has been suggested (from ESC studies) this could be via a dimerising interaction with SOX17 expressed within differentiating PrE cells (Aksoy *et al.*, 2013). Hence, OCT4 may cell autonomously contribute to both EPI specification and PrE differentiation via switching its dimerisation partner between available SOX2 or SOX17 proteins, respectively.

It is generally known that mitogen-activated-kinase (MAPK) signalling pathways are able to mediate/regulate many cellular processes linked to development, such as cell differentiation events, proliferation, growth and death (Ono and Han, 2000). MAPKs in mammals can be divided into three main families comprising, **i.** the extracellular signal regulated kinases (ERKs), **ii.** Jun-amino terminal kinases (JNKs) and **iii.** p38/stress activated protein kinases, p38-MAPKs, (Zhang, Yang and Wu, 2007).

The more classically appreciated ERK1/2 module is known to primarily respond to and become activated by specific growth factors and mitogens, in order to induce cell growth and differentiation (Shaul and Seger, 2007). Indeed it has been shown in the blastocyst ICM, that FGF4-based signalling is absolutely required for PrE differentiation (via combined reports of the genetic knockout of both the *Fgf4* and *Fgfr1/2* receptor genes – Kang *et al.*, 2013; Kang, Garg and Hadjantonakis, 2017). Indeed, the combined inhibition of FGFRs and MEK1/2

kinases (responsible for activating ERK1/2 in the MAPK cascade) blocks PrE differentiation, whereas blastocyst exposure to exogenously provided recombinant FGF4 ligand can drive all ICM cells to adopt a PrE fate (Yamanaka, Lanner and Rossant, 2010). Interestingly, whilst FGF4 is required for PrE differentiation and expressed and secreted by specified EPI progenitors (Guo *et al.*, 2010), combined evidence suggests it signals to both EPI and differentiating PrE (primarily via FGFR1 as the principle receptor – Kang, Garg and Hadjantonakis, 2017). Consistently, Azami and co-workers recently reported the presence of phosphorylated ERK1/2 in all nascent and unspecified ICM cells of the early blastocyst, and in specified and differentiating EPI and PrE cells, respectively. They argue that it is the differential expression of factors regulating the ERK1/2 MAPK pathways that are ultimately responsible for the emergence of the EPI (in volving the transcription factor ETV5) and PrE (involving the phosphatase DUSP4) lineages and how they interact in the maturing blastocyst ICM (Azami *et al.*, 2019). The p38-MAPK family represents another MAPK pathway implicated in cell specification during preimplantation mouse embryo development. Using targeted pharmacological inhibition, Natale and colleagues have shown p38-MAPK inhibition from the 2-cell stage, results in arrested development around the 8- to 16-cell stages with complete loss of filamentous actin (Natale *et al.*, 2004). Research from our own laboratory has also shown p38-MAPK activity is required to specify PrE cells, from the initially uncommitted cells of the early blastocyst ICM; with p38-MAPK inhibition provided from the early blastocyst stage resulting in peri-implantation mouse blastocysts comprising ICM cells either solely expressing NANOG (indicative of EPI specification) or uncommitted cells co-expressing NANOG and GATA6 (indicative of a failure in PrE specification/differentiation – Thamodaran and Bruce, 2016). Such necessary p38-MAPK activity, is temporally required in only the earliest stages of blastocyst maturation, is associated with both protecting specifying and/or differentiating ICM cells from oxidative stress (Bora *et al.*, 2019) and priming specifying PrE progenitor cells for differentiation, via a mechanism potentiating protein synthesis/translation (Bora, Gahurova, Hauserova, *et al.*, 2021; Bora, Gahurova, Mašek, *et al.*, 2021). Further research relating to MAPKS has revealed a role in facilitating blastocyst cavity formation, whereby inhibition of p38-MAPK and JNK (but not ERK/12) pathways during

blastocyst formation impairs cavity volume (Maekawa *et al.*, 2005; Bora, Gahurova, Mašek, *et al.*, 2021).

1.2. Mammalian Target Of Rapamycin (mTOR).

The Target Of Rapamycin (TOR) signalling pathway (Fig. 5) is present in all eukaryotes. This protein kinase is a central regulator of cell growth and metabolism and is duly often researched in relation to cancer and as a potential therapeutic target. Mammalian TOR (mTOR) is also associated with neurodegeneration and diabetes and there is evidence that mTOR may also mediate aging and lifespan in general. Specifically, mTOR function is regulated in response to growth factor signalling, nutrient availability and ATP levels. mTOR can exist in one of two multiprotein complexes, referred to as mTORC1 and mTORC2; standing for mTOR containing complexes 1/2 (Dowling *et al.*, 2010; Dazert and Hall, 2011).

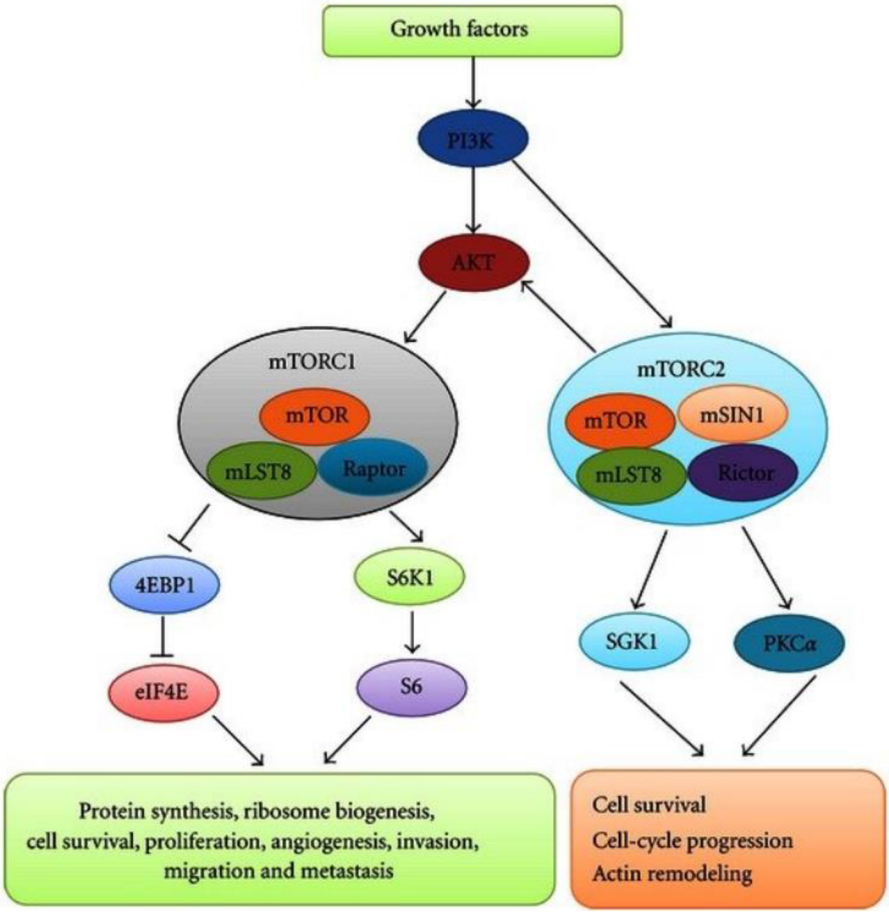

Fig. 5: The mTOR signalling pathway. mTOR can exist in one of two multiprotein complexes (mTORC1, mTORC2) under the control of growth factor signalling and other nutrient sensing mechanisms (e.g. AKT pathway). mTORC1 is composed of Raptor, mLST8 and mTOR protein subunits (with Rictor and mSIN1 replacing Raptor in the mTORC2 complex). Active mTORC1 regulates protein synthesis and degradation and in turn acts as a driver of the rate of cell proliferation and growth etc.; whereas, active mTORC2 is implicated in cell survival and regulation of cell cycle and senescence (Gao *et al.*, 2012)

However, mTORC2, unlike mTORC1, is known to be Rapamycin insensitive; although Sarabassov and co-workers have shown Rapamycin inhibits assembly of mTORC2 after prolonged treatment, eventually leading to reduced levels of mTORC2 signalling with consequent effects for downstream cellular processes (Sarbassov *et al.*, 2006); *i.e.* cell survival, cell-cycle progression and actin remodelling (Gao *et al.*, 2012).

mTORC1 is Rapamycin sensitive and is composed of three main protein subunits: Raptor, mLST8 and mTOR. This complex controls a high number of cellular processes, including regulating protein synthesis and degradation and in turn acts as a driver of the rate of cell growth and proliferation (Guertin and Sabatini, 2007). In regard to its regulation of protein synthesis, mTORC1 is

known to interact with, and phosphorylate, two important substrates; eukaryotic initiation factor 4E (eIF4E) -binding protein 1 (4EBP1) and p70 ribosomal S6 kinase 1 (S6K1) – see Fig. 6 (Gao *et al.*, 2012). mTORC1 dependent phosphorylation of 4EBP1 blocks its inhibitory interaction with eIF4E (a translation initiation factor, that functions as part of the 7-methyl-guanosine-mRNA-cap binding complex, eIF4F, needed to initiate mRNA protein translation) thus promoting enhanced levels of protein synthesis (*i.e.* cellular anabolism - (Richter and Sonenberg, 2005)). Similarly, mTORC1 mediated phosphorylation of S6K6 supports mRNA translation via a mechanism involving subsequent phosphorylation of other protein substrates including programmed cell death 4 (PDCD4), eukaryotic initiation factor 4B (eIF4B) and eukaryotic elongation factor-2 kinase (eEF-2K) (Ma and Blenis 2009). Additionally, elevated levels of active mTORC1 signalling are known to mediate the facilitated translation of specific mRNA transcripts that contain so-called terminal oligopyrimidine (TOP-) motifs in their 5´untranslated region (5´UTR); transcripts that under reduced levels of mTORC1 signalling, capable of supporting general protein synthesis, remain refractory to translation (Thoreen *et al.*, 2012). Indeed, it has been shown that the translation of many ribosomal protein related mRNAs is regulated by TOP-motifs and other proximal cis-acting regulator sequence elements, in an apparent positively reinforcing feedforward mechanism (Hamilton *et al.*, 2006).

More recently, Fonseca *et al.* have demonstrated the phosphorylation of a third mTORC1-specific substrate called the La-related protein 1 (LARP1); via a direct interaction with the Raptor subunit. The authors show that after mTORC1 dependent phosphorylation, LARP1 can bind to 5´ TOP-motifs and suppress the hosting mRNA transcript's translation; in a mechanism involving the competition of phosphorylated LARP1 with the eukaryotic initiation factor 4G (eIF4G) for TOP-motif binding. The importance of LARP1 to regulating the translation of TOP-motif containing mRNAs was further demonstrated by the blunted effect of reduced translation of TOP-motif containing mRNAs caused by mTORC1 inhibition (using both Rapamycin and another pharmacological inhibitor, Torin1, or amino acid starvation), under conditions of experimentally reduced LARP1 expression (Fonseca *et al.*, 2015). Subsequent studies also confirm LARP1 as a major mTORC1 substrate and identify specific serine and threonine target

residues (up to 26); including S689 in the C-terminal DM15 domain, that when phosphorylated, mediate the association of LARP1 with the 5´UTR TOP-motif of the ribosomal protein RPS6 encoding mRNA (Fonseca *et al.*, 2018). Most, recently research by Fuentes and co-workers shows protein complexes including LARP1 can bind, and protect from degradation, specific TOP-motif containing mRNAs essential for protein synthesis. Consequently, they claimed that the identified mTOR-LARP1-5′UTR TOP-motif axis acts at the translational level as a primary guardian of cellular anabolic capacity (Fuentes *et al.*, 2021).

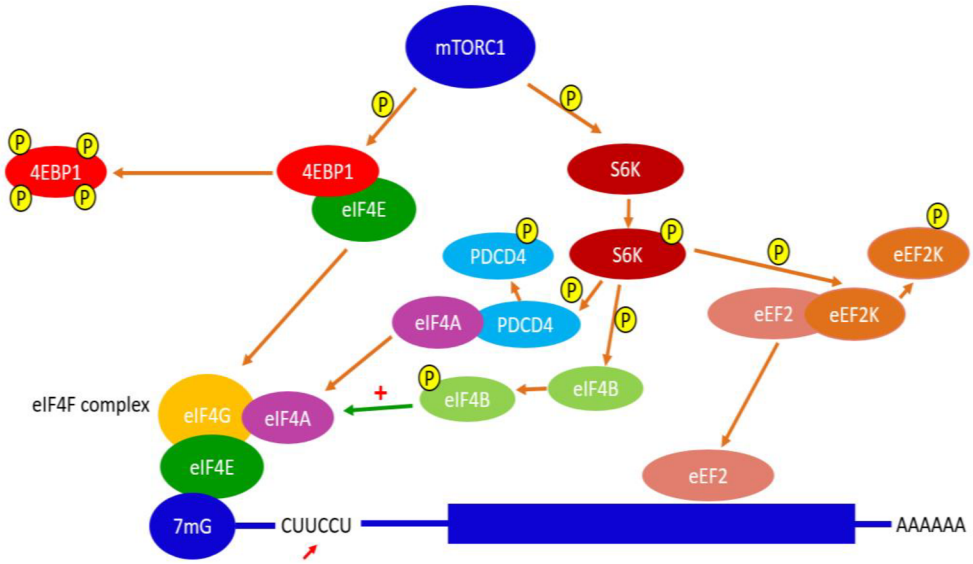

Fig. 6: mTORC1 translation regulatory cascade. mTORC1 phosphorylates two important substrates 4EBP1 and S6K1. mTORC1 dependent phosphorylation of 4EBP1 blocks its inhibitory interaction with eIF4E thus promoting enhanced levels of protein synthesis (via formation of the 7-mG-cap-binding complex, eIF4F). mTORC1 also catalyses phosphorylation of S6K1 and supports mRNA translation via a mechanism involving subsequent phosphorylation of the PDCD4, eIF4B, eEF2K.

1.2.1. mTOR in oocytes.

The activity and functioning of the mTOR pathway has been examined in mammalian (mostly murine) oocytes. Research by Severance and Latham has shown that inhibition of the PLK1 (Polo-like-kinase 1) signalling pathway disrupts meiotic spindle formation, chromosome congression and spindle-associated phospho-4EBP1 (a major mTORC1 substrate – see above) in both metaphase-I (MI) and MII arrested oocytes (Severance and Latham 2017). Against this backdrop, research by Jansova *et al.,* have confirmed that the main regulators of 4EBP1 phosphorylation in this context are indeed mTOR and cyclin

dependent kinase1 (CDK1), and not directly PLK1. Moreover, although they detected equal and homogenous expression levels of 4EBP1 and 4EBP1 phosphorylated on Thr37/46 in oocytes during meiosis I, they did observe an uneven distribution and localisation of other phospho-4EBP1 isoforms. For example phospho-4EBP1 phosphorylated on Ser65 was localised around the spindle whereas that phosphorylated on Thr70 was localised to the spindle itself. They also observed that, via a mechanism requiring phosphorylation and activation of mTOR, it is CDK1 that asserts 4EBP1 phosphorylation. Accordingly, mTOR and CDK1 were shown to be present on the meiotic spindle and to colocalise with 4EBP1 phosphorylated on Thr70 (Jansova *et al.*, 2017). Hence the activity of mTOR is closely bound with successful meiotic maturation of mouse oocytes.

The work of Heasman and Ridley has identified the small GTPases RHOA, RAC1 and CDC42 as key regulators of cell motility and actin cytoskeletal dynamics (Heasman and Ridley, 2008). During periods of cell motility and F-actin reorganisation (processes themselves under the regulation of mTORC1 mediated S6K1 and 4EBP1 pathways), the expression of such small GTPases is known to be mediated via mTORC2 (Zeng *et al.*, 2007). Indeed, it is also known that small GTPases themselves are an important downstream mTOR target substrates during cell growth. In the meiotically maturing mouse oocyte, the highly asymmetric cell division that leads to the formation of the first polar body (and the MII arrested oocyte) are known to rely on extensive remodelling of the actin cytoskeleton and the action of small GTPases. The work of Lee and colleagues has shown mTOR protein localises around the spindle proximal ooplasm. Moreover, that treatment with Rapamycin reduces mTOR expression (both at the mRNA and protein levels) and impairs cortical migration of the MI-spindle, blocks asymmetric cell division and polar body formation/extrusion and reduces mRNA expression of the small GTPases *Rhoa*, *Rac1* and *Cdc42* genes (Lee *et al.*, 2012). Additionally, research from the Susor laboratory demonstrates unique sensitivity of the translation of specific mRNAs containing 5´UTR TOP-motifs to the availability eIF4E and their role in ensuring appropriate chromosomal segregation and meiotic spindle positioning in the mouse oocyte (Susor *et al.*, 2015). Thus, in oocytes these studies collectively implicate the role

of an active mTOR pathway in the regulation of cytoplasmic dynamics that mechanistically underpin specialised, highly asymmetric, meiotic cell divisions.

Indeed, in other cell context, experimental evidence shows that protein synthesis and activity of GTPases RHOA, RAC1 and CDC42 can be inhibited by rapamycin and is associated with impaired cell motility(Liu *et al.*, 2010). Moreover, Sato and colleagues have shown that mTORC2 can also phosphorylate filamin A (an actin cross-linking protein, at serine 2152 (S2152)) and regulates its focal adhesion and cell migration (Sato *et al.*, 2016). Other research has demonstrated the deletion of the *Mtor* gene causes defective development of multiple cell layers, resulting as a tooth malformation and cystogenesis and proved mTOR regulated enamel organ development through via the mTORC1 pathway (Nie *et al.*, 2020). Thus, taken together with the above described evidence of mTOR regulation of cytoskeletal regulation on oocytes, such studies infer a possible role for similar roles underpinning the generation of the first inner and outer cell populations within the mouse embryo, following the 8- to 16-cell transition.

1.2.2. mTOR in mouse preimplantation embryos.

Several researchers have sought to clarify the role of mTOR in mouse preimplantation development. The findings of Bulut-Karslioglu *et al.,* have shown inhibition of mTOR can induce a reversible state of developmental diapause, when provided to early mouse blastocysts (E3.5 stage), and retain individual ICM residing blastomeres in a state of pluripotency; moreover, active mTOR also regulates developmental timing at the peri-implantation stage (Bulut-Karslioglu *et al.*, 2017). Reduced mTOR activity (confirmed by depleted levels of phospho-4EBP1 and SK61), in *in vitro* cultivated preimplantation mouse embryos deprived of growth media supplemented with amino acid, has been shown to cause developmental defects that can nevertheless be rescued by replenishment of exogenous amino acids (Zamfirescu, Day and Morris, 2021). Additionally, phenotypes associated with mouse preimplantation embryos heterozygotic or homozygotic for the disrupted *Mtor* gene have been reported; whereas, heterozygotes exhibit a normal developmental phenotype (despite a detected 50% reduction in mTOR protein expression and S6K1 phosphorylation/activity), homozygotes arrest development, shortly after uterine

implantation at E5.5 and show many abnormal developmental phenotypes (Gangloff *et al.*, 2004; Shor, Cavender and Harris, 2009).

1.2.3. mTOR and related signalling pathways.

It is appreciated that, in many diverse studied cell paradigms, mTOR is functionally connected to a spectrum of cellular signalling pathways (Fig. 7). For example, Kimura and colleagues identified a link with the AMPK (adenosine monophosphate activated protein kinase) pathway, involving the phosphorylation of S6K1 (Kimura *et al.*, 2003), whereas Tillu *et al.,* proved AMPK activation can directly cause inhibition of mTOR and even ERK1/2 kinases (Tillu *et al.*, 2012). Another associated mTOR pathway involves AKT (a serine/threonine protein kinase under the control of PI3Ks - phosphoinositide 3-kinases), as it has been demonstrated AKT activity is required in the signalling cascade that ultimately leads to phosphorylation of the mTORC1 substrate 4EBP1 (Gingras *et al.*, 1998). Also, research from our own laboratory has functionally associated p38-MAPK activity with activation of mTOR within the ICM cells of maturing mouse blastocysts (Thamodaran and Bruce, 2016; Bora *et al.*, 2019; Bora, Gahurova, Mašek, *et al.*, 2021). Specifically, that failed specification and differentiation of PrE (but not EPI) cells in the ICM of maturing blastocysts exposed to pharmacological inhibition of p38-MAPK can be partially rescued by induced activation of mTOR (Bora, Gahurova, Mašek, *et al.*, 2021).

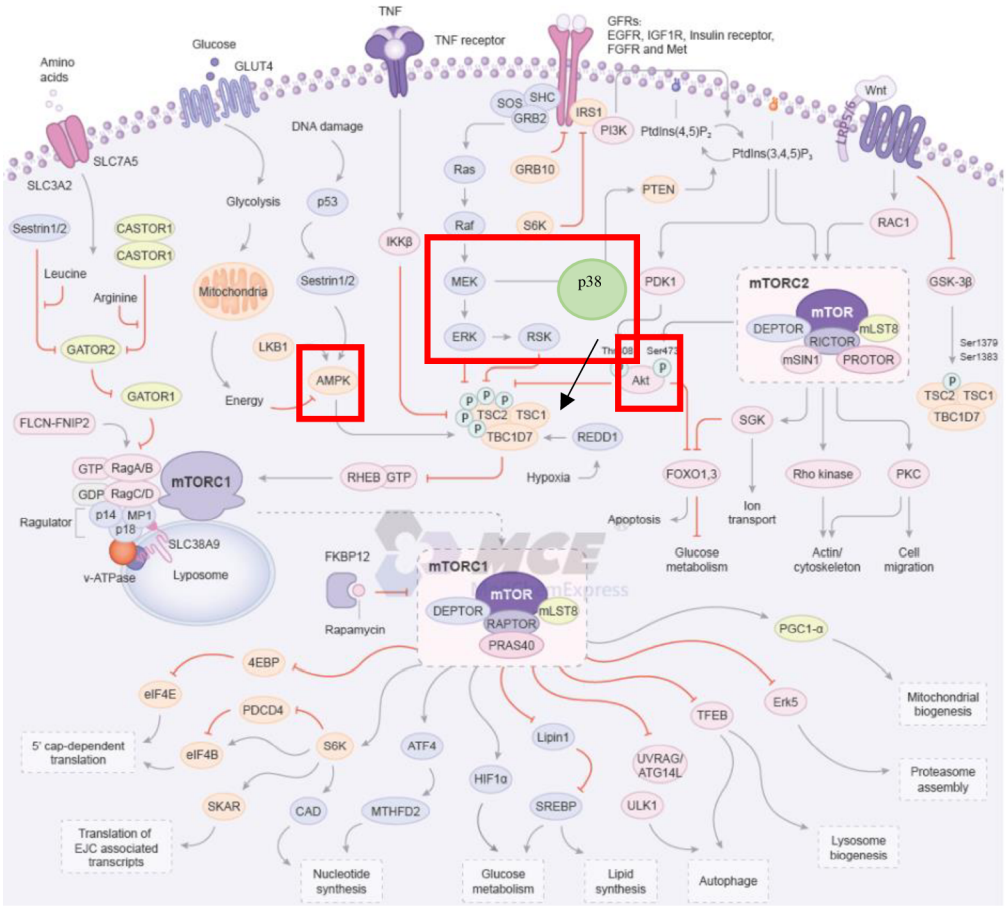

Fig. 7: Scheme of mTOR and related signalling pathways. Marked (red squares) are pathways of interest to this thesis. (https://www.medchemexpress.com/Targets/mTOR/mtor-signaling-pathway.html)

In our laboratory, we seek to further explore the role of active mTOR signalling, and potential regulation of protein translation, during the preimplantation stages of mouse embryo development and the derivation of the three blastocyst cell lineages. Accordingly, an on-going project in our group has been the investigation of the generation of the nascent inner cell founder populations under conditions with or without mTOR inhibition. This work was largely informed by observations in meiotically maturing mouse oocytes that showed the highly asymmetric cell division that segregate homologous chromosomes to generate the first polar body and the MII-arrested oocyte is under the control of active mTOR; whereby such divisions are blocked when oocytes are *in vitro* matured in the presence of mTOR inhibitors (*i.e.* Torin1 and/or Rapamycin) and also associated with impaired phosphorylation of the translational inhibitor protein

4EBP1 (that in its unphosphorylated state binds to the translation initiation factor EIF4E, preventing its association within the mRNA 7-methyl-guanosine-cap binding complex EIF4F needed to promote protein translation (Lee *et al.*, 2012)). Our unpublished observations show that, in mouse embryos, Torin1 mediated inhibition of mTOR shortly before and during the 8- to 16-cell transition is associated with the generation of statistically fewer inner cells by the mid-16 cell stage, compared to vehicle controls. However, this effect is restricted to the this first wave of inner cell internalisation and does not apply to the second wave, during the 16- to 32-cell transition (Bruce & Gahurova – *unpublished observations*). We hypothesise this phenotype of reduced numbers of primary ICM founder cells is predicated on translational regulation of key mRNA transcripts (potentially harbouring 5'UTR localised TOP-motifs) during this distinct cell-division associated window. Therefore, we set out to test the penetrance of the observed Torin1 mediated mTOR inhibition effects on cell number, in embryos containing blastomeres over-expressing 4EBP1 (or its non-phosphorylatable mutant – in which the four characterised mTOR target Serine/Threonine residues have been mutated to Alanine) or 4EIF4E. We predicted such over-expression would stoichiometrically provide enough excess EIF4F 7-methyl-guanosine-cap-binding translation initiation complex to facilitate the required translation of key mRNA transcripts and (partially) restore inner cell number by the mid-16-cell stage.

2. Goals of the thesis.

- To assess the effect on 16-cell embryos after inhibition of the mTOR pathway by the compound Rapamycin
- To determine which signalling pathways are upstream of mTOR in the context of early preimplantation embryonic development (and the generation of inner cells at the 16-cell stage)
- To determine whether mTOR plays a role in translational regulation in early preimplantation embryos (around the 8- to 16-cell stage transition)

3. Materials and Methods.

3.1. Preparation of 4EBP1, 4EBP1-4Ala and EIF4E protein encoding cDNA constructs.

The plasmid pRN3P, previously acquired in our laboratory, was used as a cloning vector. It consists of a multiple cloning site (MCS) containing recognition sites for several restriction enzymes – for experiments described below, the restriction sites for enzymes *BglII* and *BamHI* were used. MCS is flanked by sequences derived from the 5' and 3' untranslated regions (UTRs) of the *Xenopus laevis* beta-globin gene and provide high stability to any future derived mRNAs from cloned cDNA inserts (*i.e.* derived by *in vitro* transcription - IVT). Upstream a promoter sequence for the bacteriophage T3 RNA polymerase resides, that enables transcription (via IVT) of the UTRs and cloned cDNAs from a linearised plasmid template (by restriction enzyme digestion using the *SfiI* site downstream of the 3´UTR).

As a first step, *4ebp1*, *4ebp1-4Ala* (*4ebp1* with four serine and threonine sites mutated into alanine (T37A, T46A, S65A, T70A) to prevent phosphorylation at these positions) and *Eif4e* cDNA sequences (for *4ebp1* and *Eif4e* sequences were derived from mouse blastocyst cDNA, for *4ebp1-4Ala* rat cDNA was used) were cloned into pRN3P IVT plasmid vector, containing an ampicillin resistance (Amp^r) selection gene (Fig. 8). To generate *4ebp1*, *4ebp1-4Ala* and *Eif4e* cDNA inserts, polymerase chain reactions (PCR) utilising oligonucleotide primers (all used primers were purchased from Sigma Aldrich), incorporating specific restriction sites for appropriate plasmid cloning, were employed. The sense oligonucleotide primers also incorporated a sequence encoding a Haemagglutinin-epitope tag (HA-tag), to ensure future derived recombinant proteins would contain an amino-terminal epitope HA-tag allowing their discrimination from endogenous proteins. In the case of *4ebp1* and *Eif4e*, mouse blastocyst (E4.5) cDNA, previously generated in our laboratory, was used as a template, utilising specific sense and antisense primers; for *4ebp1* and *Eif4e*, primers pairs designated 446 & 445, in our internal archive, respectively were used – Table 1. Relating to generation of the *4ebp1-4Ala* cDNA sequence, the insert was PCR amplified from an obtained pre-existing plasmid clone, pCW57.1–4E-BP1–4Ala plasmid (Thoreen *et al.*, 2012), using a *4ebp1* primer pair designated 447, that was specific for the cloned rat, rather than mouse

sequence – Table 1. The high-fidelity PCR reaction composition, and cycling conditions, are summarised in Tables. 2 and 3, as informed by manufacturer's protocol (Pfusion – NEB).

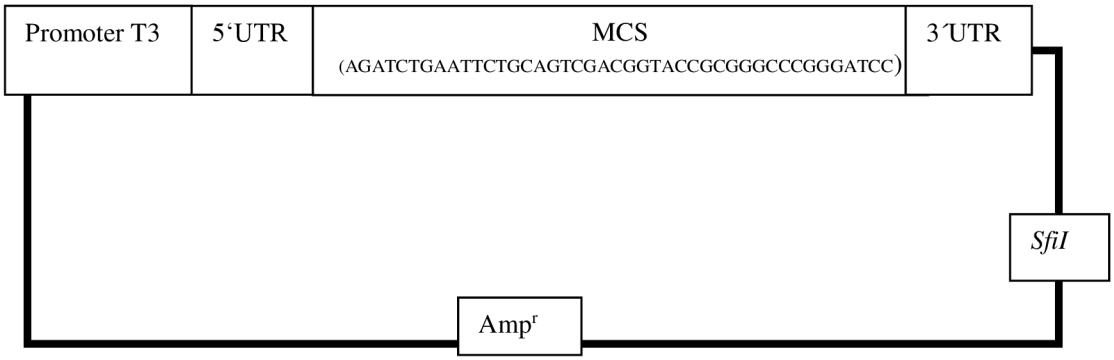

Fig. 8: Organisation of pRN3P plasmid, consisting of a bacteriophage T3 promoter sequence, 5´UTR from the frog-beta globin locus, a multiple cloning site, 3´UTR from the frog beta-globin locus, restriction site for *SfiI* enzyme and the sequence for an Ampicillin resistance selectable marker gene (Amp^r)

Tab. 1: Oligonucleotide PCR primers used for *4ebp1, 4ebp1-4Ala, Eif4e* cDNA construct generation.

Oligo-nucleotide primers 5'-3'	**Related insert**	**Sequence**
S 445	*Eif4e*	gactatAGATCTgccaccATGggctacccatacgatgttcctgactatgctGCGACTG TGGAACCG
A 445	*Eif4e*	gactatGGATCCTTAAACAACAAACCTATTTTTAGTGG
S 446	*4ebp1*	gactatAGATCTgccaccATGggctacccatacgatgttcctgactatgctTCGGCGG GCAGCAGC
A 446	*4ebp1*	gactatGGATCCTTAAATGTCCATCTCAAATTGTGACTCTTCAC
S 447	*4ebp1-4Ala*	gactatAGATCTgccaccATGggctacccatacgatgttcctgactatgctTCCGGGG GCAGCAGC
A 447	*4ebp1-4Ala*	gactatGGATCCTTAAATGTCCATCTCAAACTGTGACTCTTC

Numbers refer to our laboratory's archive nomenclature and complementarity to either sense (S) or anti-sense (A) strands.
Spacer – aids required restriction enzyme digest needed for insert cloning.
BglII site – introduced restriction enzyme site for insert cloning into pRN3P.
BamHI site – introduced restriction enzyme site for insert cloning into pRN3P.
Kozak sequence – aids translation of derived and microinjected recombinant mRNA.
Start codon.
HA tag – to permit immuno-staining of derived recombinant protein expression, after mRNA mouse embryo microinjection.

Tab. 2: PCR reaction composition for *4ebp1, 4ebp1-4Ala, Eif4e* cDNA insert generation.

Reagents	**Volume**
2x Master mix (Pfusion)	25 µl
DMSO	2 µl
Primer S 445/446/447 (10 µM)	2 µl
Primer A 445/446/447 (2 µM)	2 µl
Template (cDNA/plasmid – 30ng)	1 µl
Water	18 µl

Tab. 3: PCR reaction cycling conditions used for *4ebp1, 4ebp1-4Ala, Eif4e* cDNA insert generation**.**

Process	**Temperature (°C)**	**Duration**	
Initial Denaturation	96	1 m	
Denaturation	96	30 s	35x
Annealing	56	30 s	
Elongation	72	60 s	
Terminal Elongation	72	10 m	

The correct length of the generated PCR products was verified by electrophoresis of 2 µl aliquots, in 1% agarose and 0.5X TBE (Tris-Borate-EDTA) containing ethidium bromide stained gels and comparison with the migration of 1Kb+ standard markers (Carl Roth inc.). After verification, the remaining volumes of PCR product were purified using a QIAquick PCR purification kit (Qiagen), according to manufacturer's protocol, and the final eluate concentration was measured via Nanodrop-mediated UV spectroscopy.

The purified PCR-generated inserts (comprising cDNAs encoding HA-tagged mouse 4EBP1, rat 4EBP1-4Ala and mouse EIF4E proteins) and the recipient host plasmid vector (pRN3P) were then subject to double restriction enzyme digestion, using *BglII* and *BamHI* (following manufacturer's guidelines – NEB), thus, preparing cohesive ends for insert-plasmid ligation (the restriction digest reactions were assembled as described - Table 4). Assembled and thoroughly mixed reactions were incubated for 3 hours at 37°C (in a water bath) and then heat killed by a 2 minute incubation at 96°C on a heat block (and pulse spun in a microfuge).

Tab. 4: Double restriction enzyme digestion reaction of *4ebp1, 4ebp1-4Ala, Eif4e* cDNA PCR product inserts and pRN3P plasmid.

Reaction composition for PCR products		**Reaction composition for pRN3P plasmid**	
NEBuffer 3.1	5 µl	NEBuffer 3.1	5 µl
PCR product (from reaction in Tab. 2)	33 µl	pRN3P plasmid (5.0 µg)	13 µl
Water	10 µl	Water	30 µl
BglII (10 units)	1 µl	*BglII* (10 units)	1 µl
BamHI (10 units)	1 µl	*BamHI* (10 units)	1 µl

Following the restriction digestion, successful linearisation of pRN3P plasmid was verified by 1% gel agarose electrophoresis (as described above for PCR generated inserts) and the remaining digested (confirmed linearised) plasmid was then purified using a QIAquick PCR purification kit (Qiagen), according to the manufacturer instructions, followed by an alkaline phosphatase (NEB) treatment to prevent future self-ligation (as informed by manufacturers guidelines). The composition of the alkaline phosphatase reaction is given - Table 5), and the sample was incubated for one hour at 37°C, heat treated at 96°C for 2 minutes and pulse spun.

Tab. 5: Alkaline (Alk.) phosphatase treatment of pRN3P plasmid.

Reagents	**Volume**
10x buffer	5 µl
Linearised (*BglII* & *BamHI*) pRN3P plasmid (~1.5 µg)	20 µl
Water	22 µl
Alk. phosphatase	3 µl

To both the *BglII* and *BamHI* treated alkaline phosphatase treated linearised pRN3P plasmid and PCR generated cDNA encoding insert DNAs, an organic phenol-chloroform extraction was performed. Firstly, individual total sample volumes were increased to 300 µl by the addition of HPLC-grade water, to which 300 µl of Tris-HCl saturated phenol:chloroform mixture (Sigma Aldrich – Merck, pH 8.0) was added and thoroughly mixed in a 1.5 ml Eppendorf tube on a vortex machine. The mixed samples were then centrifuged for 5 minutes at 16000g in a bench top microfuge and the upper aqueous phase transferred into a new 1.5 ml Eppendorf tube and an equal volume of chloroform added. The samples were again subject to an identical round of vortex mixing and centrifugation, the upper phase transferred into new Eppendorf tube and combined with 3M NaAC (sodium acetate - 10% of sample volume), 100%

ethanol (250% of sample volume) and 2 µl of glycogen (ThermoFisher Scientific). The vortexed mixtures were then incubated overnight at -20°C to permit precipitation of the restriction enzyme linearised/prepared pRN3P plasmid vector and DNA inserts, respectively. The next day the samples were centrifuged at 16000g, at 4°C for 30 minutes; to pellet the precipitated DNA (and the inert carrier glycogen facilitating DNA precipitation and pelleting). The supernatant was removed and the pellets were washed by the addition of 750 µl of 70% ethanol and repeated chilled centrifugation (4°C) at 16000g, for 10 minutes. Following removal of the supernatant, the pellets were air-dried and dissolved in 12 µl of nuclease-free water. 1 µl of each sample were then used for UV-spectroscopy based (Nanodrop) measurement of purified restriction enzyme digested plasmid/insert DNA concentration.

The now purified plasmid and insert restriction digests were then appropriately combined for subsequent ligation (using T4 DNA ligase (Roche Diagnostics)), in a composition described in Table 6. Note, a control condition was prepared that lacked the addition of any DNA insert to measure the background frequency of vector self-ligation/carried over undigested pRN3P plasmid vector DNA, thus enabling an indication of the success of cDNA insert to vector ligation success (by comparison of the number of colonies on experimental and control ligation plates after transformation – *i.e.* there should be significantly more colonies on the experimental versus vector alone control plates).

Tab. 6: *4ebp1, 4ebp1-4Ala, Eif4e* cDNA PCR product inserts and pRN3P ligation reactions.

+insert		**-insert (control)**	
Reagents	**Volume**	**Reagents**	**Volume**
10x buffer	2 µl	10x buffer	2 µl
BglII/BamHI digested plasmid vector (pRN3P)	50 ng	Vector	50 ng
BglII/BamHI digested PCR insert (*4ebp1, 4ebp1-4Ala, Eif4e*)	20/40 ng		
Water	To 20 µl	Water	To 20 µl
T4 DNA ligase	1 µl	T4 DNA ligase	1 µl

The reactions mixtures were assembled at room temperature (to prevent precipitation of the reaction buffer) until the final addition of the T4 DNA ligase, which was performed on ice. The samples then were incubated at 4°C for 6-8 hours. Each ligation product (both samples +insert and negative control sample without insert) were then transformed into chemically competent DH5α *E-coli*

bacteria. Thus, 5 µl of ligation mix was combined and mixed with 45 µl of DH5α competent cells, incubated on ice for 30 minutes, then heat shocked for 90 seconds at 42°C (in a prepared water bath) and placed back on ice for a further 10 minutes. To each sample, 250 µl of pre-warmed (37°C) Lysogeny broth (LB) was added, mixed and incubated for 30 minutes at 37°C on a 1.5 ml Eppendorf tube heated shaker (300 r.p.m.; thus allowing successfully transformed bacterial cells to express the Amp^r gene). Following brief centrifugation in a bench top microfuge, the bacterial pellets were resuspended in the residual volume of LB broth and spread over LB agar (containing the antibiotic ampicillin – 100 µg/ml) Petri dishes were placed at 37°C for 12-20 hours. A selection of the supernumerary colonies from experimental (+insert) plates, when compared to the negative control plate (*i.e.* following transformation of ligation mix lacking the inert), were selected and individually streaked over new LB ampicillin containing agar plates and again incubated at 37°C for 12-20 hours.

Next colony PCR was performed to identify colonies containing pRN3P plasmid vector with the desired inserts ligated, as follows. First, PCR template samples were prepared from streaked bacterial colonies by transferring a small amount of bacteria on the end of a pipette tip into 100 µl of HPLC grade water, mixing, incubating in a PCR tube/block at 96°C for 20 minutes and then placing on ice for 20 minutes (thus, lysing the bacterial cells and liberating the potential plasmid DNA templates into solution). Such template preparations (1 µl - plus water only negative controls) were then combined with 4 µl of DreamTaq PCR Master Mix (ThermoFisher Scientific) and oligonucleotide primers specifically designed to amplify only the correctly cloned inserts (*i.e.* comprising sense primers complementary to the vector encoded T3 RNA polymerase promoter and the antisense primers specific to the relevant insert itself, as originally used to derive the insert – as described in Table 1) to a total volume of 5 µl. The composition of the prepared PCR master mixes are shown in Table 7 and these were subject to the PCR thermal cycling, as described in Table 8.

Tab. 7: *4ebp1, 4ebp1-4Ala, Eif4e* insert/pRN3P ligation specific colony PCR master mix compositions (*i.e.* enough for x9, 4 µl aliquots per reaction).

Reagents	**Volume**
2x DreamTaq PCR Master Mix	22.5 µl
Primer T3 (10 µM) – GCAATTAACCCTCACTAAAGG	2 µl
Primer A (10 µM) – insert specific (445,446,447)	2 µl
Water	9.5 µl

Tab. 8: PCR cycling program used for colony PCR reactions.

Process	Temperature (°C)	Duration	
Initial Denaturation	98	1 m	
Denaturation	98	30 s	35x
Annealing	58	30 s	
Elongation	72	60 s	
Terminal Elongation	72	30 m	

The presence/absence of a PCR product (indicative of successful or unsuccessful cloning) was verified by 1% agarose gel electrophoresis (as described above). Accordingly, plasmids from positive clones (in which a PCR product DNA of the anticipated length was generated) were isolated, after inoculation of 4 ml liquid LB broth cultures (+ampicillin; 100 μg/ml), using QIAprep Spin Miniprep Kits (Qiagen), according to the manufacturer instructions. The concentrations of the purified plasmids were then measured by UV spectroscopy on a Nanodrop and final confirmation and sequence verification of the inserted PCR product was determined by out-sourced Sanger DNA sequencing. Similarly, long-term live bacterial -80^{o}C glycerol stocks were also prepared for our laboratory archive.

3.2. Synthesis of *in vitro* transcription (IVT) derived recombinant mRNAs encoding 4EBP1, 4EBP1-4Ala and EIF4E from inserts successfully cloned into pRN3P plasmid vector.

Purified pRN3P plasmids confirmed to contain the required HA-tagged 4EBP1, 4EBP1-4Ala and EIF4E encoding cDNA inserts, were subject to linearisation using the atypical restriction enzyme *SfiI* (the restriction site for which is not present in any insert and is found in one copy downstream of the 3' frog-globin UTR of the cloned plasmids – see figure 8). Such linearisation is a pre-requisite for IVT to ensure derived mRNAs are all of the same length and plasmid backbone sequence is not transcribed. The *SfiI* linearisation reactions were prepared as shown (Table 9). using manufacturer's guidelines (NEB) and incubated for 6 hours at 50°C (in a water bath).

Tab. 9: *SfiI* linearisation of pRN3P vector containing *4ebp1, 4ebp1-4Ala, Eif4e* cDNA inserts.

Reagents	**Volume**
CutSmart buffer	5 µl
Sfi I restriction enzyme (40 units)	2 µl
Relevant plasmid (5.0 µg)	x µl
Water	To 50 µl

Post-*SfiI* digestion (after first confirming successful linearisation on a 1% agarose gel – as previously described), individual reactions were then subject to TRIS-saturated phenol-chloroform organic extraction and ethanol precipitation, as described above, and the purified linearised plasmid was quantified (Nanodrop).

The confirmed linearised plasmid DNAs (~5 µg per reaction) were then subject to IVT utilising the upstream vector encoded bacteriophage T3 RNA polymerase sequence (present in pRN3P vector backbone see figure 8) and the mMessage mMachine T3 Transcription Kit (Invitrogen), strictly observing the manufacturer provided instructions. The concentration and purity of the derived recombinant mRNAs were confirmed using the Nanodrop and their approximate size and integrity checked by electrophoresis on a 1% agarose gel (under ordinary, not denatured conditions).

3.3. Mouse preimplantation stage embryo collection and cultivation.

The first step was the superovulation of 8-week old F1 hybrid (C57Bl6♀×♂CBA/W) female mice by two successive intraperitoneal injections of reproductive hormones (this regime ensures the maximal possible number of recovered embryos per individual female mouse – helping to reduce the number of mice sacrificed per experiment). Accordingly, F1 female mice were first injected with 7.5IU of pregnant mare serum gonadotrophin extract (PMSG; Sigma Aldrich). After 48 hours a second injection of 7.5IU of recombinant human chorionic gonadotrophic hormone (hCG; Sigma Aldrich) was administered and the females were immediately placed with F1 stud males mice for overnight mating (no more than two females per stud). Successful mating was confirmed by the presence of a vaginal sperm plug and females were then separated from studs until the desired stage of preimplantation embryo collection. On the day of embryo recovery, dissection plates containing M2 medium

(prepared in-house, from the recipe described in Table 10) and washing plates containing 10 µl drops of M2 media over-laid with mineral oil were prepared and equilibrated at 37°C. Additionally, mineral oil over-laid drop culture plates of KSOM medium (Embryo-Max; Millipore) were also prepared and similarly equilibrated in an incubator at 37°C in a 5% CO_2 containing atmosphere. Such preparations were made at least two hours prior to sacrificing pregnant F1 females for embryo recovery. Preimplantation stage embryos were then recovered at the desired developmental stage (most typically at the 2-cell/E1.5 stage – 42-44 hours post hCG injection) from dissected oviducts in M2 media. At this point they could either then be microinjected (in single blastomeres – see below) or directly transferred to KSOM containing culture plates, where they were again serially washed through a series of KSOM drops (to remove trace amounts of M2 media). The plates containing the KSOM washed embryos were then transferred to the incubator (37°C in a 5% CO_2) for *in vitro* culture to the required developmental stage (as would also be the case after successful microinjection).

Tab. 10: Composition of M2 medium.

Medium	**Volume**	**Ingredients**	**g/100ml**
A(10x)	10ml	NaCl	5.534
		KCl	0.356
		KH_2PO_4	0.162
		$MgSO_4x7H_2O$	0.293
		Na-Lactate 60% sirup	3.2
		Glucose	1
		Penicillin	0.06
		Streptomycin	0.05
B(10x)	1.6ml	$NaHCO_3$	2.101
		Phenol Red	0.01
C(100x)	1ml	Na pyruvate	3.6
D(100x)	1ml	$CaCl_2x2H_2O$	2.52
E(10x)	8.4ml	HEPES	5.958
F	400mg	BSA	
G	78ml	H2O	

3.4. Preimplantation mouse embryo microinjections (*e.g.* recombinant IVT-derived mRNAs).

Microinjection of IVT-derived (see above) HA-tagged recombinant *4ebp1*, *4ebp1-4Ala* and *Eif4e* (derived from pRN3P plasmid clone) encoding mRNAs was performed by a Ph.D. student laboratory colleague (Pablo Bora); using routine laboratory techniques. Individual 2-cell stage mouse embryos were microinjected into one blastomere with a final concentration of candidate gene mRNA of 200 ng/µl. Simultaneously, recombinant mRNA for a routinely utilised Venus-histone-H2B fusion protein reporter (final concentration 60 ng/µl) or rhodamine dextran beads (diluted 1:5) was also microinjected in the same microinjection mixture to provide a marker of successful microinjection and to enable the clonal distribution of the progeny of the microinjected cell to be identified, as development progressed.

3.5. Pharmacological/chemical inhibition of cultured preimplantation stage mouse embryos.

Experiments exposing developing mouse preimplantation stage embryos in culture to different chemical inhibitors or activators, specific to varied signalling pathways were performed as follows. Recovered 2-cell (E1.5) stage embryos were cultured in KSOM (37°C and 5% CO_2) until the 8-cell stage (specifically, E2.5+4 hours). At this point (~4 pm) the experimental group of embryos were transferred into pre-equilibrated KSOM drop culture plates containing the appropriate concentration of inhibitor/activator, whereas the control group were transferred into drops containing only the vehicle control (v/v), DMSO (Sigma). In the case of the inhibitor LB100, which is not soluble in DMSO, the vehicle control (v/v) consisted of water. Transferred embryos were cultivated in the incubator (37°C and 5% CO_2) until the late 16-cell stage (E3.0+5 hours) and processed/fixed for further phenotypic analyses. The utilised chemical inhibitors and activators (and the pathways they target) and the relevant concentrations employed are summarised in Table 11.

The same inhibition procedure, with Torin1, was also used for embryos microinjected with recombinant *Eif4e* mRNA.

Tab. 11: Summary of chemical inhibitors and activators (and combinations thereof), and the concentrations employed, utilised in this study.

Chemical	Targeted signalling pathway (protein)	Pharmacological effect	Concentration used	Supplier
Torin1	mTOR	inhibitor	20µM	Selleckchem
Rapamycin	mTOR	inhibitor	5µM	VWR
GSK621	AMPK	activator	20 µM	Selleckchem
Roscovitine	CDK1	inhibitor	20µM	Selleckchem
LJH685	RSK	inhibitor	20µM	Selleckchem
LB100	PP2A	inhibitor	20µM	Selleckchem
BI2536	PLK1	inhibitor	20µM;10µM;1,25µM	Selleckchem
PD0325901	MEK1/2	inhibitor	1µM	Sigma Aldrich
SB220025	p38	inhibitor	20µM	Calbiochem, Millipore
SB220025+ MYH 1485	p38+mTOR	inhibitor+activator	20µM each	Calbiochem,Millipore +Selleckchem
GSK690693	AKT	inhibitor	10µM	Selleckchem
SU5402	FGFR	inhibitor	10 µM	Calbiochem, Millipore

3.6. Preimplantation stage mouse embryo fixation and (immuno-fluorescent) staining.

3.6.1. Pharmacologically treated embryos.

Pharmacologically treated embryos at the late 16-cell stage (E3.0+5 hours) were washed in Tyrode's solution (Sigma) to remove the *zona pellucida*. Embryos were then fixed for 20 minutes in prewarmed (37°C) 4% paraformaldehyde (PFA) (Santa Cruz Biotechnology) in a 96-well plate, at room temperature (RT). Fixed embryos were then subject to three RT washing steps in a 0.15% Tween-20 solution diluted with phosphate buffered saline (PBST); entailing individual 20 minute incubations. Fixed embryo membranes were then permeabilised (if they were to be processed for immuno-fluorescent staining – see below) by the incubation in 0.5% Triton-X100 (Sigma-Aldrich) for 20 minutes (RT), followed by three additional 20 minute washing steps in PBST (RT). Embryo blastomere cortical F-actin was then fluorescently stained by a 30 minute incubation (RT) in Oregon-green^{488nm} conjugated Phalloidin (ThermoFisher Scientific), followed by three 20 minute washing steps (RT) in PBST. In a final step, embryos were incubated for 15 minutes (RT) in pure Vectashield (Vector) containing DAPI, to enhance the fluorescent signal and stain the DNA (for subsequent confocal microscopy).

3.6.2. Microinjected embryos.

The employed protocol for fixing and staining microinjected embryos was very similar to that described above for pharmacologically inhibited embryos. The only difference was Rhodamine conjugated Phalloidin (ThermoFisher Scientific) was used instead of Oregon green^{488nm} Phalloidin. In some experiments, the translation of recombinant proteins derived from microinjected recombinant mRNA transcripts (*e.g.* relating to *4ebp1, 4ebp1-4Ala* and mRNAs) was confirmed by antibody mediated immuno-fluorescent staining, targeting the incorporated HA-tag, using the protocol described below.

3.7. Embryo immuno-fluorescent staining (to detect the expression of specific proteins).

The fixation, washing, membrane permeabilization and second washing steps were exactly as described above for pharmacologically treated/microinjected embryos. However, after the second round of PBST washes, a 30 minute incubation (4^{o}C) in 3% bovine serum albumin-PBST (BSA) (Sigma-Aldrich) was included (in order to block nonspecific epitopes). Primary antibody staining, using anti-sera specific for the assayed endogenous mouse 4EBP1 and LARP1 proteins, was performed by diluting the rabbit anti-phospho-4EBP1-T36 (Abcam, ab47365, at 1:100 or 1:200) or rabbit anti-LARP1 (Abcam, ab229164, at 1:100) in BSA and incubation at 4^{o}C overnight. In the case of embryos microinjected with mRNAs encoding HA-tagged recombinant proteins a rat anti-HA primary antibody (Sigma Aldrich), diluted at 1:100 in 4% BSA was used. The following day the embryos were washed through three 20 minute (RT) PBST washing wells, followed by a further 30 minutes (RT) blocking incubation in 3% BSA. Embryos were then transferred into a well containing either a donkey anti-rabbit IgG secondary antibody conjugated to Alexa^{488nm} (Abcam, ab150073 at a dilution 1:500 in BSA) for the immuno-staining of LARP1 and phospho-4EBP1-T36, or goat anti-rat IgG Alexa^{555nm} (Abcam, ab150158 diluted to 1:500 in BSA) for detection of recombinant HA-epitope protein expression. Such secondary antibody staining was performed at 4°C for 1 hour, before the embryos were processed through three 20 minute (RT) PBST washes and finally counter-stained with DAPI-containing Vectashield, as described above.

3.8. Preimplantation mouse embryo confocal microscopy.

Fixed (immuno-) fluorescently stained embryos were moved into PBST drops on a glass (microscope cover-slip) bottomed culture plate. Image acquisition was performed on an inverted confocal microscope (Olympus FLUOVIEW FV10i), employing laser excitation and emission wavelength settings corresponding to detection of Oregon green Phalloidin, Rhodamine phalloidin, DAPI, Alexa^{488nm} and Alexa^{555nm} as appropriate. Each embryo was scanned in a complete series of z-sections through the whole embryo (with a step-size of 2µm). Optimised (non-saturated) image settings (regarding laser output, detector gain and captured image resolution/quality) were adjusted and kept constant for all scanned embryos in both experimental and control conditions.

3.9. Preimplantation mouse embryo confocal micrograph image analyses (cell counting).

Acquired embryo images were analysed using FV10-ASW 4.2 Viewer (Olympus) and IMARIS software (BitPlane) and all z-sections per embryo were analysed to distinguish and quantify three distinct types of cells: **i.** outer cells that have an apparent contactless outer (apical) membrane, **ii.** inner cells that are completely surrounded by other cells and are allocated to the encapsulated inside compartment (*i.e.* do not comprise any outer/apical membrane), and **iii.** so-called "SAD" (short-hand for "Small Apical Domain") cells that almost entirely reside within the embryo but nevertheless retain a minimal outer membrane surface/contact (example micrographs of the three classifications are provided in Fig. 9). For quantification of detected fluorescence in immuno-fluorescently stained embryos the freeware program Fiji (NIH) was utilised; where the quantification unit *CTCF* = Integrated Density – (Area of selected cell x Mean fluorescence *of* background).

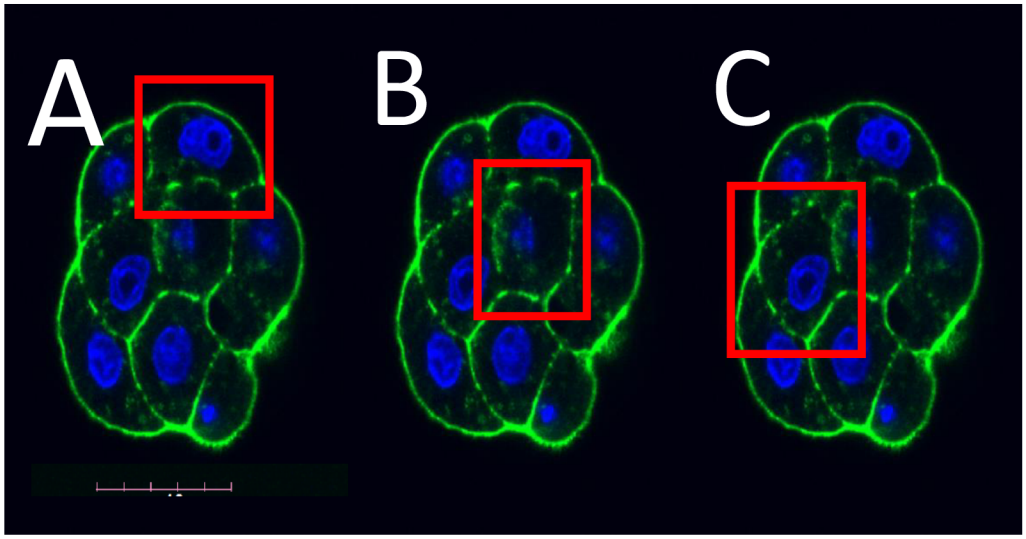

Fig. 9: The three designated categories of preimplantation mouse embryo blastomeres/cells (typically at the 16-cell stage), as revealed by confocal microscopy, and quantified in our analyses. Illustrative, single z-section confocal micrographs, exemplifying: A – an outer cell, B – an inner cell, C – a designated SAD ("Small Apical Domain") cell. Note, cortical F-actin staining using Oregon-green phalloidin (green) is used to distinguish cell type designations and DAPI (blue) counterstain marks cell nuclei. Scale bar = 40 μm

3.10. Preimplantation mouse embryo cell counting; data analysis.

For pharmacologically treated, microinjected and immuno-fluorescent embryos a Shapiro-Wilk test (to ascertain normality in each data set) was initially applied. If the data distribution was not normal (p-value < 0.05) in at least one of the datasets we wanted to compare, a Mann-Whitney U test was used to compare the datasets. If the data distribution was normal (p-value > 0.05), F-tests were used to measure variance of the two datasets. Depending on the F-test outcome, datasets were compared by t-tests specifying equal or unequal variance in the parameters. The following p-value significance cut-offs were employed. ≥ 0.05 – not significant, <0.05 – significant (*), ≤ 0.005– very significant (**) and ≤ 0.0005 – extremely significant (***). For microinjected and immuno-fluorescent embryos the graphical output detailing the quantified immuno-fluorescence as a correlate of protein expression were performed in the program R (as per the following code) - `boxplot(data=larp1,value~cat, col = "white")`

```
> stripchart(value ~ cat, data = larp1, method = "jitter", pch
= 19, col = c("grey","orange"), vertical = TRUE, add = TRUE)
```

4. Results.

4.1. Assaying the generation of inner cells in embryos under conditions of specific pathway pharmacological inhibition/activation.

As introduced above, unpublished observations from our laboratory show pharmacological inhibition of mTOR, using Torin1, in embryos transiting the 8- to 16-cell stage, is associated with a statistically significant reduction of generated mid-/late-16-cell stage inner cells versus vehicle controls. Therefore, the first task was to confirm the Torin1 obtained results and observe if a phenocopy could be obtained using the alternative mTOR inhibitor Rapamycin (that should only inhibit mTOR as part of mTORC1). Additionally, a selection of several other inhibitors and activators, known from the literature to be functionally connected with mTORC1 (see Tables 11 & 12), were also assayed in this same developmental time window and their effect on the generation of inner cells recorded.

Tab. 12: Summary of chemical inhibitors and activators (and combinations thereof) utilised (during the 8- to 16-cell mouse embryo transition) in this study.

Inhibitor/Activator	Targeted signalling pathway (protein)	Pharmacological effect
Torin1	mTOR	inhibitor
Rapamycin	mTOR	inhibitor
GSK621	AMPK	activator
Roscovitine	CDK1	inhibitor
LJH685	RSK	inhibitor
LB100	PP2A	inhibitor
BI2536	PLK1	inhibitor
PD0325901	MEK1/2	inhibitor
SB220025	p38-MAPK	inhibitor
SB220025+MYH 1485	p38-MAPK+mTOR	inhibitor+activator
GSK690693	AKT	inhibitor
SU5402	FGFR	inhibitor

Accordingly, 2-cell (E1.5) stage mouse embryos were cultured until the 8-cell stage (specifically, E2.5+4 hours). At this point, they were transferred into culture plate media drops containing the relevant inhibitor/activator (or combination thereof) and the control group were transferred into drops containing DMSO or water (depending on the inhibitor/activator), as a vehicle control (v/v). Transferred embryos were the cultivated in the incubator until the late 16-cell stage (E3.0+5 hours). At this stage, only embryos comprising exactly 16-cell were analysed to distinguish and quantify three distinct types of blastomere: outer cells having an apparent outer and cell contactless apical membrane, cells we

designate with the acronym "SAD" that are largely inside the embryo but still retain very small outer membrane contacts and inner cells completely located inside of the embryo (*i.e.* no outer membrane); real examples of all three cell designations is provided in the Materials and Methods (Fig. 9). All experiments have an extra supplementary table showing numbers of concrete embryos which were used for analysis.

Concentrating on the data generated with the alternative mTOR inhibitor Rapamycin first, a clear effect on the generation of inner cells during 8- to 16-cell transition was observed (Fig. 10). In the control embryo group the average number of inner cells generated was 1.82±0.16 whereas this was 0.91± 0.16 in the Rapamycin mTOR inhibited embryos (p-value of 1.8E-04) but there were no significant differences in the number of SAD cells generated. There is a supplementary table with extra and comprehensive experimental information (Suppl. Tab. 1)

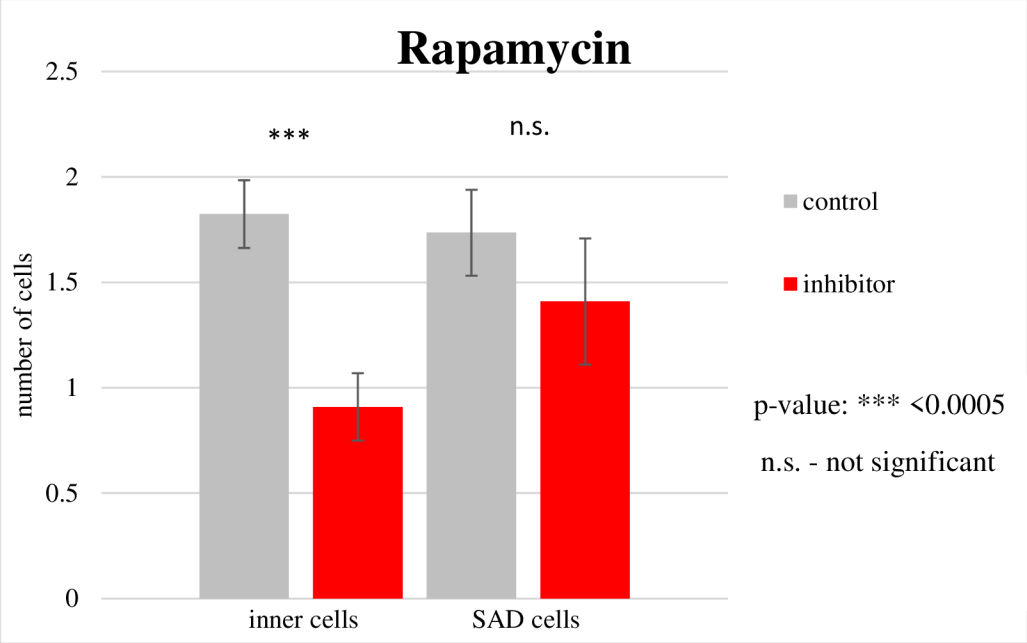

Fig. 10: Analysis of the average frequency of generated inner and SAD cells in 16-cell (E3.0+5 hours) mouse embryos after mTOR inhibition by Rapamycin (from E2.5+4 hours). Error bars are indicative of the standard error of the mean.

The obtained Rapamycin related results are in agreement with our previously observed data regarding reduced inner cell generation in 16-cell stage embryos obtained using the alternative mTOR inhibitor Torin1 (Bruce & Gahurova – *unpublished observations* - Fig. 11). Moreover, as Rapamycin selectively inhibits

the enzymatic activity of mTOR in mTORC1, the combined results suggest Torin1 induced phenotypes are also exclusively mediated via mTORC1 without an input from mTORC2. Hence, the data place mTORC1 mediated enzymatic activity during the 8- to 16-cell transition as a regulator of initial inner cell generation, relevant to the first cell fate decision, in mouse embryos.

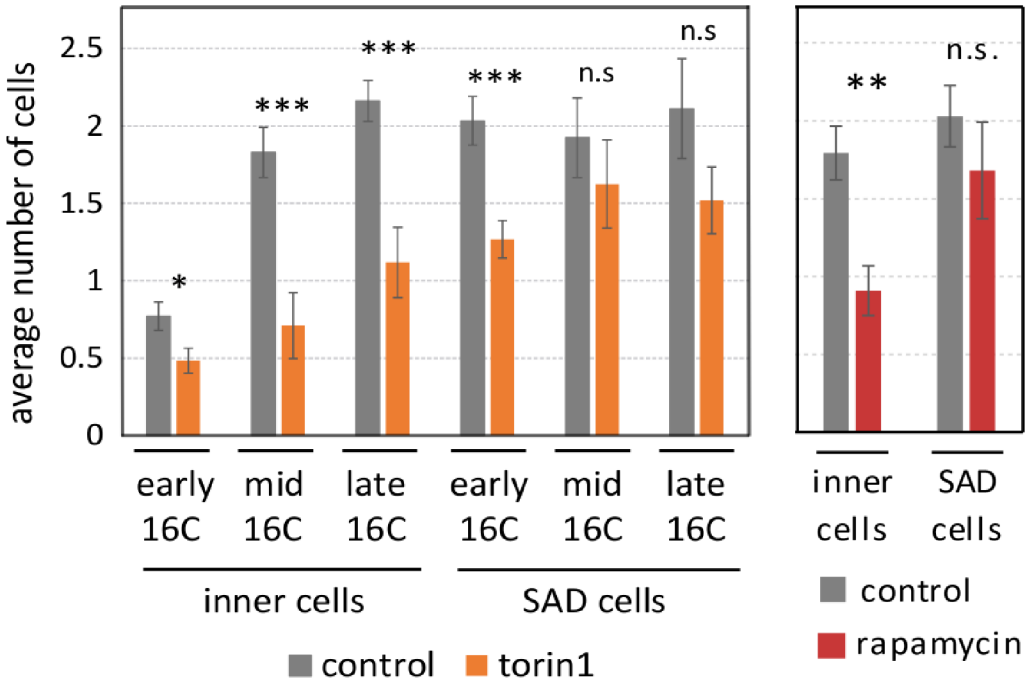

Fig.11: Analysis of Torin1 experiment (Bruce & Gahurova – *unpublished observations*) in comparison to Rapamycin results (Fig.10). Analysis of the average frequency of generated inner and SAD cells in early (E3.0), mid (E3.0+3 hours) and late (E3.0+5 hours) 16-cell mouse embryos after mTOR inhibition by Torin1 (from E2.5+4 hours). Error bars are indicative of the standard error of the mean.

In an attempt to mechanistically dissect the confirmed mTORC1 inhibition mediated inner cell phenotypes further, similar experiments utilising small chemical inhibitors/activator of several pathways, related or connected to mTORC1 (described in the theoretical section above) were conducted and similar phenotypes affecting inner cell generation at the late-16-cell stage assayed for (Fig. 12).

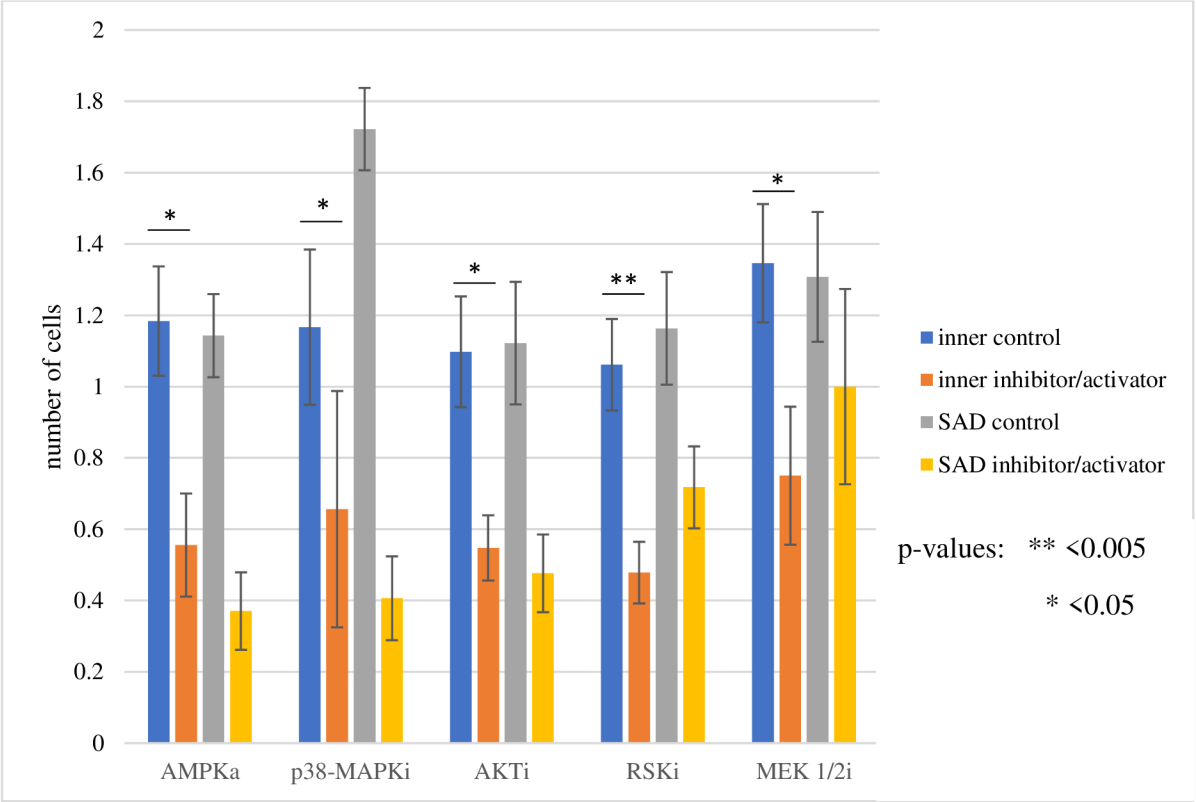

Fig. 12: Analysis of inner control vs inner inhibited/activated cells and SAD control vs SAD inhibited/activated cells in 16-cell (E3.0+5 hours) mouse embryos after inhibition (i)/activation (a) (from E2.5+4 hours) of AMPK, p38-MAPK, AKT, RSK, MEK 1/2 pathways. Error bars are indicative of the standard error of the mean.

Across the following individual conditions (from Table 11), targeting the AMPK (activation), p38-MAPK (inhibition), AKT (inhibition), RSK (inhibition) and MEK1/2 (inhibition – targeting upstream activating kinases of the ERK1/2 family of MAPKs), statistically significant decreases in inner cell numbers were observed in late 16-cell stage embryos, versus their appropriate control condition. Unlike mTORC1 mediated inhibition by Rapamycin (*see above* Figs. 10, 11) all conditions (with the exception of MEK1/2 inhibition) also caused reductions in the number of SAD cells generated.

Specifically, under AMPK activation conditions the average number of inner cells was 0.56± 0.14 compared to 1.18± 0.15 in the control group (p-value equals 8.961E-03) and the average of SAD cells was 0.37± 0.11 and 1.14± 0.12 (p-value equals 4.278E-05) respectively. Other data relevant to the generation of the AMPK activation related data is given in the supplementary information table (Suppl. Tab. 2).

The results relating to p38-MAPK inhibition, specifically reveal a reduction in the average number of inner cells, comprising 0.66±0.12 versus 1.17±0.22 under control conditions (p-value equals, 9.534E-03). The average of SAD cells was also reduced from 1.72±0.33 in control embryos to 0.41±0.12 under p38-MAPK inhibited cultures (p-value equals, 2.082E-04). The related subsidiary data relating to the p38-MAPK inhibition, and appropriate control conditions, is given in the supplementary information table (Suppl. Tab. 3).

In the experiments relating to inhibition of the AKT pathway, the concentration of chemical inhibitor GSK690693, was reduced to 10 µM (from that suggested by literature precedent and the manufacturer's guidelines) because 35% of embryos in the original experiments (utilising a concentration of 20 µM) developmentally arrested at the 8-cell. However, even at this revised concentration AKT inhibition caused a statistically significant and marked reduction in the average number of inner cells, numbering only 0.55±0.09 versus 1.1±0.16 in the appropriate control embryo group (p-value equals 7.891E-03), as well as SAD cells; numbering 0.48±0.11 compared to 1.12±0.17 (p-value equals, 3.265E-03), respectively. Other AKT inhibition related experimental details/data are given in the supplementary information table (Suppl. Tab. 4).

Regarding the RSK inhibition experimental results, a reduction in the average number of inner cells to 0.48±0.09 from 1.06±0.13 was observed in comparison with the appropriate control embryos (p-value, 8.33E-04). Additionally, the average of SAD cells was slightly reduced to 0.72±0.11 from 1.16±0.16, although this reduction still equated with statistical significance (p-value equals, 4.836E-02) Other relevant experimental details/data are described in the supplementary information table (Suppl. Tab. 5).

Lastly, the specific results from the MEK1/2 inhibition experiment (targeting the ERK1/2 MAPK pathway), caused late 16-cell stage average inner cell numbers to fall, in a statistically significant manner, from 1.35±0.17 in the control condition to 0.75±0.19 (p-value equals, 3.239E-02). The average number of SAD cells was 1.31±0.18 in the control embryo group and was not statistically significant from the value of 1±0.27 in the inhibited embryos (p-value equals p-value = 2.562E-01); note, such a reduction in inner cell generation but lack of effect on SAD cell number is consistent with mTOR inhibition using either

Rapamycin (see Figs. 10 & 11 – *above*) or Torin1 (Fig. 11 Bruce & Gahurova – *unpublished observations*). The other MEK1/2 inhibition relevant details/data are summarised in the supplementary information table (Suppl. Tab. 6).

A further group of individual experimental conditions (also stated in Table 11 above) did not result in any statistically significant differences in the average number of inner/SAD cells generated in late 16-cell stage embryos, when comparted to their appropriate control groups. These represented pharmacological targeting of the PP2A (inhibition - PP2A is a protein phosphatase involved in regulation of 4EBP1 and S6K1 phosphorylation status (Peterson, Randall *et al.*, 1999)), CDK1(inhibition - a protein kinase asserting 4EBP1 phosphorylation in oocytes (Kalous, Jansova and Šušor, 2020)) and FGFRs (inhibition - receptors for the fibroblast-growth-factor/FGF family of inter-cellular signalling ligands (Yang *et al.*, 2015)) (Fig. 13).

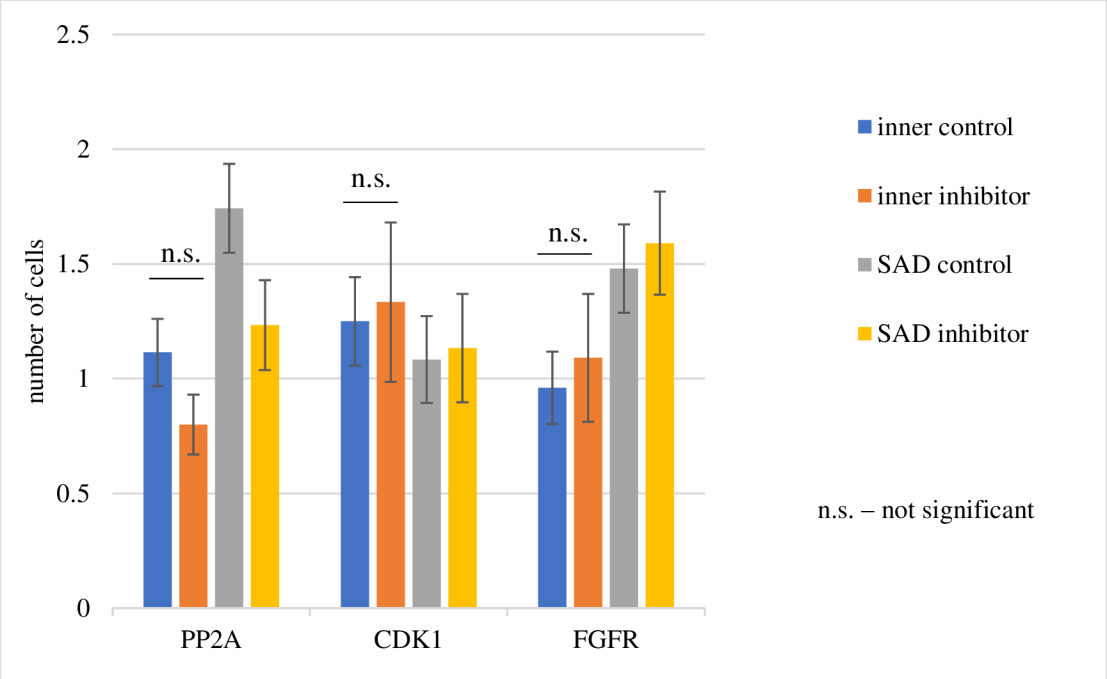

Fig. 13: Analysis of the average frequency of generated inner and SAD cells in 16-cell (E3.0+5 hours) mouse embryos after inhibition of PP2A, CDK1 and FGFR pathways (from E2.5+4 hours). Error bars are indicative of the standard error of the mean.

Specifically, in the experiments targeting PP2A, the average number of inner cells was 1.11±0.15 in control embryos and was not statistically significant from the average of 0.8±0.13 inner cells observed in inhibited embryos (p-value, 1.234E-01). Neither were the differences in the average number of SAD cells observed, amounting to 1.74±0.19 in control embryos versus 1.23±0.2 in

inhibited group (p-value, 8.052E-02). Supplementary data relating to the PP2A inhibition experiments are given below in the supplementary information table (Suppl. Tab. 7). T-tests show that inhibited embryos were slightly delayed from control ones in terms of total cell number, indicating PP2A inhibition had a negative effect on embryo development *per se*; notwithstanding this slight delay the experimental data did not show any significant difference in the number of inner cell generated after PP2A inhibition.

In relation to the experiments targeting CDK1, the results detail an average number of inner cells in the control embryo group of 1.25 ±0.19 compared to the similar number of 1.33±0.35 in the inhibited embryos (p-value, 7.785E-01). Similarly, the average number of SAD cells was statistically equal with 1.08±0.19 in control and 1.13±0.24 in inhibited conditions (p-value, 9.757E-01). The provided supplementary tables summarise the additional relevant information regarding the described CDK1 inhibition experiments (Suppl. Tab. 8).

Regarding the results from the FGFR inhibition experiments, the average number of inner cells was 0.96±0.16 in control embryos and 1.09±0.28 in the inhibited group (p-value, 8.302E-01) and the corresponding figures for SAD cells were 1.48±0.19 and 1.59±0.22, respectively (p-value, 7.976E-01). Additional experimental data is provided in the supplementary data table (Suppl. Tab. 9).

An additional experimental condition was performed and involved simultaneous pharmacological p38-MAPK inhibition and activation of the mTOR pathway (i.e. the same p38-MAPK inhibitor that had previously used was employed in combination with the mTOR activator – Fig. 14).

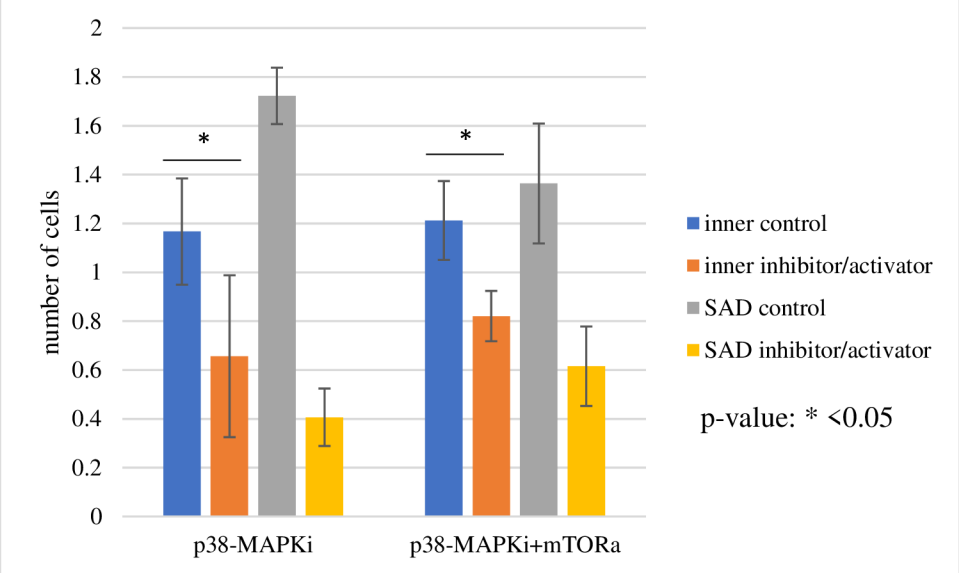

Fig. 14: Analysis of the average frequency of generated inner and SAD cells in 16-cell (E3.0+5 hours) mouse embryos after inhibition of p38-MAPK pathway and inhibition of p38-MAPK and activation of mTOR at the same time (from E2.5+4 hours) to see the rescue effect. Error bars are indicative of the standard error of the mean.

This was because it had already been observed in our laboratory, that p38-MAPK inhibition during mouse blastocyst maturation (E3.5-E4.5) results in failed specification/differentiation of the primitive endoderm (PrE) lineage, but simultaneous inhibition of p38-MAPK and activation of mTOR could partially restore PrE formation (Bora, Gahurova, Mašek, *et al.*, 2021); potentially, functionally placing mTOR downstream of p38-MAPK. It was therefore hypothesised the reduced numbers of inner and SAD cells observed in late 16-cell stage embryos after p38-MAPK inhibition from the late 8-cell stage, may similarly be rescued by concomitant pharmacological activation of mTOR. As can be seen (Fig. 14), this experiment did not show any significant or partial rescue of the p38-MAPK reduced inner cell phenotype. Specifically, in the p38-MAPK inhibited condition alone the average number of inner cells was 0.66±0.12 versus 1.17±0.22 in the appropriate control embryos; a statistically significant reduction (p-value equals, 9.534E-03). Likewise, when the p38-MAPK inhibition was repeated in the presence of the mTOR activator, the average number of inner cells was still significantly reduced at 0.82±0.1 versus 1.21±0.16 in the control group. A similar trend regarding the generation of SAD cells was observed. Specifically, p38-MAPK inhibition alone lead to an average of number of SAD cells of 0.41±0.12 compared to 1.72±0.33 in control (another statistically significant reduction - p-value, 2.082E-04), with p38-MAPK

inhibition plus co-stimulation of mTOR resulting in 0.62±0.16 SAD cells versus 1.36±0.25 in the control (p-value equals, 3.678E-03). Additional supplementary data for the combined p38-MAPK inhibition plus simultaneous mTOR activation experiment can be found in the supplementary table (Suppl. Tab.10).

The last of the tested inhibitors was BI2536, which targets PLK1 (polo-like-kinase 1); a cell cycle regulated kinase that plays role in mitotic spindle orientation. PLK1 inhibition is known to disrupt meiotic spindle formation, chromosome congression and spindle-associated localisation of phospho-4EBP1 in meiotically maturing murine oocytes (Severance, A. and Latham, K., 2017). In the first iteration of the PLK inhibition experiment on embryos, an inhibitor concentration of 20 µM was employed but caused arrested development at the 8-cell stage (*i.e.* the stage at which the inhibitor was initially administered). Accordingly, lower concentrations were applied in subsequent experiments (*i.e.* 10µM and 1.25µM) but equally caused 8-cell stage arrested phenotype; most likely due to the PLK1 essential role in mitotic cell division (Kim and Griffin, 2021).

From these pharmacologically treated embryo experimental results, we can link several pathways to that of mTOR and the potential regulation of protein translation, in regard to generating the first population of founder inner cells in the 16-cell stage mouse embryo. It was proved that mTOR inhibitor Rapamycin (specifically targeting mTORC1) negatively affects the generation of inner cells during 8- to 16-cell stage transition; an effect that can be extended to the pharmacological activation of the AMPK pathway and the inhibition of the related p38-MAPK, AKT, RSK, MEK1/2 signalling cascades, potentially implicating them in a broader mTOR mediated regulative mechanism governing initial inner cell generation. It was also shown that such mTOR inhibition related phenotypes are not extendable to the appropriate functioning of the PP2A, CDK1 and FGFR pathways. Equally, nor does PLK1 inhibition affect the generation of the first population of inner cells during the 8- to 16-cell transition, but PLK1 activity is essential to promote transition through the 8- to 16-cell transition without resulting in arrested development.

4.2. Cloning of cDNA inserts encoding HA-tagged 4EBP1, 4EBP1-Ala and EIF4E into the *in vitro* transcription (IVT) vector pRN3P.

In order to assay the potential component of regulated protein translation (possibly of specific 5'UTR TOP-motif containing mRNA transcripts) related to our unpublished observation of Torin1 mediated inhibition of mTOR (shortly before and during the 8- to 16-cell transition) and which causes the generation of fewer initial inner cells at the mid-16-cell stage (Bruce & Gahurova – *unpublished observations*), we first needed to clone cDNA inserts related to the mTOR sensitive translation initiation complex, EIF4F. These included three constructs, that all incorporate a N-terminal HA-epitope tag, and encode either; **i.** 4EBP1, **ii.** 4EBP1-4Ala (a non-phosphorylatable dominant-negative mutant, in which the four characterised mTOR target Serine/Threonine residues have been mutated to Alanine) or **iii.** EIF4E. It was our intention to clone the gene specific PCR generated inserts into the multiple cloning site of our preferred *in vitro* transcription (IVT) plasmid vector pRN3P (Fig. 8). This would permit T3 bacteriophage RNA polymerase mediated transcription of gene cDNA insert specific and linearised plasmid template that would also incorporate transcript stablishing 5' and 3'-UTRs from the frog beta-globin gene locus. Therefore, after *in vitro* poly-adenylation, yielding stable recombinant mRNA transcripts that could be microinjected into single embryonic blastomeres (typically at the 2-cell stage – E1.5), together with a lineage tracer, to create marked clones of progeny cells. The spatial allocation of such marked clones (to the nascent 16-cell stage ICM founder population), harbouring microinjected recombinant mRNAs and consequently overexpressed and relevant EIF4F complex components, could then be assayed under control or mTOR inhibited conditions. We would predict an excess of either recombinantly expressed 4EBP1 or EIF4E (but not 4EBP1-4Ala) could restore or partially rescue the number of mid-16-cell stage inner cells under mTOR inhibited conditions.

Therefore, the first step involved in cloning the three EIF4F complex related cDNAs was to independently confirm the activity of the required restriction enzymes (*i.e. BamHI* and *BglII*). Accordingly, we individually tested each enzymes ability to linearise an existing plasmid containing one copy of each restriction site (*i.e.* pRN3P-GFP). Post-digestion a sample of either *BamHI* or *BglII* digested plasmid DNA was ran alongside an equal amount of undigested

pRN3P-GFP plasmid on an ethidium-stained agarose gel (Fig. 15). Whilst the uncut plasmid resolved into three bands of differing mobility (indicative of supercoiled and nicked DNA species) both the restriction enzyme digested samples ran at the correct and anticipated molecular weight (when compared to the 1 Kbp DNA marker lane) of 4.2 Kbp; thus confirming the activity of both enzymes (Figure 15 – panel A). Therefore, in order to prepare the empty pRN3P plasmid vector for cloning of the EIF4F related cDNA inserts, an aliquot was subsequently digested with both *BamHI* and *BglII* simultaneously. As shown in Figure 15 – panel B, successful linearisation of the empty pRN3P vector was confirmed by agarose gel electrophoresis, when compared to a sample of uncut plasmid on the same gel, and migrated at the correct size (3.3 Kbp).

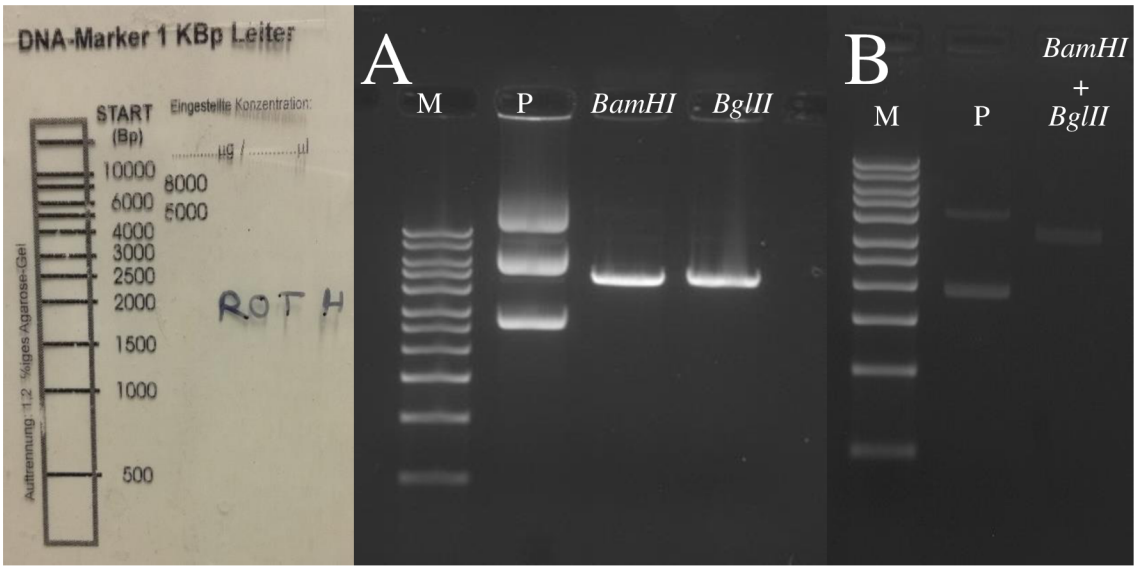

Fig. 15: Panel A - Control digests confirming the activity of restriction enzymes *BamHI* and *BglII*; marker (M) – 1KBp marker ladder (key shown on right), uncut pRN3P-GFP plasmid (P). Panel B – Agarose gel after restriction digest of empty pRN3P vector using *BamHI* + *BglII*, marker (M) – 1KBp ladder, uncut control pRN3P plasmid (P)

Following restriction digest preparation of the host pRN3P vector, specific oligonucleotide primers were utilised in high-fidelity PCR reactions to derive the *4ebp1, 4ebp1-4Ala* and *Eif4e* cDNA inserts. The inserts for *4ebp1* and *Eif4e* were amplified using existing mouse blastocyst cDNA, previously generated in our laboratory, and the *4ebp1-4Ala* insert was PCR amplified from an obtained rat cDNA and sequenced plasmid clone; pCW57.1–4E-BP1–4Ala (Thoreen *et al.*, 2012). Note, in all cases the sense oligonucleotide primer included sequences corresponding to *BglII* and a HA-epitope tag, that was 5' to, and in frame with, the gene specific sequence. Likewise, the antisense primer comprised a *BamHI*

sequence, also to the 5' side of the gene specific sequence. Hence the derived PCR products would not only comprise the gene specific cDNA but also the necessary restriction enzyme sites needed for cloning into the pRN3P vector and an encoded N-terminal HA-epitope tag (to permit the potential discrimination of the over-expressed recombinant proteins by immuno-fluorescence). After PCR amplification, an aliquot of each reaction was resolved on an agarose gel and the size of the obtained product determined and verified against the correct size (*i.e.* for *4ebp1 and 4ebp1-4Ala* - 417 bp and for *eif4e* - 717bp) As can be seen, the PCR reactions yielded single products of the correct size for eacch of the three EIF4F related cDNA inserts (Fig. 16).

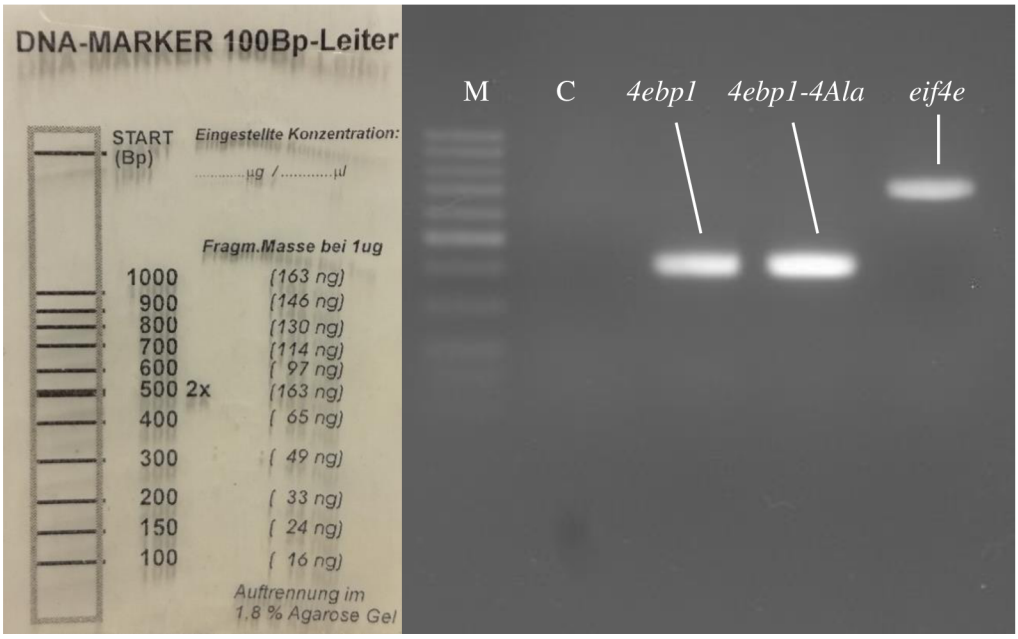

Fig. 16 : Agarose gel detailing the correct size of PCR generated cDNA inserts encoding *4ebp1, 4ebp1-4Ala, Eif4e*, compared to a 100bp marker lane (M – key shown on the left), and negative PCR control lane (lacking template – C).

Having verified the size of the cDNA inserts, the PCR reactions were purified and double digested with *BamHI* and *BglII* to generate the necessary cohesive ends required for ligation (cloning) into the already prepared/digested pRN3P vector (*see above*). Following restriction digestion, the cDNA inserts were again purified and combined with linearised pRN3P plasmid in a DNA ligation reaction, before transformation into competent bacteria. Colonies arising from successful transformants of individual ligations were then screened by colony PCR to confirm the presence of the desired cloned inserts. Accordingly, template

samples were prepared from streaked and indexed bacterial colonies and using a vector encoded sense oligonucleotide primer and an insert specific anti-sense primer, PCR reactions conducted. The expected sizes, indicative of successfully cloned cDNA inserts corresponded to 450bp for *4ebp1* and *4ebp1-4Ala* and 750bp for *Eif4e* (Figs. 17, 18 & 19). Bacterial colonies/clones harbouring the required pRN3P-EIF4F related cDNA inserts, were expanded, plasmid DNA preparations purified, sequence verified (by out-sourced Sanger DNA sequencing) and long-term -80^{o}C glycerol storage stocks prepared.

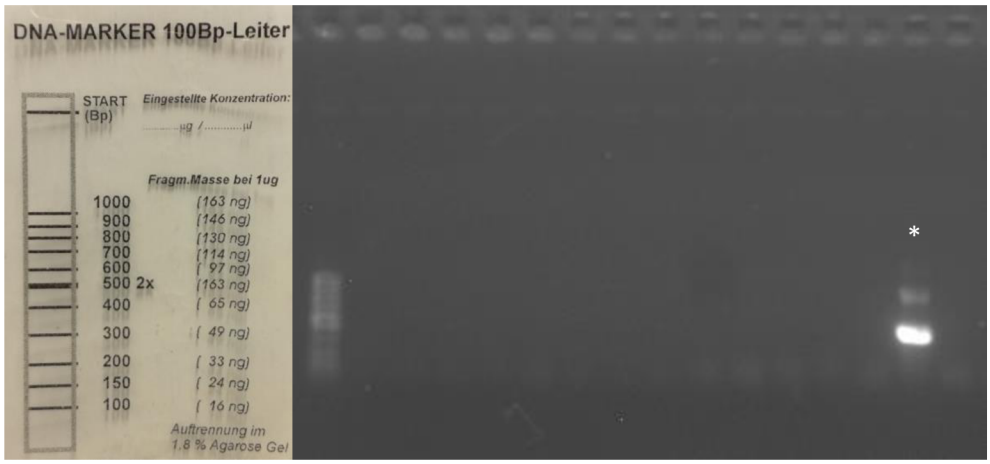

Fig. 17: Agarose gel showing derived colony PCR products for transformed pRN3P-*4ebp1* ligation mixtutres (the lanes corresponsing to a bacterial clone containing the desired cDNA insert are highlighted *). The size of derived colony PCR products are compared to a 100bp marker lane – lane 1 (M – key shown on the left).

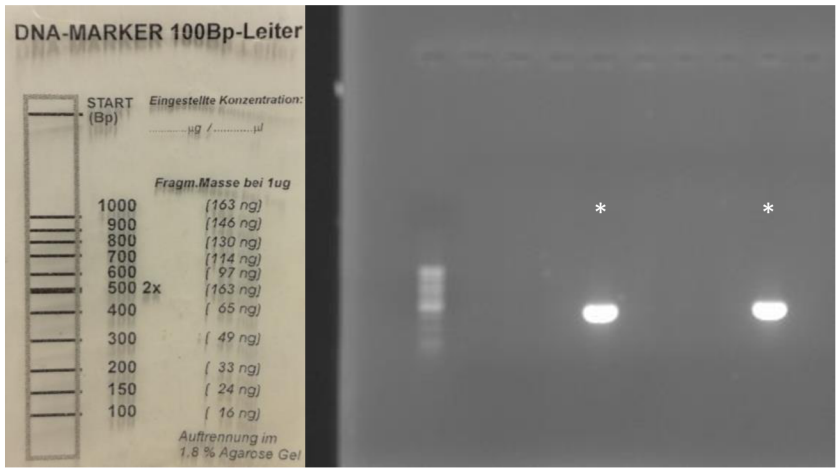

Fig. 18: Agarose gel showing derived colony PCR products for transformed pRN3P-*4ebp1-4Ala* ligation mixtutres (the lanes corresponsing to a bacterial clone containing the desired cDNA insert are highlighted *). The size of derived colony PCR products are compared to a 100bp marker lane – lane 1 (M – key shown on the left).

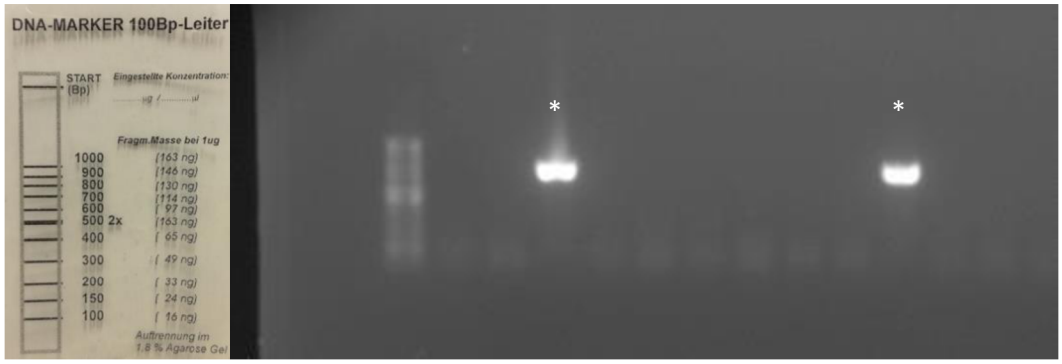

Fig. 19: Agarose gel showing derived colony PCR products for transformed pRN3P- *eif4e* ligation mixtutres (the lanes corresponsing to a bacterial clone containing the desired cDNA insert are highlighted *). The size of derived colony PCR products are compared to a 100bp marker lane – lane 1 (M – key shown on the left).

In order to prepare the three EIF4F related pRN3P plasmid DNA clones for *in vitro* transcription (IVT) it was first necessary to linearise using the restriction enzyme *SfiI* (a restriction enzyme that recognises an atypical sequence present in one copy downstream of the cloned inserts and the 3´frog-globin UTR and is not present in any of the three insert sequences themselves). Successful *SfiI* restriction digestion/linearisation was confirmed by agarose gel electrophoresis (Fig. 20).

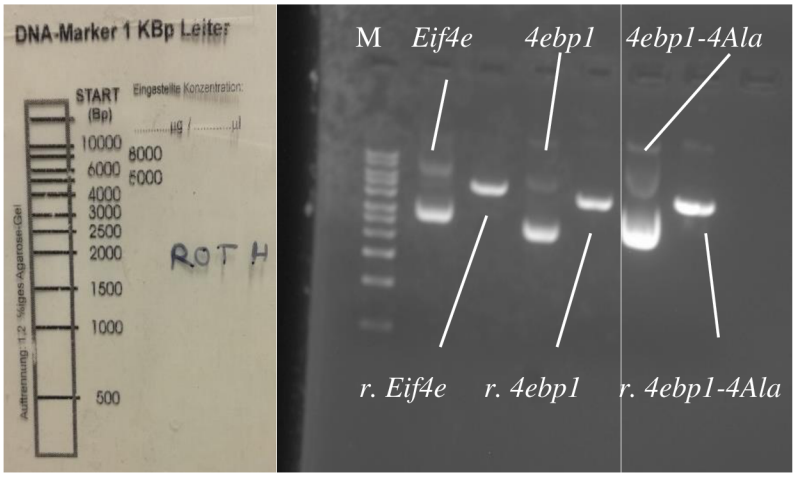

Fig. 20: *SfiI* restriction digestion/linearisation of pRN3P clones containing *Eif4e*, *4ebp1* and 4*ebp1-4Ala* encoding cDNA inserts, compared to the relevant undigested parental plasmid as indicated (r. denotes + *SfiI*), as preparation for IVT. Correct size of linearised plasmid templates was compared against 1Kbp ladder (key on left).

Following confirmed linearisation of pRN3P clones containing the relevant EIF4F related gene cDNA inserts, the individual plasmid DNAs were used as templates in IVT reactions utilising the vector encoded T3 bacteriophage RNA polymerase promoter to transcribe the relevant recombinant cDNA inserts. For each insert the expected mRNA transcript size/length was approximately 500bp for *4ebp1, 4ebp1-4Ala* and 800bp for *Eif4e.* During this time in the laboratory there were some technical problems regarding the use of denaturing agarose gels, meaning the exact size of the IVT products could not be verified. However, using normal agarose gel electrophoresis did allow the sizes of IVT products to be estimated and to also ensure the products were not degraded (Fig. 21). The IVT reactions were then quantified by U.V. spectroscopy (nanodrop) and stored at -80^{o}C for subsequent microinjection into single preimplantation stage mouse embryo blastomeres (*see below*).

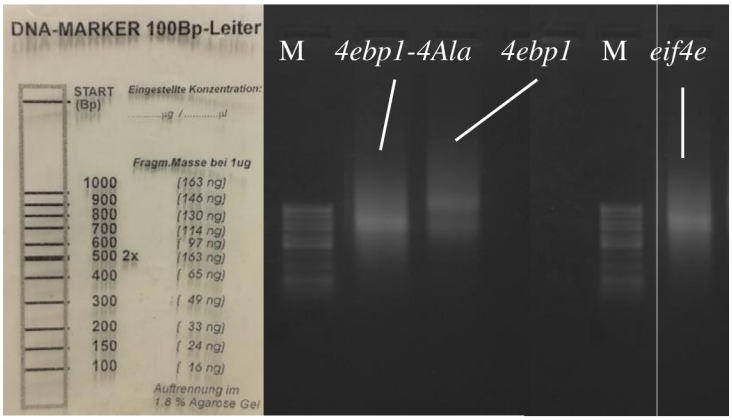

Fig. 21: Verification of approximate size of recombinant IVT derived mRNA products transcribed from pRN3P-*4ebp1-4Ala*, pRN3P-*4ebp1* and pRN3P-*Eif4e* (as indicated). Product sizes were judged against the 100 bp marker (M – key shown on the left)

4.3. Microinjection of the recombinant EIF4F-related mRNAs into 2-cell stage embryos to assay their effect regarding mTOR inhibition.

The first step after cloning the N-terminally HA-tagged 4EBP1 (encoded by pRN3P-4ebp1), 4EBP1-4Ala (pRN3P-4ebp1-4Ala) and EIF4E (pRN3P-Eif4e) cDNAs and then generating the corresponding IVT derived capped and poly-A+ tailed mRNAs (as described above), was to microinject them into individual mouse embryo blastomeres and confirm recombinant protein expression. Accordingly, all three mRNAs (*HA-4ebp1*, *HA-4ebp1-4Ala* and *HA-Eif4e*) were co-microinjected in one blastomeres of 2-cell stage (E1.5) embryos (at a concentration 200 ng/µl) with Venus-histone-H2B fusion reporter encoding

mRNA (final concentration 60 ng/µl); enabling the successfulness of the microinjection procedure and the clonal identification of subsequent progeny cells to be determined, by presence or absence of fluorescence. Microinjected 2-cell embryos were then *in vitro* cultured until the late 16-cell stage (E3.0+5h), fixed, stained/immuno-fluorescently stained (using a primary antibody specific for the N-terminal HA-epitope tag) and processed for confocal microscopy imaging (using techniques essentially similar to those described above for the pharmacologically inhibited embryos; the only difference was Rhodamine conjugated Phalloidin (ThermoFisher Scientific) was used as well as Oregon green^{488nm} Phalloidin to test which cells exhibit detected HA-tag fluorescence – presented micrograph images show Oregon green^{488nm} Phalloidin. As can be observed from the inspection of exemplar single z-section confocal images of the recombinant mRNA microinjected embryos, the appropriate expression of recombinant HA-4EBP1 (Fig. 22), HA-4EBP1-4Ala (Fig. 23) and HA-EIF4E (Fig. 24) protein was exclusively confirmed in the 16-cell stage progeny of the injected 2-cell blastomere; via co-expression of the Venus-histone-H2B fusion reporter protein (within cell nuclei – as marked also marked by DAPI staining). The cell progeny of the non-microinjected clones (unmarked by Venus-histone-H2B fusion reporter protein expression) consistently did not provide any detectable anti-HA-tag immunofluorescence. Collectively, these results confirm the successful and clonal over-expression of the in-house cloned recombinant EIF4F complex/mRNA 7-methyl-guanosine-cap-binding subunit related proteins in the mouse preimplantation stage embryo.

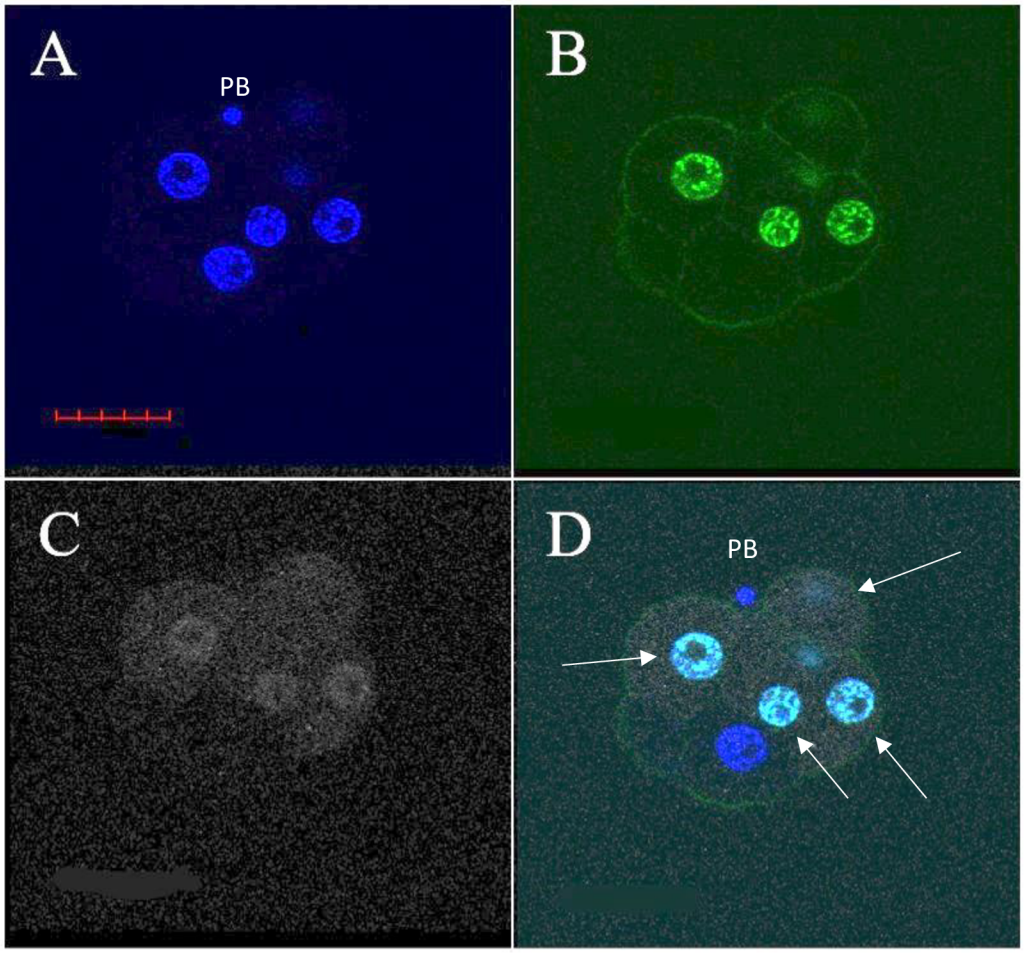

Fig. 22: Immuno-fluorescent staining of clonal HA-tagged 4EBP1 protein expression following *HA-4ebp1* mRNA microinjection (in one blastomere at the 2-cell stage): A - DAPI DNA stain (blue), marking all embryonic nuclei (plus second polar body – PB), B - Histone H2B-Venus (injection marker) expression (green nuclear signal) and cortical F-actin phalloidin staining (weak green cell membrane localised signal), C – Anti-HA tag immuno-fluorescence stain (grayscale) – note cytoplasmic and nuclear HA-4EBP1 protein expression/localisation. D – Three channel merge – note, restricted HA-4EBP1 expression in only the progeny of the microinjected cell, as marked by co-expression of histone H2B-Venus (arrow heads). Scale bar = 30 µm.

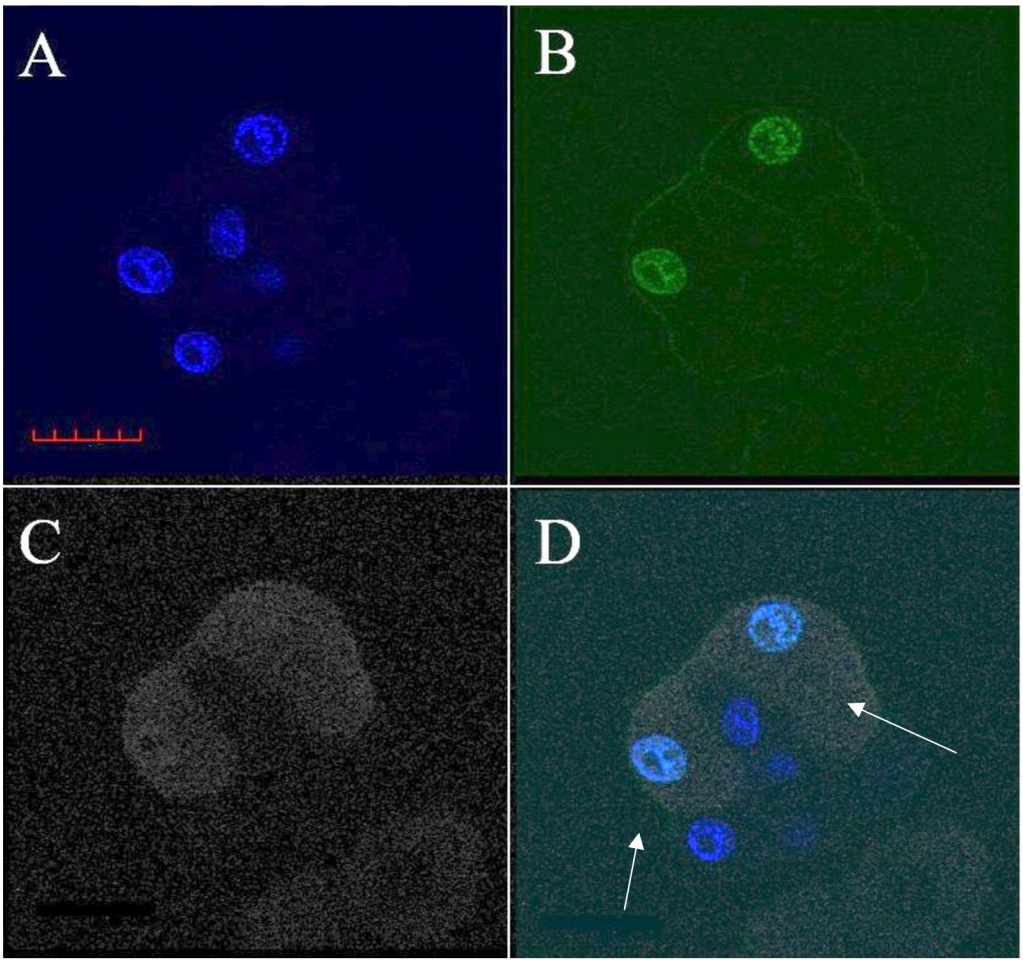

Fig. 23: Immuno-fluorescent staining of clonal HA-tagged 4EBP1-4Ala protein expression following *HA-4ebp1-4Ala* mRNA microinjection (in one blastomere at the 2-cell stage): A - DAPI DNA stain (blue), marking all embryonic nuclei, B - Histone H2B-Venus (injection marker) expression (green nuclear signal) and cortical F-actin phalloidin staining (weak green cell membrane localised signal), C – Anti-HA tag immuno-fluorescence stain (grayscale) HA-4EBP1-4Ala protein expression/localisation. D – Three channel merge – note, restricted HA-4EBP1-4Ala expression in only the progeny of the microinjected cell, as marked by co-expression of histone H2B-Venus (arrow heads). Scale bars = 30 µm.

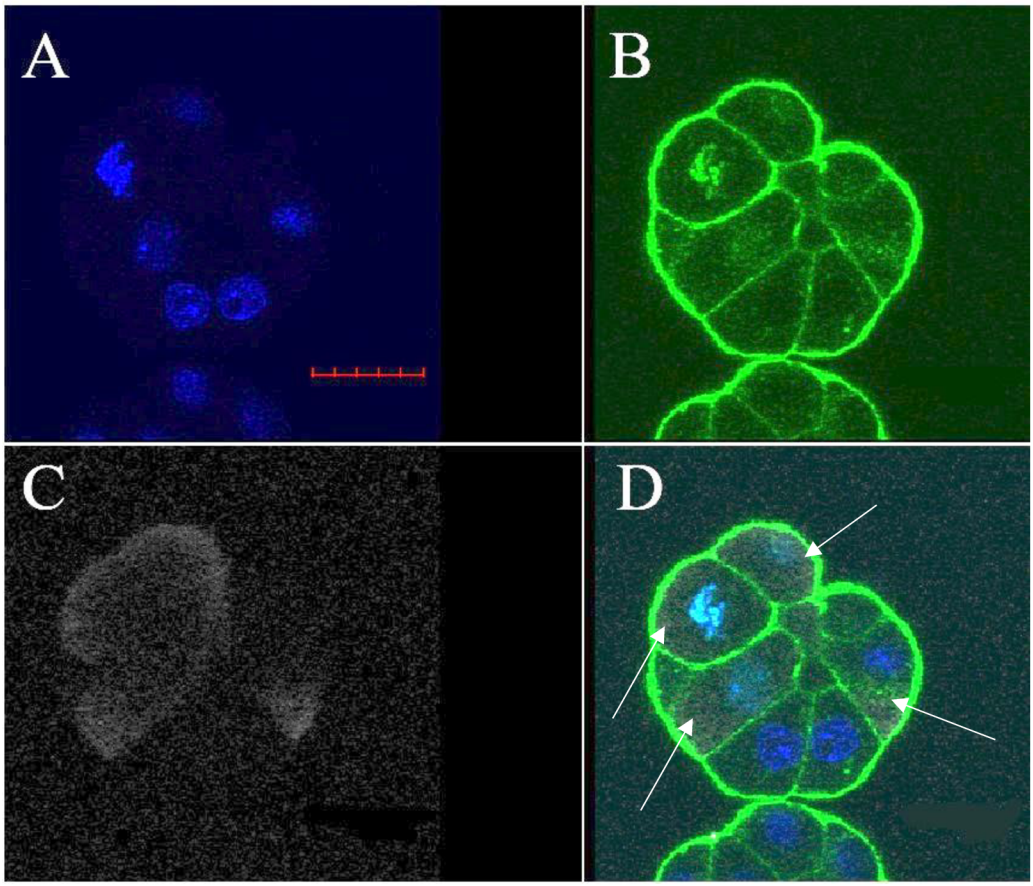

Fig. 24: Immuno-fluorescent staining of clonal HA-tagged EIF4E protein expression following *HA-Eif4e* mRNA microinjection (in one blastomere at the 2-cell stage): A - DAPI DNA stain (blue), marking all embryonic nuclei, B - Histone H2B-Venus (injection marker) expression (green nuclear/mitotic chromosome signal) and cortical F-actin phalloidin staining (cell membrane localised signal), C – Anti-HA tag immuno-fluorescence stain (grayscale) – note cytoplasmic HA-EIF4E protein expression/localisation. D – Three channel merge – note, restricted HA-EIF4E expression in only the progeny of the microinjected cell, as marked by co-expression of histone H2B-Venus (arrow heads). Scale bars = 30 µm.

After confirming recombinant protein expression, any potential effect on the average spatial allocation of cells (to the nascent inner compartment of fixed late 16-cell stage embryos), from both the fluorescently microinjected clones expressing recombinant EIF4F/mRNA 7-methyl-guanosine-cap-binding complex related proteins and the non-microinjected sister clone from the same embryo groups was compared. It was hypothesised recombinant HA-4EBP1 over-expression may either, **i.** phenocopy pharmacological inhibition of mTOR by sequestering available endogenous EIF4E protein from the EIF4F/ mRNA 7-methyl-guanosine-cap-binding complex to reduce functionally- or phenotype-

relevant protein translation, or **ii.** have little or no effect on spatial allocation as endogenous levels of mTOR activation would be sufficient to liberate EIF4E from 4EBP1 containing inhibitor complexes regardless of endogenous or recombinant origin. In relation to expression of recombinant HA-4EBP1-4Ala it was predicted that the over-expressing clones would be impaired in their contribution to the nascent late-16-cell stage inner cell compartment; as the lack of phosphorylatable regulation by mTOR (due to the alanine substitution of mTOR target residue substrates) would in effect mimic mTOR inhibition; permitting the mutant recombinant protein to interact with, and sequester, the endogenous levels of EIF4E protein (impairing EIF4F/mRNA 7-methyl-guanosine-cap-dependent translation). Lastly, it was hypothesised recombinant HA-EIF4E expression would most probably have little effect on 16-cell stage blastomere allocation on its own (as alone it would be unlikely to affect functionally- or phenotype-relevant protein translation). However, it was predicted such clonal HA-EIF4E over-expression in the context of mTOR inhibition could be sufficient to rescue the pharmacologically induced late-16-cell reduced inner cell phenotype, as the capacity of endogenous levels of 4EBP1 to bind to and inactivate both endogenous EIF4E and recombinant HA-EIF4E could be exceeded. In such a circumstance, unbound/free EIF4E (regardless of endogenous or recombinant origin) could facilitate the necessary functionally- and phenotype-relevant protein translation (by contribution to the EIF4F/mRNA 7-methyl-guanosine-cap-binding complex) that circumvents and negates the effect of inhibited mTOR activity.

Considering the clonal *HA-4ebp1* and *HA-4ebp1-4Ala* microinjections first. We did not observe any statistically significant difference in the average late-16-cell stage inner cell allocation between the microinjected (0.74±0.2) and non-microinjected (0.85±0.14) clones, when microinjecting *HA-4ebp1* mRNA (p-value, 2.632E-01 - Fig. 25); suggesting clonal overexpression of HA-4EBP1 does not interfere with protein translational mechanisms that would influence allocation of inner cells in a manner reminiscent of mTOR inhibition (see above – Fig. 22). However, when recombinant *HA-4ebp1-4Ala* mRNA was microinjected, the contribution of cells to the late-16-cell inner embryo compartment was significantly attenuated in the microinjected (0.21±0.11) versus non-microinjected (1 ± 0.26) cell clones (p-value, 1.406E-02 - Fig.25).

Such reduced inner cell contribution of cell clones over-expressing the mutant HA-4EBP1-4Ala recombinant protein, confirmed the above stated hypothesis. Such data most likely relates to a sequestering of available endogenous EIF4E into a non-functional and HA-4EBP1-4Ala interacting pool, that cannot be retrieved by active mTOR signalling due to a lack of the key regulatory and phosphorylatable target substrate residues. Therefore, this reduced inner cell allocation phenocopy of pharmacological inhibition of mTOR strongly suggests the mechanism by which the originally observed (and confirmed here – Fig.10; using Rapamycin) mTOR inhibition induced reduction in late-16-cell inner cells is mediated, acts via regulation of 4EBP1 phosphorylation and regulation of EIF4E availability to drive necessary EIF4F/mRNA 7-methyl-guanosine-cap dependent protein translation. Interestingly, the clonal over-expression of neither HA-4EBP1 nor HA-4EBP1-4Ala protein had any statistically significant effect on the average number of SAD cells (as was the case for mTOR inhibition – Fig. 12) observed between the microinjected or non-microinjected clones (Fig. 26 - *i.e.,* 0.96±0.16 & 1.17±0.15 for HA-*4ebp1* mRNA injected embryos, and 0.9±0.18 & 0.8±0.29 for HA-*4ebp1-4Ala* mRNA injected embryos, respectively; associated p-values 7.05E-02 & 8.43E-01).

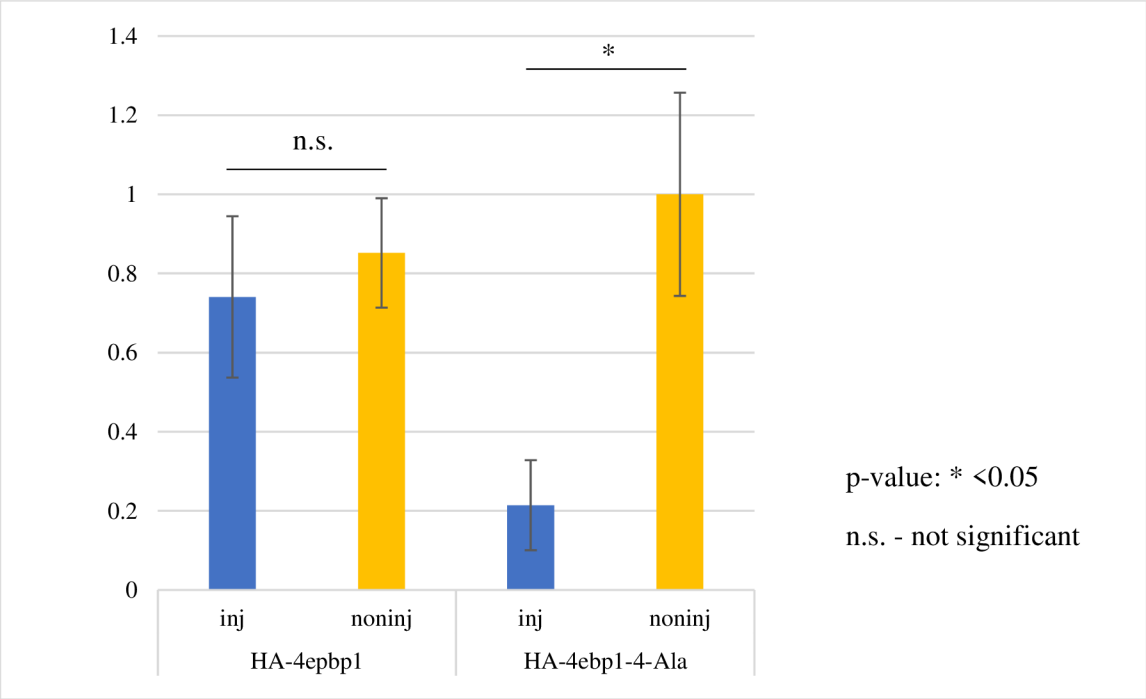

Fig. 25: Analysis of the average frequency of generated inner cells in 16-cell (E3.0+5 hours) mouse embryos after microinjection of *HA-4epbp1* mRNA and *HA-4ebp1-4-Ala* mRNA (in one blastomere at 2-cell stage). Error bars are indicative of the standard error of the mean.

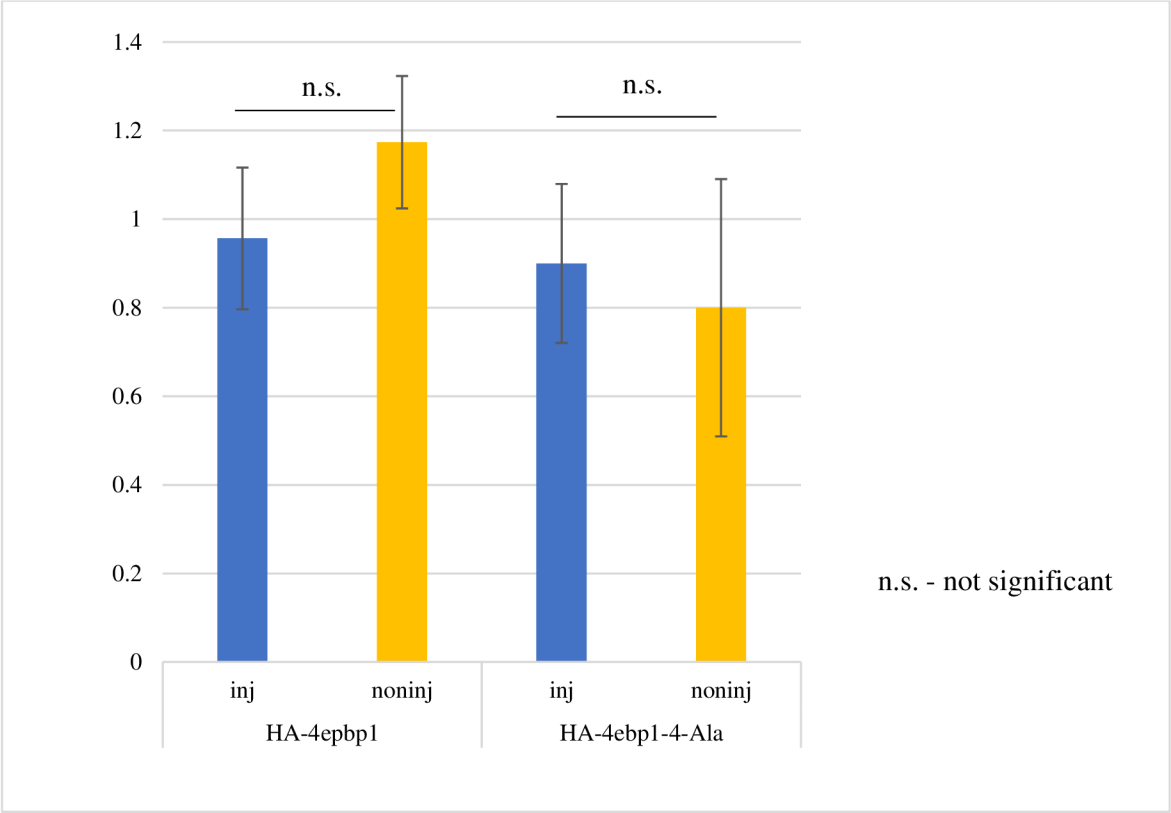

Fig. 26: Analysis of the average frequency of generated SAD cells in 16-cell (E3.0+5 hours) mouse embryos after microinjection of *HA-4epbp1* mRNA and *HA-4ebp1-4-Ala* mRNA (in one blastomere at 2-cell stage). Error bars are indicative of the standard error of the mean.

The next experiment was to compare the late-16-cell stage inner cell contribution of mTOR (+Torin1) inhibited embryos comprising non-microinjected and microinjected clones, derived from the microinjection of *HA-Eif4e* recombinant mRNA. As described above, it was hypothesised the confirmed recombinant HA-EIF4E protein expression would be able to rescue the average inner cell number deficit caused by mTOR inhibition (from the late-8-cell stage to the late 16-cell stage) and that this effect would be limited to the marked microinjected clone. Accordingly, 2-cell stage (E1.5) embryos were co-microinjected in one blastomere with *HA-Eif4e* recombinant mRNA and the fluorescent histone-H2B-Venus fusion microinjection marker/lineage tracer mRNA (that in of itself does not lead to any inter-clone variation in late-16-cell stage inner cell numbers – *data not shown*). A second control group, in which only the fluorescent histone-H2B-Venus fusion microinjection marker/lineage tracer mRNA was injected, was similarly prepared. The two microinjected embryo groups were then *in vitro* cultured until the late 8-cell stage and each further then split into two equal

treatment conditions. In the first treatment condition, embryos were transferred into Torin1 containing media drops (*i.e.* the mTOR inhibited experimental treatment groups), whilst the embryos of the second treatment condition were transferred into solvent vehicle control DMSO containing media (*i.e.* the control treatment groups). Both treatment conditions (per microinjection group) were then further cultured until the late-16-cell stage, fixed and imaged by fluorescent confocal microscopy to ascertain the average inner cell number contribution.

As shown in Fig. 27, the treatment of the control group of embryos microinjected solely with the histone H2B-Venus mRNA with Torin1 caused a reduction in the late-16-cell stage inner cell contribution of both the injected and non-injected clones, when compared with DMSO treated embryos (as would be expected given our previously observed data on unmanipulated Torin1 treated embryos – Bruce & Gahurova, *unpublished observations* – Fig.11, and supported by similar results using the alternative mTOR inhibitor compound Rapamycin - Fig. 10 - *see above*). Contrary to our initial hypothesis, this trend was replicated in embryos microinjected with *HA-Eif4e* mRNA (in addition to H2B-Venus mRNA encoding the fluorescent marker – Fig. 27). It had been expected that the progeny of the microinjected clone, may have been able to restore (at least partially) the reduced late-16-cell stage inner cell phenotype caused by Torin1 mediated mTOR inhibition (whereas the non-microinjected clone would remain compromised). However, this was not the case with both clones exhibiting reduced inner cell number under Torin1 induced mTOR inhibition.

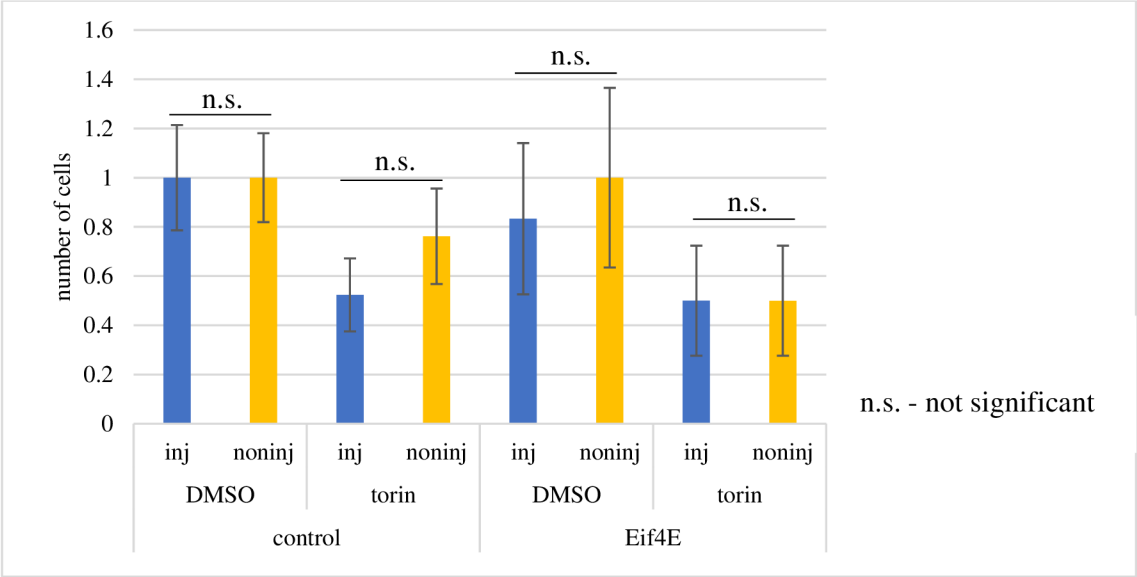

Fig. 27: Analysis of the average frequency of generated inner cells in 16-cell (E3.0+5 hours) mouse embryos after microinjection of H2B-Venus mRNA and *HA-Eif4e* mRNA (in one blastomere at 2-cell stage) and either control or mTOR inhibition (+Torin1) during the 8- to 16-cell transition. Error bars are indicative of the standard error of the mean.

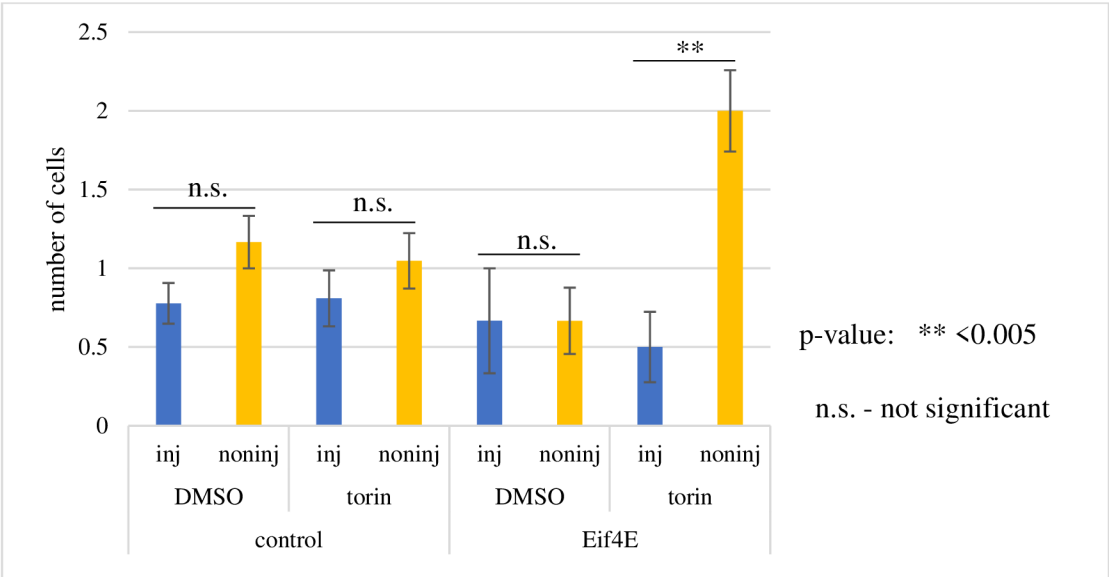

Fig. 28: Analysis of the average frequency of generated SAD cells in 16-cell (E3.0+5 hours) mouse embryos after microinjection of H2B-Venus mRNA and *HA-Eif4e* mRNA (in one blastomere at 2-cell stage) and either control or mTOR inhibition (+Torin1) during the 8- to 16-cell transition. Error bars are indicative of the standard error of the mean.

Examining the same dataset, the average clonal number of SAD cells per condition was also calculated (Fig. 28). As has been previously observed in unmanipulated embryos, treatment of the control group (*i.e.* only microinjected with the injection marker/lineage tracer mRNA) with Torin1 caused no effect on

the generation of SAD cells (in either the non-injected nor microinjected cell clones) versus DMSO treated embryos. Taken with the data revealing the concomitant reduction in the number of derived inner cells caused by Torin1 mediated mTOR inhibition (*see above* – Fig. 11), these consistent results further confirm mTOR inhibition (from the late-8-cell stage) under minimal control conditions does indeed compromise the production of late-16 stage inner cells but has no effect on SAD cell generation. Concentrating on the experimental microinjection group (*i.e.* after microinjection of *HA-Eif4e* and *H2B-Venus* mRNAs), there was no significant difference in the average SAD cell number within the microinjected clone after mTOR inhibition compared to control DMSO treatment. The corresponding number was not significantly increased in the non-injected clone (versus both the non-injected clone of the DMSO-treated embryos of same experimental embryo group or the equivalent clone in embryos solely microinjected with *H2B-Venus* mRNA; Fig. 28). The precise reasons for this compensatory behaviour in the non-microinjected clone and the fact it is only limited to embryos in which the HA-*Eif4e* mRNA was microinjected is not clear.

Taken collectively, such experiments combining microinjection based clonal overexpression of recombinant HA-EIF4E protein with Torin1 mediated mTOR inhibition between the late 8- and 16-cell stages did not result in the anticipated microinjected cell/clone autonomous rescue of average inner cell deficits observed by mTOR inhibition alone. However, it was speculated that a potential contributing factor to this lack of predicted effect may be related to the choice of microinjection marker/lineage tracer employed; namely, histone *H2B-Venus* mRNA. This was because such a marker/lineage tracer is itself reliant on translation to yield the fluorescent protein product required to distinguish clonal cell populations and indicate successful microinjection. As such, the abundant presence of such mRNA post-microinjection (and in all subsequent clonal cell progeny) may place an additional and sufficient protein translational burden on such cells, thus potentially masking any recombinant HA-EIF4E induced rescue of mTOR inhibition mediated reduced inner 16-cell stage phenotypes (*i.e.* additionally derived recombinant HA-EIF4E protein, predicted to facilitate the translation of mRNA transcripts related to regulation of inner cell generation, would be preferentially recruited to the translation of abundant recombinant and microinjected *H2B-Venus* mRNAs).

Therefore, we repeated the above-described experiment but substituted histone *H2B-Venus* mRNA for rhodamine-conjugated dextran micro-beads (RDBs) as the microinjection/lineage tracer marker. RDBs have the advantage of providing an instantly detectable post-microinjection fluorescence signal that readily persists in the clonal progeny of the microinjected cells until the mid- (E4.0) to late-blastocyst (E4.5) stages and does not burden the cellular protein translational machinery. As detailed in Figs. 29 & 30, the average number of generated inner cells in the RDB alone microinjection group of embryos was significantly impaired after addition of Torin1 (compared to DMSO control) and equally affected both injected and non-microinjected clones; moreover, there were no obvious effects on the generation of SAD cells. These expected data further still confirm the generation of inner cells between the late-8- and 16-cell stages are sensitive to levels of active mTOR signalling. In the experimental group of embryos, microinjected with RDBs and *HA-Eif4e* mRNA, the average number of generated inner cells under mTOR (+Torin1) inhibited conditions was lower than after the addition of DMSO (SAD cell generation remained statistically unaffected across all examined conditions). However, unlike in embryos solely microinjected with RDBs, such reductions did not reach statistical significance. Whilst this could be interpreted as potentially reflecting the predicted partial rescue effect, it was not limited to the microinjected clone (overexpressing the recombinant HA-EIF4E protein) as anticipated. Additionally, the average inner cell contribution of both clones under control DMSO conditions was not obviously below that observed in the equivalent clones of embryos microinjected with RDBs alone (indeed not higher after exposure to Torin1). Such an alteration in the baseline contribution of cells of both clones to the late-16-cell inner compartment associated with clonal HA-EIF4E expression, makes it difficult to unequivocally interpret or judge the potential rescue effect in regard to mTOR inhibition (+Torin1 conditions). However, the basic fact clonal expression of recombinant HA-EIF4E protein appears to impair general late-16-cell inner cell generation supports a wider role for regulated protein translation as being an important mediator of spatial cellular allocation during this developmental window. Moreover, the fact the magnitude of the reduction in generated inner cells caused by mTOR (+Torin1) inhibition is lessened under such conditions

supports but does not prove this role, although why this effect is not specific to the microinjected clone is currently not known.

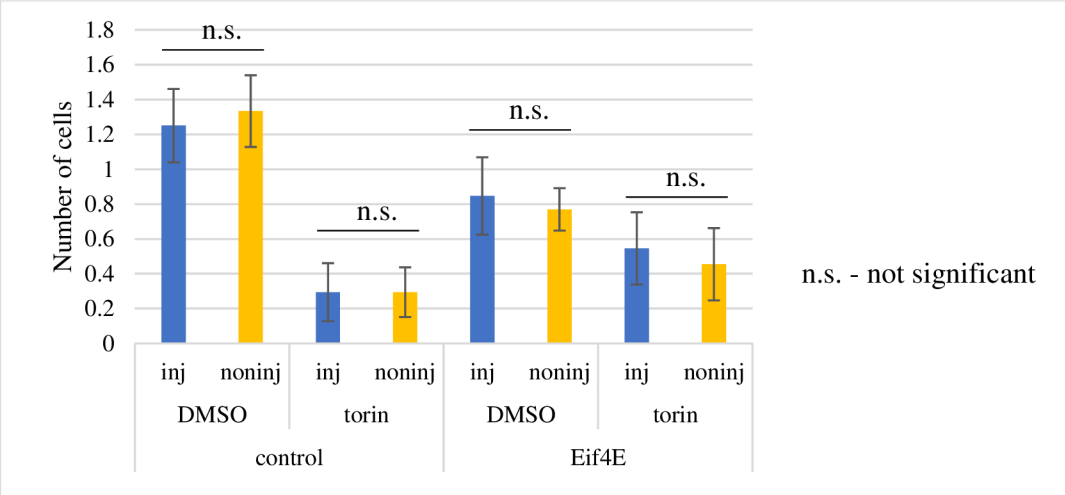

Fig. 29: Analysis of the average frequency of generated inner cells in 16-cell (E3.0+5 hours) mouse embryos after microinjection of RDBs ±*HA-Eif4e* mRNA (in one blastomere at 2-cell stage) and either control or mTOR inhibition (+Torin1) during the 8- to 16-cell transition. Error bars are indicative of the standard error of the mean.

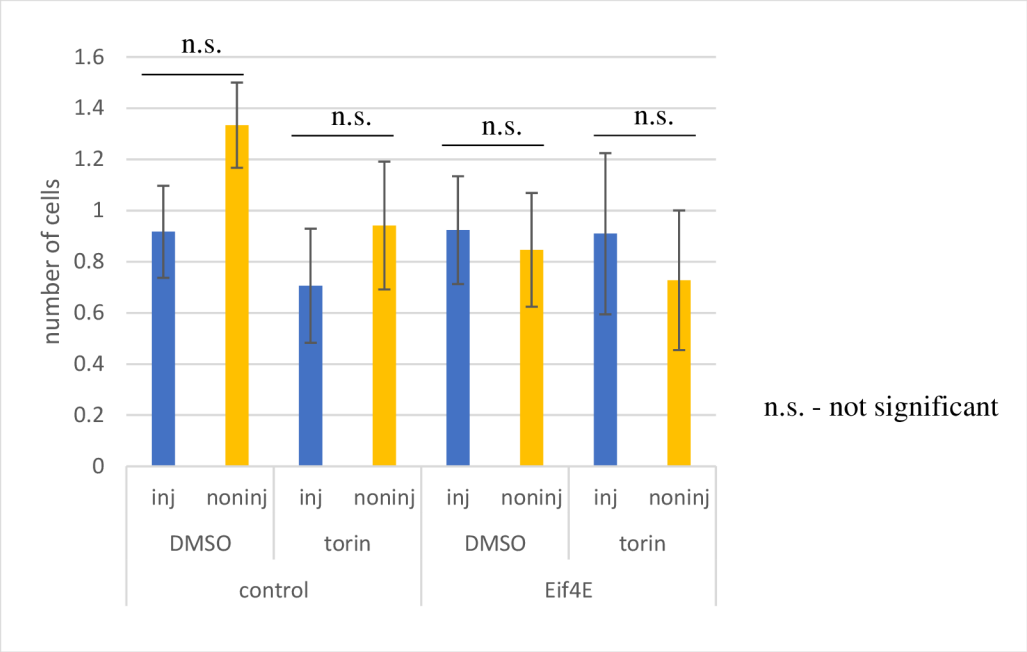

Fig. 30: Analysis of the average frequency of generated SAD cells in 16-cell (E3.0+5 hours) mouse embryos after microinjection of RDBs ±*HA-Eif4e* mRNA (in one blastomere at 2-cell stage) and either control or mTOR inhibition (+Torin1) during the 8- to 16-cell transition. Error bars are indicative of the standard error of the mean.

4.4. Embryo immuno-fluorescent staining for mTOR related proteins during and around the 8- to 16-cell stage embryo transition.

As stated in the introduction, the mTOR pathway regulates many cellular cascades and acts as a central nutrient sensor and regulator of catabolic and anabolic metabolism (Dazert and Hall, 2011). Amongst such pathways, is the regulation of 7-methyl-guanosine-cap-dependent mRNA translation involving the phosphorylation of the mTOR (mTORC1) target protein 4EBP1 to promote enhanced levels of translation (Gao *et al.*, 2012); in addition to mTOR interaction/regulation of LARP1 (implicated in regulating mRNAs containing so-called TOP-motifs in their 5'UTRs, with conflicting reports as to the effect on eventual transcript translation (Fonseca *et al.*, 2015, 2018; Fuentes *et al.*, 2021)). Additionally, such mTOR regulated mechanisms of enhanced translation (involving phosphorylation of 4EBP1) have been implicated in meiotically maturing mouse oocytes as being crucial for temporally and spatially regulated protein translation necessary to ensure appropriate meiotic spindle formation, migration and the asymmetric cell division involving the extrusion of the first polar body (Susor *et al.*, 2015). Therefore, given pharmacological mTOR inhibition (plus that of related pathways – including AMPK (activation), p38-MAPK, AKT, RSK & MEK1/2 – *see above*, Figs. 10, 11 & 12) during the 8- to 16-cell transition is also associated with impaired derivation of late-16-cell stage inner cells (*i.e.* what could be classified as defective asymmetric cell divisions in regard to eventual spatial positioning of daughter cells in the embryo), it was decided to directly assay the phosphorylation of 4EBP1 (*i.e.* p4EBP1 - using phospho-specific anti-sera recognising two individually targeted amino residues; *i.e.* Thr37/46 for 4EBP1) and general LARP1 expression in culture mouse embryos, with or without mTOR inhibition, around this developmental window.

Accordingly, 2-cell stage mouse embryos were *in vitro* cultured until the late 8-cell stage (E2.5+4 hours) and split in to two equal groups. One group were further cultured to the 8- to 16-cell stage transition in media drops containing the mTOR inhibitor Torin1, whereas the second group were similarly cultured in control DMSO supplemented media. At this transitionary stage both embryo groups were fixed and immuno-fluorescently stained for p4EBP1 or LARP1 and imaging by confocal microscopy. Image analysis of specifically immuno-fluorescently stained individual blastomeres per embryo group was then conducted to quantify

the normalised expression levels of p4EBP1 and LARP1 in undivided/8-cell stage blastomeres, actively dividing blastomeres (*i.e*. undergoing mitosis) and divided daughter/16-cell stage blastomeres, under control DMSO or Torin1 mediated mTOR inhibited conditions. It was predicted the levels of pEBP1 expression would peak during cell division but would be blunted by mTOR inhibition, whereas due to the conflicting nature of the reports of LARP1 function on 7-methyl-guanosine cap-dependent and 5' UTR TOP-motif containing mRNA translation, it was difficult to predict whether LARP1 levels were expected to reduce or enhance (although a significant change in expression levels was anticipated). Figure 31 provides normalised quantification of the detected anti-p4EBP1 fluorescence, as a correlate of its endogenous expression results, obtained under the above stated conditions. Figure 32 details exemplar single z-stack confocal micrographs of such embryos stained with anti-p4EBP1 antibody under control DMSO and Torin1 mTOR inhibited conditions.

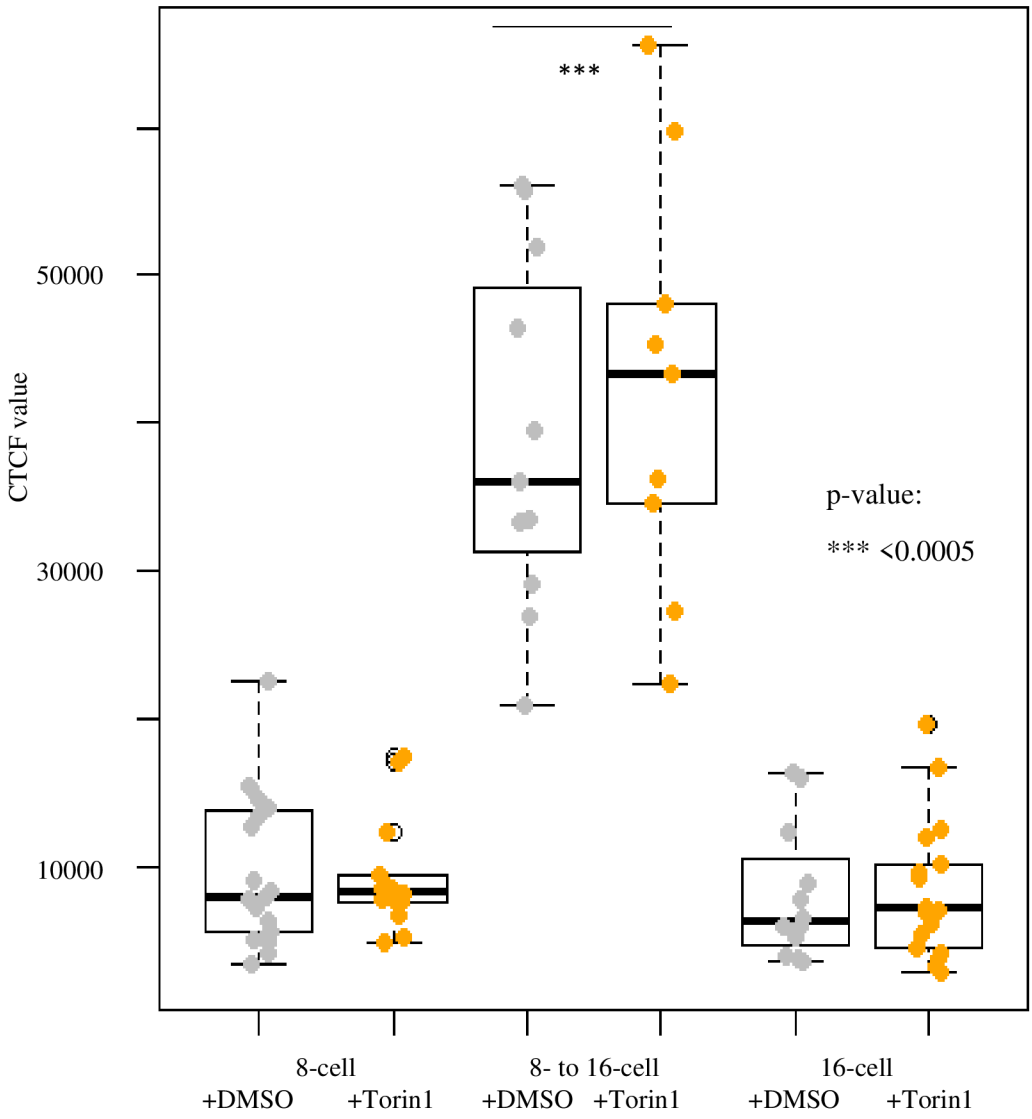

Fig. 31: A comparison of the normalised quantification (CTCF) of detected anti-p4EBP1 fluorescence of embryos cultivated from the late-8-cell (E2.5+4 hours) stage in DMSO or Torin1 at the 8-cell stage, during the 8- to 16-cell stage transition at the 16-cell stage.

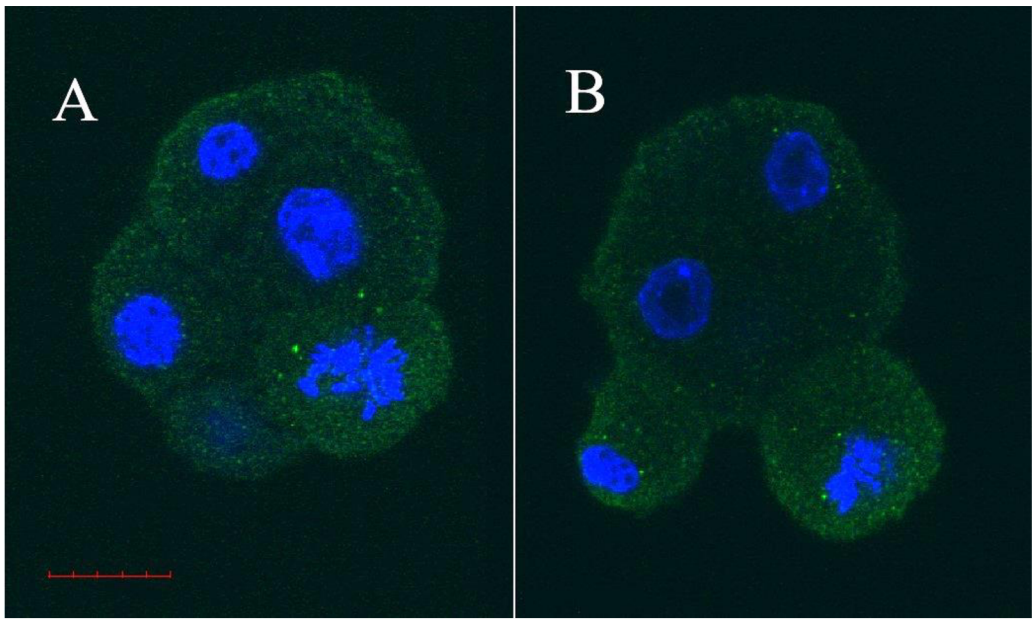

Fig. 32: Single z-stack confocal micrographs of embryos stained with anti-p4EBP1 antibody A – embryo cultivated in DMSO condition, B- embryo cultivated in Torin1 condition, Scale bar = 20µm

As can be seen, p4EBP1 (pThr37/46) expression levels were surprisingly not significantly altered between pairs of control DMSO or mTOR inhibited Torin1 conditions in either undivided 8-cell, mitotic or post-division 16-cell stage blastomeres. However, there was a clear and statistically significant increase in p4EBP1 expression as 8-cell stage blastomeres entered mitosis, with expression returning to levels in 16-cell stage interphase blastomeres statistically equivalent to those of interphase 8-cell stage blastomeres; also clearly visible in the illustrative confocal micrographs. These data suggest, if the specific p4EBP1 anti-sera are indeed specific, no change in the phosphorylation of Thr37 nor Thr46 of 4EBP1 under mTOR inhibited conditions at any one stage occurs but levels increase during mitosis and could reflect elevated levels of mRNA protein translation during active cell division. Whilst these specific amino acids represent known and reported mTOR substrates, they have also been described as target residues for other kinases (GSK3, Proto-oncogene serin / threonin-protein kinase, Leucine-rich repeat kinase 2)(Qin, Jiang and Zhang, 2016). It is therefore possible phosphorylation of these residues is important during 8-cell stage blastomere division, possibly to drive translation of mRNA transcripts important for deriving proteins involved in subsequent spatial allocation of daughter cells at the 16-cell stage, but are not targeted by mTOR directly (although this would only represent

informed speculation). There are however still other residues on 4EBP1 that may play an active role and have also been shown to be mTOR targets (Ser 65, Thr 70, Ser 83, Ser 101, and Ser 112)(Qin, Jiang and Zhang, 2016). Interestingly, subsequent work independently conducted by others in the laboratory, using phospho-specific anti-4EBP1 antibodies targeting such residues, have revealed similar M-phase associated elevations in expression that are indeed blunted by inhibition of mTOR (Bruce & Gahurova – *unpublished observations* – further commented upon in the Discussion section to this thesis).

In addition to assaying p4EBP1 protein expression levels, the expression of LARP1 protein was also assayed using a similar immuno-fluorescent staining experimental approach (note, the anti-LARP1 antibody used only recognises general LARP1 protein, irrespective of phosphorylation status – no phospho-specific anti-sera currently exist). However, rather than making individual blastomere observations and associated anti-LARP1 immuno-fluorescent quantification measurements, the expression level in the entire embryo as a whole was quantified (because there were no difference between dividing and nondividing cells). Accordingly, the experimental groups included embryos transiting the 8- to 16-cell stages and those which had completed the transition (*i.e.* comprised 16 individual interphase cells), under both DMSO control and Torin1 mediated mTOR inhibition conditions. Normalised quantification of the detected fluorescence, as a correlate of LARP1 protein expression levels, are summarised in figure 33 and illustrative fluorescent confocal micrographs (representing projected z-sections of the entire imaged embryo) of the four measured experimental conditions are provided in figure 34. The data report statistically significant increases in general LARP1 expression levels in 8- to 16-cell stage-transiting embryos comprising mitotic cells, compared to those that have completed entry into the 16-cell stage. Moreover, treatment with Torin1 to inhibit mTOR activity actually significantly increased the expression of LARP1 protein in both stage-transiting and *bona fide* 16-cell stage embryos; indicative of a feed forward loop that may act to potentiate impaired protein translation (although this only represents informed speculation - *see Introduction section of this thesis*).

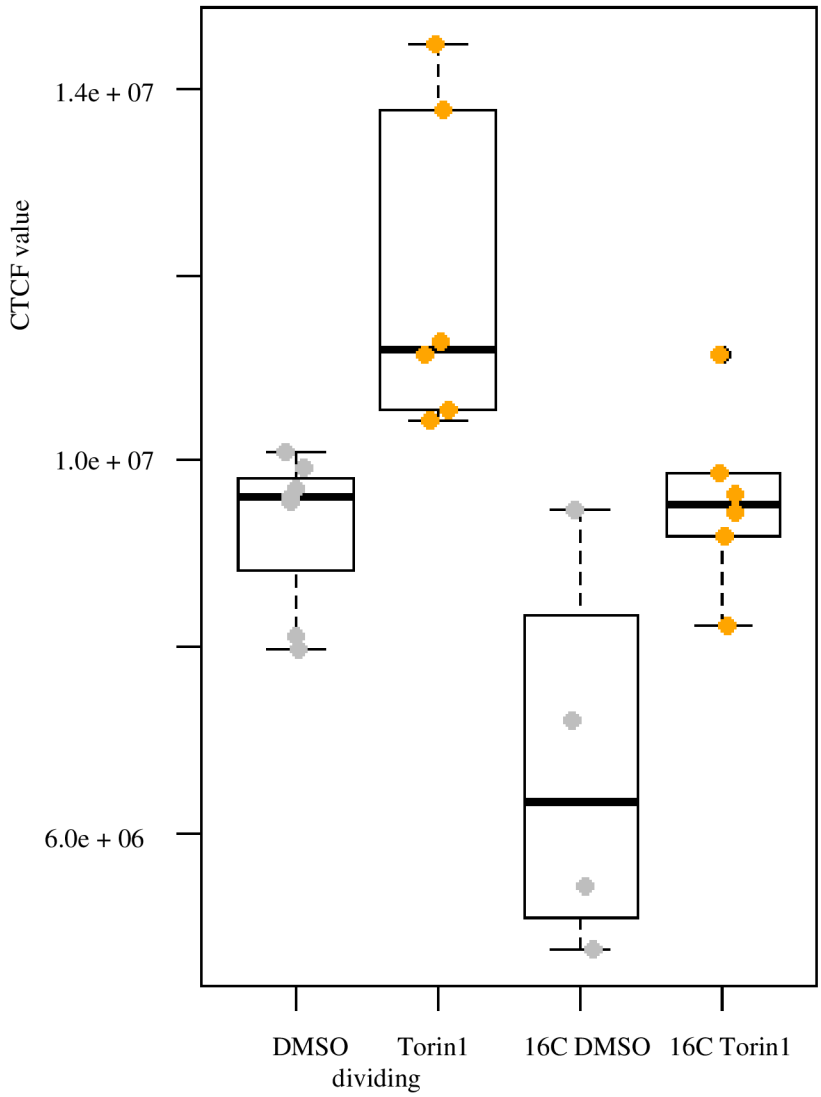

Fig. 33: A comparison of the normalised quantification of detected anti-LARP1 antibody fluorescence (CTCF) of embryos cultivated from the late-8-cell (E2.5+4 hours) stage in DMSO or Torin1, during the 8- to 16-cell stage transition or in confirmed 16-cell stage embryos.

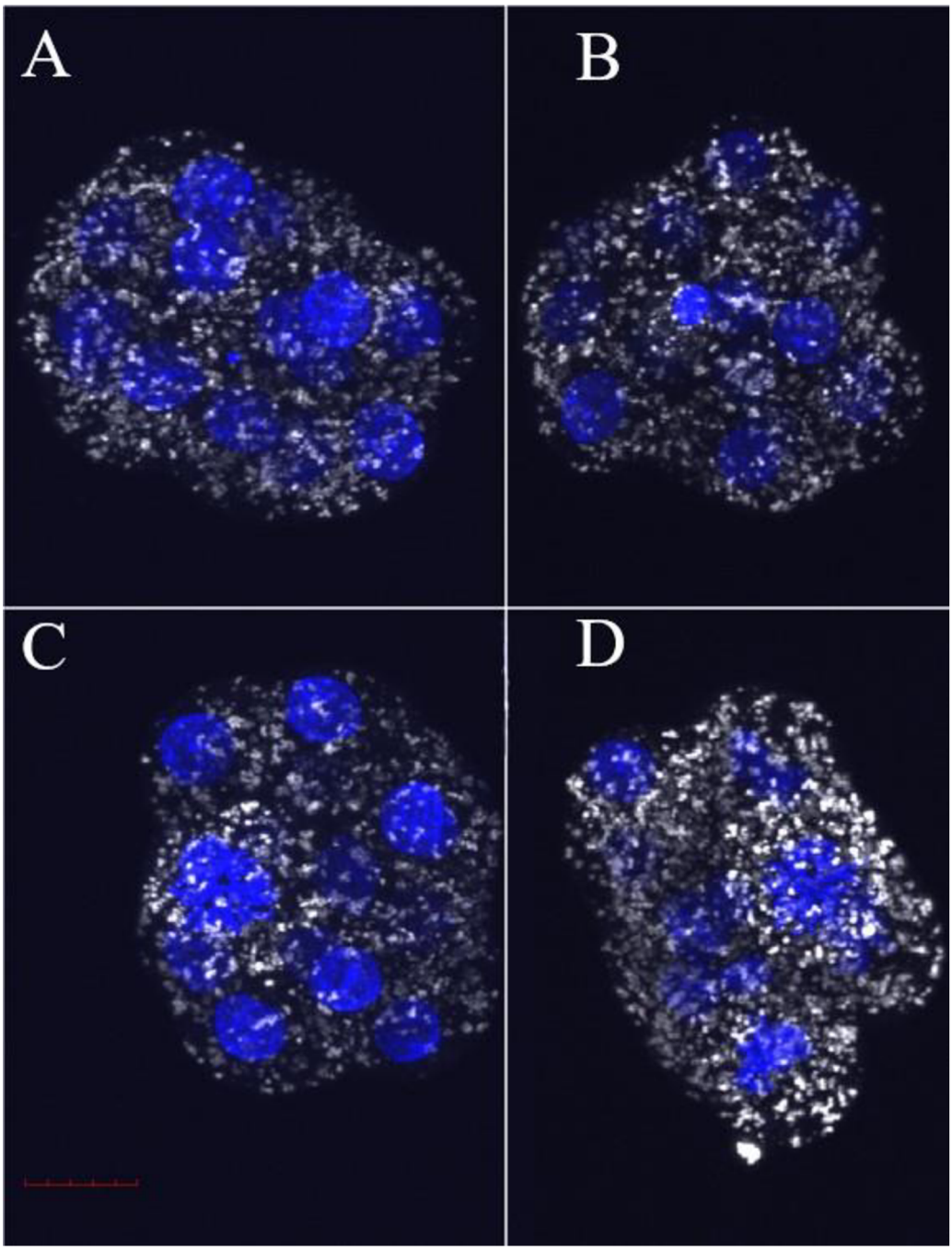

Fig. 34: Illustrative projected z-series confocal micrographs of whole embryos stained with anti-LARP antibody under the following conditions: A. 16-cell stage embryo cultivated in DMSO containing medium, B. 16-cell stage embryo cultivated in Torin1 (mTOR inhibition) containing media, C. Dividing 8-cell stage embryo cultivated in DMSO containing media, D. Dividing 8-cell stage embryo cultivated in Torin1 (mTOR inhibited) containing media. Scale bar = 30µm

5. Discussion.

The first aim of this thesis was to investigate the effect of mTOR inhibition on 16-cell stage embryos after using the drug Rapamycin. It was assumed that Rapamycin, as a known mTOR inhibitor, would have the same inhibitory impact on the generation of 16-cell stage inner cells as Torin1, (which caused a decreased number of inner cells following the 8-cell to16-cell transition). This hypothesis was confirmed and independently verified the role active mTOR signalling in the generation of the first wave of inner ICM founder cells. Additionally, as Rapamycin selectively targets mTOR as part of the mTORC1 and not mTORC2 complexes (unlike Torin1) these data refine such a role for mTOR acting within the context of the mTORC1 complex. The precise regulatory mechanism by which active mTOR/mTORC1, during and shortly after the 8- to 16-cell stage transition, results in the generation of an appropriate number of inner cells at the 16-cell stage is unknow. However, we hypothesise (partly based on data presented in this thesis and other results in the laboratory) that it is predicated upon regulated protein translation, potentially involving a subset of specific and functionally relevant mRNA transcripts. Several studies have been published, attempting to clarify the role of mTOR during murine preimplantation development. Zamfirescu and colleagues show that blastocysts cultivated for a couple of hours in medium without amino acids have decreased mTORC1 activity (with similar but greater effects observed in earlier stage embryos also cultured in the absence of amino acids) and that this signalling activity can be partially restored by provision of exogenous amino acids (Zamfirescu, Day and Morris, 2021); providing evidence of a consistent feedback link mechanism between amino-acid availability and necessary mTORC1 activity required to sustain protein translation. Susor and co-workers have also clarified that in the meiotically maturing mouse oocyte, mTOR actively controls protein translation and hence impacts normal spindle assembly, chromosome alignment, chromosome segregation and extrusion of the first polar body (Susor *et al.*, 2015). It is tempting to speculate similar mTOR/mTORC1 dependent mechanisms are operative in regulating relative spatial positioning of daughter cells as a consequence of the 8- to 16-cell transition. However, other evidence emerging from our laboratory strongly suggests spindle positioning and a regulation of cell division planes are not significantly affected under conditions of mTOR

inhibition (Bruce & Gahurova – *unpublished confocal microscopy time-lapse observations*) It has also been shown that mice homozygous for the disrupted *Mtor* gene can arrest development shortly after uterine implantation at E5.5 or are severely runted and display an aberrant developmental phenotype (Gangloff *et al.*, 2004; Shor, Cavender and Harris, 2009); that may be related to sub-optimal blastocyst formation, possibly involving the impaired segregation of initial ICM founding cells at the 16-cell stages, as implicated from our mTOR inhibition results (plus pharmacological intervention of related pathways). Although, pharmacological inhibition of mTOR activity in maturing mouse blastocysts from E3.5 has also been implicated with inducing a reversible state of developmental diapause (Bulut-Karslioglu *et al.*, 2017), suggesting the observed E5.5. embryonic lethal phenoype of *Mtor* knockout mice is likely to be multi-factorial in nature.

Interestingly, it also seems the mTOR dependent positioning of cells during/after the 8- to 16-cell transition in 16-cell stage embryos is unique to this cleavage division (developmental time point), as we are unable to demonstrate further mTOR sensitivity in regard to generating additional inner cells during the 16- to 32-cell transition (*i.e.* from outer-residing dividing cells – the second wave of cell internalisation); moreover, the deficit number of early 32-cell stage (E3.5) blastocyst inner cells caused by mTOR inhibition from the 8- to 16-cell stage transition (or indeed limited to it) can be naturally corrected during blastocyst maturation, to reflect a germane number by the time of peri-implantation (*i.e.* E4.5 - possibly via a reduced rate of apoptosis that normally occurs in the ICM during this developmental window; Bruce & Gahurova – *unpublished observations*). Such eventual correction in ICM cell number clearly demonstrates the remarkable regulative capacity of the embryo and its ability to adapt its development under abnormal circumstances; helping to explain why preimplantation mammalian development is so regulative (rather than deterministic) in nature.

As referenced above, the Rapamycin related results presented in this thesis indicate the mTOR inhibition phenotypes in 16-cell stage inner cell number are mediated by mTORC1 and not mTORC2 complexes, and potentially to one of the known cellular processes mTORC1 regulates. Indeed, mTORC1 and not mTORC2 is known participate in the regulation of mRNA translation; thus, these

results provide extra confidence that such impaired inner cell allocation phenotypes have their foundation in regulation of protein synthesis and potentially of specific mRNAs, containing so-called TOP-motifs in their 5'UTR, via 7-methyl-guanosine-cap-dependant mechanisms requiring elevated levels of mTOR signalling compared to more general transcripts (as described in the *Introduction* section of this thesis). It is tempting to speculate that such specific/individual mRNA transcripts maybe related to regulation of cytoskeletal function and/or dynamics, possibly involving small GTPase regulation as observed mTOR control of mouse oocyte meiotic maturation and first polar body extrusion (Lee *et al.*, 2012); although this still remains to be directly and completely addressed in our laboratory. One way in which this dependency on protein translation may be experimentally tested independently would be to employ other small molecule inhibitors that directly target the ribosome and protein synthesis during the same mTOR inhibition sensitive window (*i.e.* the 8- to 16-cell transition), and assay for phenocopies of reduced inner cell allocation. One such compound could be the naturally occurring fungicide cycloheximide, that blocks the translocation step of the elongation phase of the ribosome cycle (Beugnet *et al.*, 2003); however, this treatment may prove too generic in blocking translation of all mRNAs rather than those hypothesised to be especially sensitive to levels of mTOR signalling (as suggested above)[1].

In an attempt to better understand the mTOR inhibition mediated 16-cell stage inner cell phenotypes, a number of other pathways, known in the literature exhibit regulatory inputs to mTOR activity (Zoncu, Sabatini and Efeyan, 2012), were similarly screened in pharmacologically based assays; including such upstream regulators of mTOR as AMPK, p38-MAPK, AKT, RSK, MEK 1/2 (Gingras *et al.*, 1998; Kimura *et al.*, 2003; Thamodaran and Bruce, 2016; Bora *et al.*, 2019). Interestingly, we found that inhibition of all of these pathways, during the same brief 8- to 16-cell transition employed for Rapamycin or Torin1 mediated mTOR inhibition, resulted in varying degrees of reduced 16-cell stage inner cell

[1] Since completing this thesis, a successor student in the laboratory has attempted such cycloheximide based experiments and found the treatment, under a range of concentrations regimes, to result in arrested development shortly after administering the drug (*i.e.* during the 8- to 16-cell transition); precluding an assay of 16-cell stage inner cell generation. This most probably reflects the identified concern such general inhibition of translation is not the primary mechanism of the mTOR inhibition effects we observe but leaves the possibility of regulation of specific mRNA translation as a contributing mechanism.

generation phenocopy. These data suggest functional inputs from multiple intra-cellular signalling cascades all contribute to attain a level of sufficient mTOR/mTORC1 activity required to generate an appropriate number of ICM founder cells, by the 16-cell stage, during the first wave of potential blastomere internalisation. The exact mechanistic triggers responsible for the activation of such pathways, in the context of the preimplantation mouse embryo, remain unknown but could potentially arise from both extra-cellular communication by secreted signalling ligands interacting with their plasma membrane bound receptors and/or intrinsic mechanism such as nutrient sensing or mechanosensory inputs.

As signalling via the FGF family of ligands has been implicated in both first (TE versus ICM – via FGF2 (Hermitte and Chazaud, 2014)) and second (EPI versus PrE - via FGF4 (Yang *et al.*, 2015) cell fate decisions, it was hypothesised similar FGF-based signalling may provide an input to regulate mTOR activity around the 8- to 16-cell transition, especially as activation of FGF-receptors (or their pharmacological inhibition) has also been linked to the activation of ERK1/2 mitogen-activated-kinase pathway (Yamanaka, Lanner and Rossant, 2010); a pathway that when inhibited as described herein (via targeted inhibition of the intermediary, and ERK1/2 activating, MEK1/2 kinases), resulted in fewer inner 16-cell stage blastomeres. However, using an inhibitor (SU 5402) that that targets all three murine FGF-receptor isoforms (*i.e.* FGFR1, FGFR2 and FGFR3), and that had previously been shown in the laboratory to block PrE formation when administered to maturing mouse blastocysts (Thamodaran and Bruce, 2016), we were not able to elicit a reduced inner cell 16-cell stage phenocopy of mTOR inhibition (or, indeed, MEK1/2 inhibition). This result suggests that whilst FGF-based cell signalling is undoubtedly crucial for preimplantation mouse embryo development and derivation of the three blastocyst lineages, it is not important in regulating 16-cell stage inner cell derivation and is unlikely to affect the critical activity of mTOR during the important 8- to 16-cell transition. Similar negative results were also obtained when targeting CDK1, PLK1 and PP2A by chemical inhibition, despite reports emanating from studies in meiotically maturing mouse oocytes (sometimes conflicting – see below) that suggest the involvement of mTOR in controlling enhanced spindle localised protein translation, via direct and indirect mechanisms of 4EBP1 phosphorylation, and regulation of germane

meiotic cell division (*i.e.* appropriate segregation of homologous chromosomes in meiosis I and first polar body extrusion/formation (Susor *et al.*, 2015; Jansova *et al.*, 2017)). These presented CDK1, PLK1 and PP2A inhibition-based results suggest such pathways are not important for mTOR mediated spatial separation of blastomeres by the 16-cell stage, despite the similar and/or related precedents in oocyte maturation. Thus, confirming the regulatory output of mTOR activity in relation to cell division is most probably highly context dependent. Indeed, even in the studies of the meiotic mouse oocyte model, the exact role of mTOR in relation to 4EBP1 and regulation of protein translation is contested, with one group implicating mTOR and CDK1 (Jansova *et al.*, 2017) and another proposing PLK1 (Jansova *et al.*, 2017; Severance, A. and Latham, K., 2017); highlighting the complexity and current lack of clarity in the early developmental field.

The last aim of the project was to test our hypothesis that mTOR does indeed play a specific role in translation regulation, that is important for spatial allocation of blastomeres by the 16-cell stage. The described experiments in which recombinant mRNA encoding either wild-type 4EBP1 (as explained in the *Introduction,* an inhibitory factor of protein translation that in its non-phosphorylated state acts by sequestering the translation initiation factor EIF4E from the EIF4F/mRNA 7-methyl-guanosine-cap binding complex (Richter and Sonenberg, 2005)) or the non-phosphorylatable 4EBP1-4Ala dominant negative mutant (lacking substrate Serine/Threonine residues for mTOR phosphorylation, needed to liberate its sequestering interaction with EIF4E) were microinjected into one cell of 2-cell stage mouse embryos, provided additional evidence of this link to specific protein translation as being important. This was because the clonal progeny of cells microinjected with *4ebp1-4Ala* mRNA significantly contributed less 16-cell stage inner blastomeres (compared to controls including the recombinant *4ebp1* mRNA microinjected embryos and noninjected embryo controls), in a phenocopy of mTOR inhibition during the 8- top 16-cell transition. Hence, implicating the phosphorylation of 4EBP1, a mTOR/mTORC1 substrate (Gao *et al.*, 2012), as being an important mechanistic component regulating the generation inner (and outer) blastomeres in the 16-cell stage embryo. It had been hoped that we could develop this specific link to protein translation further by ameliorating mTOR/mTORC1 inhibition (using Torin1) induced deficits in 16-cell stage inner blastomere cell numbers by over-expressing recombinant EIF4E

(hence, circumventing the hypothesised lack of endogenous EIF4E sequestered by unphosphorylated 4EBP1, caused by mTOR/mTORC1 inhibition). However, the anticipated result was not forthcoming and no amelioration was observed. On reflection, this may be because the expression levels of recombinant EIF4E achieved after recombinant mRNA microinjection were too high, resulting in so-called 'squelching effects'. Under such circumstances, other important protein components, for example related to the overall EIF4F/ mRNA 7-methyl-guanosine-cap-binding complex, are sequestered by interaction with the over-expressed recombinant EIF4E protein. This could results in a reduction in the overall concentration of functional EIF4F complexes able to directly participate in mRNA translation. One such candidate would be the known EIF4E interactor protein EIF4G (together with EIF4A, another component of the overall EIF4F complex - (Richter and Sonenberg, 2005)). If time had permitted, one way in which to test this hypothesis would have been to perform a titration series of the concentration/amount of recombinant *Eif4e* mRNA microinjected into 2-cell stage blastomeres, and then assay the effect of mTOR inhibition (+Torin1/Rapamycin) on 16-cell stage inner blastomere generation. It might be expected that such an approach would identify a condition in which a sufficiency of over-expressed recombinant EIF4E protein could ameliorate the effects of mTOR inhibition, providing enough EIF4E protein to sustain a required population of functional EIF4F/mRNA 7-methyl-guanosine-cap-binding complex to drive translation of critically important mRNA transcripts, without generic effects of reduced translation caused by 'squelching'. Indeed, the fact that in the presented recombinant EIF4E over-expression experiments, embryonic development was not arrested (as was the case when cycloheximide was applied to embryos in the same developmental time window – see above; Bruce & Gahurova, *unpublished observations*) strongly argues the reduced 16-cell stage inner cell phenotypes caused by mTOR/mTORC1 inhibition are indeed actually caused by reduced translation of a subset of uniquely mTOR/mTORC1 sensitive mRNA transcripts (possibly defined by the presence of a 5'UTR located TOP-motif) rather than generally reduced translation. Although, this still needs to be directly tested, and the suggested titration of recombinant EIF4E protein expression under such mTOR/mTORC1 inhibited conditions would go some way to resolving this outstanding question. It is also documented in the literature that

in some mTOR inhibition based anti-tumour therapies, human cancer cells can acquire resistance to mTOR inhibition via a downregulation of EIF4E expression or genetic loss of a 4EBP1 encoding gene. Consistently, depleted expression of these targets prove the anti-tumour effects of mTOR inhibition is dependent of these key protein translational regulators (*i.e.* components of the overall EIF4F/mRNA 7-methyl-guanosine-cap-binding complex (Alain *et al.*, 2012)). Furthermore, the authors of this study propose the ratio between eIF4E and 4EBP1 protein expression is the key marker in the prediction of clinical therapeutic outcomes of mTOR inhibitor-based cancer treatments (Alain *et al.*, 2012). It is therefore possible that in the recombinant EIF4E over-expression experiments presented in this thesis, the obtained ratio between EIF4E and 4EBP1 protein expression may not have been optimal to drive the levels of 7-methyl-guanosine-cap-dependent mRNA translation needed to observe amelioration of mTOR/mTORC1 inhibition mediated deficits in 16-cell stage inner blastomere generation; these finding support the proposed experiments aimed at titrating the concentration/amount of recombinant *Eif4e* mRNA initially microinjected and thus the expression level of recombinant EIF4E protein needed to rescue the effect of mTOR/mTORC1 inhibition.

In connection to these experiments we also measured the expression levels of endogenous p4EBP1 (using a phospho-specific anti-sera recognising two known mTOR targeted amino residues *i.e.* Thr37/46 4EBP1(Qin, Jiang and Zhang, 2016)). It was expected the detected levels of p4EBP1 would increases during the 8- to 16-cell transition, as increased p4EBP1 would be needed to drive translation of mTOR sensitive TOP-motif containing mRNA transcripts, required to ensure germane inner cell generation. However, the hypothesised result was not confirmed. It is possible that this may indicate these specific mTOR target residues are not so important in the context of the generation of 16-cell stage inner cells (as reflected in studies of specific p4EBP1 iso-/phospho-form localisation around the meiotic spindles of mouse oocytes undergoing meiosis I (Jansova *et al.*, 2017)). Another explanation may be that the individual antibody used is not as specific as claimed and hence it is not possible to observe the predicted effect. To address these potential points, additional experimentation should be performed using alternative anti-p4EBP1 antibodies, including those that targeted different amino acids substrates, also known to be targeted by

mTOR[2] (Ser 65, Thr 70, Ser 83, Ser 101, and Ser 112(Qin, Jiang and Zhang, 2016)).

Regarding our measurements of LARP1 protein expression, we did not fully anticipate how expression may change during the 8- to 16-cell transition. This was mainly because there is a paucity of relevant LARP1 related literature (that depending on cell context is conflicting (Fonseca *et al.*, 2015, 2018; Fuentes *et al.*, 2021)). Nevertheless, given there are described functional links between mTOR signalling and LARP1 expression/function, in relation to TOP-motif containing mRNA transcripts, we reasoned any observed changes in LARP1 expression during the mTOR sensitive 8- to 16-cell window could be informative and contribute to the wider literature. Indeed, our data report statistically significant increases in general LARP1 (*i.e.* unphosphorylated – note, a phospho-specific anti-sera is unavailable) expression levels in embryos transiting the 8- to 16-cell stages (*i.e.* mitotic cells), compared to those that have completed entry into the 16-cell stage. However, treatment with Torin1 to inhibit mTOR activity actually significantly increased detectable expression of LARP1 protein in both transiting and *bona fide* 16-cell stage embryos. Notwithstanding this unexpected result, it is consistent with the findings of Fonsecas and colleagues who describe a blunting of the effect of reduced translation of TOP-motif containing mRNAs caused by mTORC1 inhibition, when LARP1 levels were experimentally reduced (Fonseca *et al.*, 2015). Accordingly, we conclude LARP1 may also be an important molecular component of the mTOR inhibition phenotype of reduced inner cell generation at the 16-cell stage but that this requires more in-depth investigation.

This thesis and experiments it contains form part of a wider project within the laboratory, aimed at further clarifying the cellular processes around the regulation of mTOR activity, the specific effects on protein translation and the consequences for germane cell fate derivation in the developing preimplantation mouse embryo. As part of this effort, successors students (and post-doctoral researchers – *i.e.* Lenka Gahurova) have also investigated mTOR inhibition in later embryonic stages and performed immuno-fluorescent staining of related

[2] Since completing my experimental work, another student has undertaken such experiments that focus on p4EBP1 expression during the late 8-cell stage and entry into M-phase and confirmed increased levels of p4EBP1 protein expression, that are reduced after concomitant mTOR inhibition.

proteins, to better understand how mTOR dependant translation affects generation of inner cells and the subsequently derived EPI and PrE lineages. This collective effort is currently being written up in a manuscript with the aimed intention of publication in 2022.

6. References

Ajduk, A., Biswas, S. and Zernicka-goetz, M. (2014) 'The basal position of nuclei is one pre-requisite for asymmetric cell divisions in the early mouse embryo', *Developmental Biology*. Elsevier, pp. 1–8. doi: 10.1016/j.ydbio.2014.05.009.

Aksoy, I. *et al.* (2013) 'Oct4 switches partnering from Sox2 to Sox17 to reinterpret the enhancer code and specify endoderm.', *The EMBO journal*, 32(7), pp. 938–953. doi: 10.1038/emboj.2013.31.

Alain, T. *et al.* (2012) 'eIF4E / 4E-BP Ratio Predicts the Ef fi cacy of mTOR Targeted Therapies', *Cancer Research*, 72(24), pp. 6468–6477. doi: 10.1158/0008-5472.CAN-12-2395.

Alarcon, V. B. (2010) 'Cell Polarity Regulator PARD6B Is Essential for Trophectoderm Formation in the Preimplantation Mouse Embryo 1', *Biology of Reproduction*, 83, pp. 347–358. doi: 10.1095/biolreprod.110.084400.

Anani, S. *et al.* (2014) 'Initiation of Hippo signaling is linked to polarity rather than to cell position in the pre-implantation mouse embryo', *Development*, 141(14), pp. 2813–2824. doi: 10.1242/dev.107276.

Aoki, F., Worrad, D. M. and Schultz, R. M. (1997) 'Regulation of Transcriptional Activity during the First and Second Cell Cycles in the Preimplantation Mouse Embryo', *Developmental Biology*, 181(2), pp. 296–307. doi: https://doi.org/10.1006/dbio.1996.8466.

Artus, J., Piliszek, A. and Hadjantonakis, A.-K. (2011) 'The primitive endoderm lineage of the mouse blastocyst: Sequential transcription factor activation and regulation of differentiation by Sox17', *Developmental Biology*, 350(2), pp. 393–404. doi: https://doi.org/10.1016/j.ydbio.2010.12.007.

Azami, T. *et al.* (2019) 'Regulation of the ERK signalling pathway in the developing mouse blastocyst', *Development*, 146. doi: 10.1242/dev.177139.

Bessonnard, S. *et al.* (2014) 'Gata6, Nanog and Erk signaling control cell fate in the inner cell mass through a tristable regulatory network.', *Development (Cambridge, England)*. England, 141(19), pp. 3637–3648. doi: 10.1242/dev.109678.

Beugnet, A. *et al.* (2003) 'Regulation of targets of mTOR (mammalian target of rapamycin) signalling by intracellular amino acid availability', *Biochemical Journal*, 372(2), pp. 555–566. doi: 10.1042/BJ20021266.

Bischoff, M., Parfitt, D. and Zernicka-goetz, M. (2008) 'Europe PMC Funders Group Formation of the embryonic-abembryonic axis of the mouse blastocyst : relationships between orientation of early cleavage divisions and pattern of symmetric / asymmetric divisions', 135(5), pp. 953–962. doi: 10.1242/dev.014316.Formation.

Bora, P. *et al.* (2019) 'p38-Mitogen Activated Kinases Mediate a Developmental Regulatory Response to Amino Acid Depletion and Associated Oxidative Stress in Mouse Blastocyst Embryos', *Frontiers in Cell and Developmental Biology*, 7(276). doi: 10.3389/fcell.2019.00276.

Bora, P., Gahurova, L., Hauserova, A., *et al.* (2021) 'DDX21 is a p38-MAPK-sensitive nucleolar protein necessary for mouse preimplantation embryo development and cell-fate specification', *Open Biology*, 11. doi: 10.1098/rsob.210092.

Bora, P., Gahurova, L., Mašek, T., *et al.* (2021) 'p38-MAPK-mediated translation regulation during early blastocyst development is required for primitive endoderm differentiation in mice', *communications biology*, pp. 1–19. doi: 10.1038/s42003-021-02290-z.

Bruce, A. W. and Zernicka-Goetz, M. (2010) 'Developmental control of the early mammalian embryo: competition among heterogeneous cells that biases cell fate.', *Current opinion in genetics & development*. England, 20(5), pp. 485–491. doi: 10.1016/j.gde.2010.05.006.

Bulut-Karslioglu, A. *et al.* (2017) 'Inhibition of mTor induces a paused pluripotent state', *Nature*, 540(7631), pp. 119–123. doi: 10.1038/nature20578.Inhibition.

Chazaud, C. *et al.* (2006) 'Early Lineage Segregation between Epiblast and Primitive Endoderm in Mouse Blastocysts through the Grb2-MAPK Pathway', *Developmental Cell*, 10, pp. 615–624. doi: 10.1016/j.devcel.2006.02.020.

Chazaud, C. and Yamanaka, Y. (2016) 'Lineage specification in the mouse

preimplantation embryo', *The Company of Biologists*, 143, pp. 1063–1074. doi: 10.1242/dev.128314.

Cockburn, K. *et al.* (2013) 'The Hippo Pathway Member Nf2 Is Required for Inner Cell Mass Specification', *Current Biology*. Elsevier Ltd, 23, pp. 1195–1201. doi: 10.1016/j.cub.2013.05.044.

Dard, N. *et al.* (2004) 'Phosphorylation of ezrin on threonine T567 plays a crucial role during compaction in the mouse early embryo', *Developmental Biology*, 271(1), pp. 87–97. doi: https://doi.org/10.1016/j.ydbio.2004.03.024.

Dazert, E. and Hall, M. N. (2011) 'mTOR signaling in disease', *Current opinion in cell biology*, 23, pp. 744–755. doi: 10.1016/j.ceb.2011.09.003.

Dowling, R. J. O. *et al.* (2010) 'Dissecting the role of mTOR : Lessons from mTOR inhibitors', *BBA - Proteins and Proteomics*, 1804(3), pp. 433–439. doi: 10.1016/j.bbapap.2009.12.001.

Enders, Allen, C., Given, Randall, L. and Schlafke, S. (1978) 'Differentiation and Migration of Endoderm in the Rat and Mouse at Implantation 1', *The Anatomical record*, 190, pp. 65–77.

Fonseca, B. D. *et al.* (2015) 'La-related Protein 1 (LARP1) Represses Terminal Oligopyrimidine (TOP) mRNA Translation Downstream of mTOR Complex 1 (mTORC1) * □', *The Journal of biological chemistry*, 290(26), pp. 15996–16020. doi: 10.1074/jbc.M114.621730.

Fonseca, B. D. *et al.* (2018) 'LARP1 is a major phosphorylation substrate of mTORC1', *bioRxiv*, 491274. doi: https://doi.org/10.1101/491274.

Frum, T. *et al.* (2013) 'Oct4 cell-autonomously promotes primitive endoderm development in the mouse blastocyst.', *Developmental cell*, 25(6), pp. 610–622. doi: 10.1016/j.devcel.2013.05.004.

Fuentes, P. *et al.* (2021) 'The 40 S -LARP1 complex reprograms the cellular translatome upon mTOR inhibition to preserve the protein synthetic capacity', *Science Advances*, 7(48). doi: 10.1126/sciadv.abg9275.

Gangloff, Y.-G. *et al.* (2004) 'Disruption of the Mouse mTOR Gene Leads to Early Postimplantation Lethality and Prohibits Embryonic Stem Cell Development', *Molecular and Cellular Biology*, 24(21), pp. 9508–9516. doi:

10.1128/MCB.24.21.9508.

Gao, W. *et al.* (2012) 'mTOR Pathway and mTOR Inhibitors in Head and Neck Cancer', *ISRN Otolaryngology*, 2012. doi: 10.5402/2012/953089.

Gardner, R. L. (1982) 'Investigation of cell lineage and differentiation in the extraembryonic endoderm of the mouse embryo.', *Journal of embryology and experimental morphology*. England, 68, pp. 175–198.

Gingras, A. *et al.* (1998) '4E-BP1, a repressor of mRNA translation, is phosphorylated and inactivated by the Akt(PKB) signaling pathway', *Genes & development*, 12(4), pp. 502–513. doi: 10.1101/gad.12.4.502.

Goolam, M. *et al.* (2016) 'Heterogeneity in Oct4 and Sox2 Targets Biases Cell Fate in 4-Cell Mouse Embryos Article Heterogeneity in Oct4 and Sox2 Targets Biases Cell Fate in 4-Cell Mouse Embryos', *Cell*. The Authors, 165(1), pp. 61–74. doi: 10.1016/j.cell.2016.01.047.

Guertin, D. A. and Sabatini, D. M. (2007) 'Defining the Role of mTOR in Cancer', *Cancer Cell*, 12(1), pp. 9–22. doi: 10.1016/j.ccr.2007.05.008.

Guo, G. *et al.* (2010) 'Resolution of Cell Fate Decisions Revealed by Single-Cell Gene Expression Analysis from Zygote to Blastocyst', *Developmental Cell*. Elsevier Ltd, 18(4), pp. 675–685. doi: 10.1016/j.devcel.2010.02.012.

Hamilton, T. L. *et al.* (2006) 'TOPs and their regulation', *Biochemical Society Transactions*, 34, pp. 12–16. doi: 10.1042/BST20060012.

Heasman, S. J. and Ridley, A. J. (2008) 'Mammalian Rho GTPases : new insights into their functions from in vivo studies', *Nature Reviews Molecular Cell Biology*, 9, pp. 690–701. doi: 10.1038/nrm2476.

Hermitte, S. and Chazaud, C. (2014) 'Primitive endoderm differentiation: from specification to epithelium formation', *Philosophical Transactions of the Royal Society B: Biological Sciences*, 369, pp. 81–104. doi: 10.1016/bs.ctdb.2017.12.001.

Hirate, Y., Hirahara, S., Inoue, K. I., *et al.* (2013) 'Polarity-dependent distribution of angiomotin localizes hippo signaling in preimplantation embryos', *Current Biology*. Elsevier Ltd, 23, pp. 1181–1194. doi: 10.1016/j.cub.2013.05.014.

Jansova, D. *et al.* (2017) 'Regulation of 4E-BP1 activity in the mammalian oocyte', *Cell Cycle*. Taylor & Francis, 16(10), pp. 927–939. doi: 10.1080/15384101.2017.1295178.

Jedrusik, A. *et al.* (2008) 'Role of Cdx2 and cell polarity in cell allocation and specification of trophectoderm and inner cell mass in the mouse embryo.', *Genes & development*, 22(19), pp. 2692–2706. doi: 10.1101/gad.486108.

Johnson, M. H. (2009) 'From Mouse Egg to Mouse Embryo: Polarities, Axes, and Tissues', *Annual Review of Cell and Developmental Biology*, 25(1), pp. 483–512. doi: 10.1146/annurev.cellbio.042308.113348.

Johnson, M. H. and McConnell, J. M. L. (2004) 'Lineage allocation and cell polarity during mouse embryogenesis', *Seminars in Cell & Developmental Biology*, 15(5), pp. 583–597. doi: https://doi.org/10.1016/j.semcdb.2004.04.002.

Johnson, M. H. and Ziomek, C. A. (1981) 'The Foundation of Two Distinct within the Mouse Morula', *Cell*, 24, pp. 71–80. doi: https://doi.org/10.1016/0092-8674(81)90502-X.

Kalous, J., Jansova, D. and Šušor, A. (2020) 'Role of Cyclin-Dependent Kinase 1 in Translational Regulation in the M-Phase', *Cells*, 9, pp. 1–14. doi: 10.3390/cells9071568.

Kang, M. *et al.* (2013) 'FGF4 is required for lineage restriction and salt-and-pepper distribution of primitive endoderm factors but not their initial expression in the mouse', *Development (Cambridge)*. Elsevier Inc., 140(2), pp. 496–510. doi: 10.1242/dev.084996.

Kang, M., Garg, V. and Hadjantonakis, A. K. (2017) 'Lineage Establishment and Progression within the Inner Cell Mass of the Mouse Blastocyst Requires FGFR1 and FGFR2', *Developmental Cell*, 41(5), pp. 496–510. doi: 10.1016/j.devcel.2017.05.003.

Kim, A. J. and Griffin, E. E. (2021) 'PLK-1 Regulation of Asymmetric Cell Division in the Early C. elegans Embryo', *Frontiers in Cell and Developmental Biology*, 8, p. 1853. doi: 10.3389/fcell.2020.632253.

Kimura, N. *et al.* (2003) 'A possible linkage between AMP-activated protein kinase (AMPK) and mammalian target of rapamycin (mTOR) signalling

pathway', *Genes to Cells*, 8, pp. 65–79. doi: 10.1046/j.1365-2443.2003.00615.x.

Kono, K., Tamashiro, D. A. A. and Alarcon, V. B. (2014) 'Inhibition of RHO-ROCK signaling enhances ICM and suppresses TE characteristics through activation of Hippo signaling in the mouse blastocyst.', *Developmental biology*, 394(1), pp. 142–155. doi: 10.1016/j.ydbio.2014.06.023.

Korotkevich, E. *et al.* (2017) 'The Apical Domain Is Required and Sufficient for the First Lineage Segregation in the Mouse Embryo', *Developmental Cell*, 40, pp. 235–247. doi: 10.1016/j.devcel.2017.01.006.

Krupa, M. *et al.* (2014) 'Allocation of inner cells to epiblast vs primitive endoderm in the mouse embryo is biased but not determined by the round of asymmetric divisions (8→16- and 16→32-cells)', *Developmental Biology*, 385(1), pp. 136–148. doi: https://doi.org/10.1016/j.ydbio.2013.09.008.

Lee, S. *et al.* (2012) 'mTOR Is Required for Asymmetric Division Through Small GTPases in Mouse Oocytes', *Molecular Reproduction and Development*, 79, pp. 356–366. doi: 10.1002/mrd.22035.

Leung, C. Y. and Zernicka-Goetz, M. (2013) 'Angiomotin prevents pluripotent lineage differentiation in mouse embryos via Hippo pathway-dependent and -independent mechanisms', *Nature Communications*. Nature Publishing Group, 4. doi: 10.1038/ncomms3251.

Liu, L. *et al.* (2010) 'Rapamycin inhibits cytoskeleton reorganization and cell motility by suppressing RhoA expression and activity', *Journal of Biological Chemistry*, 285(49), pp. 38362–38373. doi: 10.1074/jbc.M110.141168.

Ma, X. M. and Blenis, J. (2009) 'Molecular mechanisms of mTOR- mediated translational control', *Nature Reviews Molecular Cell Biology*, 10, pp. 307–318. doi: 10.1038/nrm2672.

Maekawa, M. *et al.* (2005) 'Requirement of the MAP kinase signaling pathways for mouse preimplantation development', *Development*, 132, pp. 1773–1783. doi: 10.1242/dev.01729.

Meilhac, S. M. *et al.* (2009) 'Active cell movements coupled to positional induction are involved in lineage segregation in the mouse blastocyst', *Developmental Biology*. Elsevier Inc., 331(2), pp. 210–221. doi:

10.1016/j.ydbio.2009.04.036.

Mihajlovic, A. I. and Bruce, A. W. (2016) 'Rho-associated protein kinase regulates subcellular localisation of Angiomotin and Hippo-signalling during preimplantation', *Reproductive BioMedicine Online*, 33, pp. 381–390. doi: 10.1016/j.rbmo.2016.06.028.

Mihajlovic, A. I. and Bruce, A. W. (2017) 'The first cell-fate decision of mouse preimplantation embryo development : integrating cell position and polarity', *Open Biology*, 7. doi: http://dx.doi.org/10.1098/rsob.170210.

Morris, S. A. *et al.* (2010) 'Origin and formation of the fi rst two distinct cell types of the inner cell mass in the mouse embryo', *Proceedings of the National Academy of Sciences of the United States of America*, 107(14), pp. 6364–6369. doi: 10.1073/pnas.0915063107.

Morris, S. A. *et al.* (2013) 'The differential response to Fgf signalling in cells internalized at different times influences lineage segregation in preimplantation mouse embryos', *Open Biology*, 3. doi: http://dx.doi.org/10.1098/rsob.130104.

Morris, S. A., Guo, Y. and Zernicka-Goetz, M. (2012) 'Developmental Plasticity Is Bound by Pluripotency and the Fgf and Wnt Signaling Pathways', *Cell Reports*. Elsevier, 2(4), pp. 756–765. doi: 10.1016/j.celrep.2012.08.029.

Nagy, A. *et al.* (2003) *Manipulating the Mouse Embryo: A Laboratory Manual*. Cold Spring Harbor Laboratory Press. Available at: https://books.google.cz/books?id=4juoa5xMs8oC.

Natale, D. R. *et al.* (2004) 'p38 MAPK signaling during murine preimplantation development', *Developmental Biology*, 268, pp. 76–88. doi: 10.1016/j.ydbio.2003.12.011.

Niakan, Kathy, K. *et al.* (2010) 'Sox17 promotes differentiation in mouse embryonic stem cells by directly regulating extraembryonic gene expression and indirectly antagonizing self-renewal', *Genes & development*, 24, pp. 312–326. doi: 10.1101/gad.1833510.8.

Nie, X. *et al.* (2020) 'mTOR plays a pivotal role in multiple processes of enamel organ development principally through the mTORC1 pathway and in part via regulating cytoskeleton dynamics', *Developmental Biology*. Elsevier Ltd, 467(1–

2), pp. 77–87. doi: 10.1016/j.ydbio.2020.08.010.

Nishioka, N. *et al.* (2009) 'The Hippo Signaling Pathway Components Lats and Yap Pattern Tead4 Activity to Distinguish Mouse Trophectoderm from Inner Cell Mass', *Developmental Cell*. Elsevier Ltd, 16(3), pp. 398–410. doi: 10.1016/j.devcel.2009.02.003.

Ohnishi, Y. *et al.* (2014) 'Cell-to-cell expression variability followed by signal reinforcement progressively segregates early mouse lineages.', *Nature cell biology*, 16(1), pp. 27–37. doi: 10.1038/ncb2881.

Ono, K. and Han, J. (2000) 'The p38 signal transduction pathway Activation and function', *Cellular Signalling*, 12, pp. 1–13. doi: 10.1016/s0898-6568(99)00071-6.

Peterson, Randall, T. *et al.* (1999) 'Protein phosphatase 2A interacts with the 70-kDa S6 kinase and is activated by inhibition of FKBP12–rapamycin- associated protein', *Proceedings of the National Academy of Sciences of the United States of America*, 96, pp. 4438–4442. doi: https://doi.org/10.1073/pnas.96.8.4438.

Piotrowska-Nitsche, K. *et al.* (2005) 'Four-cell stage mouse blastomeres have different developmental properties', *Development*, 132(3), pp. 479–490. doi: 10.1242/dev.01602.

Plusa, B. *et al.* (2008) 'Distinct sequential cell behaviours direct primitive endoderm formation in the mouse blastocyst', *Development*, 135(18), pp. 3081–3091. doi: 10.1242/dev.021519.

Posfai, E. *et al.* (2017) 'Position- and Hippo signaling-dependent plasticity during lineage segregation in the early mouse embryo', *eLiFE*, 6, pp. 1–24. doi: 10.7554/eLife.22906.

Qin, X., Jiang, B. and Zhang, Y. (2016) '4E-BP1, a multifactor regulated multifunctional protein', *Cell Cycle*, 15(6), pp. 781–786. doi: 10.1080/15384101.2016.1151581.

Richter, J. D. and Sonenberg, N. (2005) 'Regulation of cap-dependent translation by eIF4E inhibitory proteins', *Nature*, 433, pp. 477–480. doi: 10.1038/nature03205.

Rossant, J. (1976) 'Postimplantation development of blastomeres isolated from

4- and 8-cell mouse eggs.', *Journal of embryology and experimental morphology*. England, 36(2), pp. 283–290.

Rossant, J. and Tam, P. P. L. (2009) 'Blastocyst lineage formation , early embryonic asymmetries and axis patterning in the mouse', *Development*, 136, pp. 701–713. doi: 10.1242/dev.017178.

Ryan, A. Q. *et al.* (2019) 'Lumen Expansion Facilitates Epiblast-Primitive Endoderm Fate Specification during Mouse Blastocyst Formation', *Developmental Cell*, 51, pp. 684–697. doi: 10.1016/j.devcel.2019.10.011.

Samarage, C. R. *et al.* (2015) 'Cortical Tension Allocates the First Inner Cells of the Mammalian Embryo.', *Developmental cell*. United States, 34(4), pp. 435–447. doi: 10.1016/j.devcel.2015.07.004.

Sarbassov, D. D. *et al.* (2006) 'Prolonged Rapamycin Treatment Inhibits mTORC2 Assembly and Akt / PKB', *Molecular Cell*, 22, pp. 159–168. doi: 10.1016/j.molcel.2006.03.029.

Sasaki, H. (2010) 'Mechanisms of trophectoderm fate specification in preimplantation mouse development', *Development Growth and Differentiation*, 52, pp. 263–273. doi: 10.1111/j.1440-169X.2009.01158.x.

Sato, T. *et al.* (2016) 'Mammalian target of rapamycin (mTOR) complex 2 regulates filamin A-dependent focal adhesion dynamics and cell migration', *Genes to Cells*, 21(6), pp. 579–593. doi: 10.1111/gtc.12366.

Severance, A., L. and Latham, K., E. (2017) 'PLK1 regulates spindle association of phosphorylated eukaryotic translation initiation factor 4E binding protein, and spindle function in mouse oocytes', *American Journal of Physiology-Cell Physiology*, 313, pp. 501–515. doi: 10.1152/ajpcell.00075.2017.

Shaul, Y. D. and Seger, R. (2007) 'The MEK / ERK cascade : From signaling specificity to diverse functions', *Biochimica et Biophysica Acta*, 1773, pp. 1213–1226. doi: 10.1016/j.bbamcr.2006.10.005.

Shor, B., Cavender, D. and Harris, C. (2009) 'A kinase-dead knock-in mutation in mTOR leads to early embryonic lethality and is dispensable for the immune system in heterozygous mice', *Biomed Central Immunology*, 1. doi: 10.1186/1471-2172-10-28.

Susor, A. *et al.* (2015) 'Temporal and spatial regulation of translation in the mammalian oocyte via the mTOR-eIF4F pathway', *Nature Communications*. Nature Publishing Group, 6. doi: 10.1038/ncomms7078.

Sutherland, A. E., Speed, T. P. and Calarco, P. G. (1990) 'Inner cell allocation in the mouse morula: The role of oriented division during fourth cleavage', *Developmental Biology*, 137(1), pp. 13–25. doi: 10.1016/0012-1606(90)90003-2.

Suwińska, A. *et al.* (2008) 'Blastomeres of the mouse embryo lose totipotency after the fifth cleavage division: Expression of Cdx2 and Oct4 and developmental potential of inner and outer blastomeres of 16- and 32-cell embryos', *Developmental Biology*, 322(1), pp. 133–144. doi: https://doi.org/10.1016/j.ydbio.2008.07.019.

Tabansky, I. *et al.* (2013) 'Developmental bias in cleavage-stage mouse blastomeres.', *Current biology : CB*, 23(1), pp. 21–31. doi: 10.1016/j.cub.2012.10.054.

Tarkowski, A. K. (1959) 'Experiments on the Development of Isolated Blastomeres of Mouse Eggs', *Nature*, 184(4695), pp. 1286–1287. doi: 10.1038/1841286a0.

Tarkowski, A K and Wróblewska, J. (1967) 'Development of blastomeres of mouse eggs isolated at the 4- and 8-cell stage.', *Journal of embryology and experimental morphology*. England, 18(1), pp. 155–180.

Tarkowski, A. K. and Wróblewska, J. (1967) 'Development of blastomeres of mouse eggs isolated at the 4- and 8-cell stage.', *Journal of Embryology and Experimental Morphology*, 18(1), pp. 155–180.

Thamodaran, V. and Bruce, A. W. (2016) 'p38 (Mapk14/11) occupies a regulatory node governing entry into primitive endoderm differentiation during preimplantation mouse embryo development', *Open Biology*, 6. doi: http://dx.doi.org/10.1098/rsob.160190.

Thoreen, C. C. *et al.* (2012) 'A unifying model for mTORC1-mediated regulation of mRNA translation', *Nature*, 485(7396), pp. 109–113. doi: 10.1038/nature11083.A.

Tillu, D. V *et al.* (2012) 'Resveratrol engages AMPK to attenuate ERK and mTOR signaling in sensory neurons and inhibits incision-induced acute and chronic pain', *Molecular Pain*, 8, pp. 1–12. doi: 10.1186/1744-8069-8-5.

Torres-Padilla, M.-E. *et al.* (2007) 'Histone arginine methylation regulates pluripotency in the early mouse embryo', *Nature*, 445(7124), pp. 214–218. doi: 10.1038/nature05458.

Vinot, S. *et al.* (2005) 'Asymmetric distribution of PAR proteins in the mouse embryo begins at the 8-cell stage during compaction', *Developmental Biology*, 282, pp. 307–319. doi: 10.1016/j.ydbio.2005.03.001.

Watanabe, T. *et al.* (2014) 'Limited predictive value of blastomere angle of division in trophectoderm and inner cell mass specification', *Development*, 141, pp. 2279–2288. doi: 10.1242/dev.103267.

Wicklow, E. *et al.* (2014) 'HIPPO Pathway Members Restrict SOX2 to the Inner Cell Mass Where It Promotes ICM Fates in the Mouse Blastocyst', *PLOS Genetics*, 10(10). doi: 10.1371/journal.pgen.1004618.

Yamanaka, Y., Lanner, F. and Rossant, J. (2010) 'FGF signal-dependent segregation of primitive endoderm and epiblast in the mouse blastocyst', *Development*, 137, pp. 715–724. doi: 10.1242/dev.043471.

Yang, J. *et al.* (2015) 'Binding of FGF2 to FGFR2 in an autocrine mode in trophectoderm cells is indispensable for mouse blastocyst formation through PKC-p38 pathway', *Cell Cycle*, 14(20), pp. 3318–3330. doi: 10.1080/15384101.2015.1087622.

Zamfirescu, R. C., Day, M. L. and Morris, M. B. (2021) 'mTORC1/2 signaling is downregulated by amino acid-free culture of mouse preimplantation embryos and is only partially restored by amino acid readdition', *American Journal of Physiology-Cell Physiology*, 320(1), pp. C30–C44. doi: 10.1152/ajpcell.00385.2020.

Zeng, Z. *et al.* (2007) 'Rapamycin derivatives reduce mTORC2 signaling and inhibit AKT activation in AML', *Blood*, 109(8), pp. 3509–3513. doi: 10.1182/blood-2006-06-030833.The.

Zernicka-Goetz, M., Morris, S. A. and Bruce, A. W. (2009) 'Making a firm

decision: Multifaceted regulation of cell fate in the early mouse embryo', *Nature Reviews Genetics*. Nature Publishing Group, 10(7), pp. 467–477. doi: 10.1038/nrg2564.

Zhang, Y., Yang, Z. and Wu, J. (2007) 'Signaling pathways and preimplantation development of mammalian embryos', *The FEBS Journal*, 274, pp. 4349–4359. doi: 10.1111/j.1742-4658.2007.05980.x.

Ziomek, C. A. and Johnson, M. H. (1982) 'The roles of phenotype and position in guiding the fate of 16-cell mouse blastomeres', *Developmental Biology*, 91(2), pp. 440–447. doi: https://doi.org/10.1016/0012-1606(82)90050-1.

Zoncu, R., Sabatini, D. M. and Efeyan, A. (2012) 'mTOR: from growth signal integration to cancer, diabetes and ageing', *Nature Reviews Molecular Cell Biology*, 12, pp. 21–35. doi: 10.1038/nrm3025.mTOR.

7. Appendix (Supplementary Tables).

Suppl. Tab. 1: Complementary data of rapamycin inhibition experiment (Fig. 10) showing all information about used embryos.

Total number of embryos assayed per condition	151
Total embryos in control condition	72
Total embryos in experimental (inhibited) condition	79
Number of biological replicates	5
Total embryos in control condition at exactly 16-cell stage (and hence included in the chart).	35
Total embryos in experimental condition at exactly 16-cell stage (and hence included in the chart).	23
The average number of cells across all embryos in the control condition.	18.9
The average number of cells across all embryos in the experimental condition.	18.9
The statistical p-value (T-Test) describing the difference between the total number of cells in each condition across ALL embryos.	0.81

Suppl. Tab. 2: Complementary data of AMPK activation experiment (Fig. 12) showing all information about used embryos.

Total number of embryos assayed per condition	110
Total embryos in control condition	66
Total embryos in experimental (inhibited) condition	44
Number of biological replicates	2
Total embryos in control condition at exactly 16-cell stage (and hence included in the chart).	49
Total embryos in experimental condition at exactly 16-cell stage (and hence included in the chart).	27
The average number of cells across all embryos in the control condition.	15.43
The average number of cells across all embryos in the experimental condition.	16.32
The statistical p-value (T-Test) describing the difference between the total number of cells in each condition across ALL embryos.	0.09

Suppl. Tab. 3: Complementary data of p38-MAPK inhibition experiment (Fig. 12) showing all information about used embryos.

Total number of embryos assayed per condition	145
Total embryos in control condition	70
Total embryos in experimental (inhibited) condition	75
Number of biological replicates	5
Total embryos in control condition at exactly 16-cell stage (and hence included in the chart).	18
Total embryos in experimental condition at exactly 16-cell stage (and hence included in the chart).	32
The average number of cells across all embryos in the control condition.	19.25
The average number of cells across all embryos in the experimental condition.	21.4
The statistical p-value (T-Test) describing the difference between the total number of cells in each condition across ALL embryos.	0.07

Suppl. Tab. 4: Complementary data of AKT inhibition experiment (Fig. 12) showing all information about used embryos.

Total number of embryos assayed per condition	141
Total embryos in control condition	86
Total embryos in experimental (inhibited) condition	55
Number of biological replicates	3
Total embryos in control condition at exactly 16-cell stage (and hence included in the chart).	41
Total embryos in experimental condition at exactly 16-cell stage (and hence included in the chart).	42
The average number of cells across all embryos in the control condition.	15.78
The average number of cells across all embryos in the experimental condition.	16
The statistical p-value (T-Test) describing the difference between the total number of cells in each condition across ALL embryos.	0.91

Suppl. Tab. 5: Complementary data of RSK inhibition experiment (Fig. 12) showing all information about used embryos.

Total number of embryos assayed per condition	163
Total embryos in control condition	83
Total embryos in experimental (inhibited) condition	80
Number of biological replicates	3
Total embryos in control condition at exactly 16-cell stage (and hence included in the chart).	49
Total embryos in experimental condition at exactly 16-cell stage (and hence included in the chart).	46
The average number of cells across all embryos in the control condition.	15.44
The average number of cells across all embryos in the experimental condition.	15.27
The statistical p-value (T-Test) describing the difference between the total number of cells in each condition across ALL embryos.	0.70

Suppl. Tab. 6: Complementary data of MEK1/2 inhibition experiment (Fig. 12) showing all information about used embryos.

Total number of embryos assayed per condition	106
Total embryos in control condition	60
Total embryos in experimental (inhibited) condition	46
Number of biological replicates	3
Total embryos in control condition at exactly 16-cell stage (and hence included in the chart).	26
Total embryos in experimental condition at exactly 16-cell stage (and hence included in the chart).	16
The average number of cells across all embryos in the control condition.	21.13
The average number of cells across all embryos in the experimental condition.	19.8
The statistical p-value (T-Test) describing the difference between the total number of cells in each condition across ALL embryos.	0.19

Suppl. Tab. 7: Complementary data of PP2A inhibition experiment (Fig. 13) showing all information about used embryos.

Total number of embryos assayed per condition	113
Total embryos in control condition	61
Total embryos in experimental (inhibited) condition	52
Number of biological replicates	3
Total embryos in control condition at exactly 16-cell stage (and hence included in the chart).	35
Total embryos in experimental condition at exactly 16-cell stage (and hence included in the chart).	30
The average number of cells across all embryos in the control condition.	18.15
The average number of cells across all embryos in the experimental condition.	16.37
The statistical p-value (T-Test) describing the difference between the total number of cells in each condition across ALL embryos.	0.07

Suppl. Tab. 8: Complementary data of CDK1 inhibition experiment (Fig. 13) showing all information about used embryos.

Total number of embryos assayed per condition	84
Total embryos in control condition	50
Total embryos in experimental (inhibited) condition	34
Number of biological replicates	15
Total embryos in control condition at exactly 16-cell stage (and hence included in the chart).	24
Total embryos in experimental condition at exactly 16-cell stage (and hence included in the chart).	2
The average number of cells across all embryos in the control condition.	19.32352941
The average number of cells across all embryos in the experimental condition.	21.86
The statistical p-value (T-Test) describing the difference between the total number of cells in each condition across ALL embryos.	0.05

Suppl. Tab. 9: Complementary data of FGFR inhibition experiment (Fig. 13) showing all information about used embryos.

Total number of embryos assayed per condition	76
Total embryos in control condition	39
Total embryos in experimental (inhibited) condition	37
Number of biological replicates	1
Total embryos in control condition at exactly 16-cell stage (and hence included in the chart).	25
Total embryos in experimental condition at exactly 16-cell stage (and hence included in the chart).	22
The average number of cells across all embryos in the control condition.	15.86
The average number of cells across all embryos in the experimental condition.	15.92
The statistical p-value (T-Test) describing the difference between the total number of cells in each condition across ALL embryos.	0.92

Suppl. Tab. 10: Complementary data of p38+mTOR (Fig. 14) showing all information about used embryos.

Total number of embryos assayed per condition	66
Total embryos in control condition	36
Total embryos in experimental (inhibited) condition	30
Number of biological replicates	3
Total embryos in control condition at exactly 16-cell stage (and hence included in the chart).	33
Total embryos in experimental condition at exactly 16-cell stage (and hence included in the chart).	40
The average number of cells across all embryos in the control condition.	17.75
The average number of cells across all embryos in the experimental condition.	17.9
The statistical p-value (T-Test) describing the difference between the total number of cells in each condition across ALL embryos.	0.89

Suppl. Tab. 11: Complementary data of 4EBP1/4EBP1-4Ala (Fig. 14) showing all information about used embryos.

Total number of embryos assayed per condition	123
Total embryos in control condition	60
Total embryos in experimental (inhibited) condition	63
Number of biological replicates	3
Total embryos in control condition at exactly 16-cell stage (and hence included in the chart).	27
Total embryos in experimental condition at exactly 16-cell stage (and hence included in the chart).	14
The average number of cells across all embryos in the control condition.	15.33
The average number of cells across all embryos in the experimental condition.	16.16
The statistical p-value (T-Test) describing the difference between the total number of cells in each condition across ALL embryos.	0.31

Suppl. Tab. 12: Complementary data of EIF4E histone (Fig. 14) showing all information about used embryos.

Total number of embryos assayed per condition	148
Total embryos in control condition	76
Total embryos in experimental (inhibited) condition	72
Number of biological replicates	4
Total embryos in control + DMSO condition at exactly 16-cell stage (and hence included in the chart).	16
Total embryos in control + Torin condition at exactly 16-cell stage (and hence included in the chart).	21
Total embryos in experimental condition + DMSO at exactly 16-cell stage (and hence included in the chart).	6
Total embryos in experimental condition + Torin at exactly 16-cell stage (and hence included in the chart).	10
The average number of cells across all embryos in the control + DMSO condition.	16.36
The average number of cells across all embryos in the control + Torin condition.	17.46
The average number of cells across all embryos in the experimental + DMSO condition.	15.04
The average number of cells across all embryos in the experimental + Torin condition.	15.28

Suppl. Tab. 12: Complementary data of EIF4E beads (Fig. 14) showing all information about used embryos.

Total number of embryos assayed per condition	191
Total embryos in control condition	89
Total embryos in experimental (inhibited) condition	102
Number of biological replicates	3
Total embryos in control + DMSO condition at exactly 16-cell stage (and hence included in the chart).	24
Total embryos in control + Torin condition at exactly 16-cell stage (and hence included in the chart).	16
Total embryos in experimental condition + DMSO at exactly 16-cell stage (and hence included in the chart).	13
Total embryos in experimental condition + Torin at exactly 16-cell stage (and hence included in the chart).	11
The average number of cells across all embryos in the control + DMSO condition.	17.55
The average number of cells across all embryos in the control + Torin condition.	17.64
The average number of cells across all embryos in the experimental + DMSO condition.	14.96
The average number of cells across all embryos in the experimental + Torin condition.	16.56